Clinical Neuroscience Research

Editors-in-Chief

J.B.M. Kuks

University Medical Center Groningen, The Netherlands

Deqin Geng

Affiliated Hospital of Xuzhou Medical University, China

BIO-BYWORD SCIENTIFIC PUBLISHING PTY LTD
(619 649 400)
Level 10
50 Clarence Street
SYDNEY NSW 2000
Copyright © 2026. Bio-Byword Scientific Publishing Pty Ltd.
Complimentary Copy

Clinical Neuroscience Research

Focus and Scope

Clinical Neuroscience Research is a peer-reviewed articles across a wide spectrum of basic, translational, and clinical research that help improve patient care. The journal publishes original articles, editorials and reviews to educate its readers, and to better understand, treat, and prevent neurological disorders. Published papers describing the results of original research on any aspect of the scientific study of the nervous system. Any paper, however short, will be considered for publication provided that it reports significant, new and carefully confirmed findings with full experimental details.

The journal provides a platform for studies that explores the diagnosis, nature, causes, treatment, and public health aspects of neurological illnesses.

About Publisher

Bio-Byword Scientific Publishing is a fast-growing, peer-reviewed and open access journal publisher, which is located in Sydney, Australia. As a dependable and credible corporation, it promotes and serves a broad range of subject areas for the benefit of humanity. By informing and educating a global community of scholars, practitioners, researchers and students, it endeavors to be the world's leading independent academic and professional publisher. To realize it, it keeps creative and innovative to meet the range of the authors' needs and publish the best of their work.

By cooperating with University of Sydney, University of New South Wales and other world-famous universities, Bio-Byword Scientific Publishing has established a huge publishing system based on hundreds of academic programs, and with a variety of journals in the subjects of medicine, construction, education and electronics.

Publisher Headquarter

BIO-BYWORD SCIENTIFIC PUBLISHING PTY LTD
Level 10
50 Clarence Street
Sydney NSW 2000
Website: www.bbwpublisher.com
Email: info@bbwpublisher.com

2026, Volume 4, Issue 3

Table of Contents

1 **Bidirectional Causal Relationship Between Sleep Duration, Insomnia, and Cerebral Infarction: A Two-Sample Mendelian Randomization Study**
Jing Shi, Yanhua Zhao, Yangyang Wu, Jiangping Wang, Xuan Chen

12 **The Impact of Cerebral Small Vessel Disease on Hemorrhagic Transformation After Mechanical Thrombectomy in Acute Large Vessel Occlusion Ischemic Stroke**
Yangyang Wu, Jing Shi, Xuan Chen

24 **Development and Validation of a Machine Learning Model Integrating Stress Hyperglycemia for Predicting Early Neurological Deterioration in Acute Mild-to-Moderate Ischemic Stroke**
Zhihui Chen, Zhixin Huang, Kaili Huang

38 **Combined Laminotomy and Spinal Endoscopic-Assisted Decompression for Gouty Tophi Involving the Lumbar Epidural Space and Multi-level Paravertebral Regions: A Case Report**
Yaolei Chen, Shaojun Kang, Zhi Hou, Chenglong Luo, Xin He

45 **Study on Stress Response of Propofol Combined with Sevoflurane Combined IntravenousInhalation General Anesthesia in Laparoscopic Cholecystectomy**
Wenyuan Zhang, Zhiyang Sun, Yunfang Wan

52 **The Global, Regional, and National Patterns of Change in the Burden of Skull Fractures from 1990 to 2021 and the Forecast for 2036: A Global Burden of Disease Study**
Yuhang Gu, Xiaoyu Ji, Siyuan Yang, Zhengquan Yu

80 **A Case Report of Schizophrenia Presenting with "Multiple Personality"-like Manifestations as the Initial Symptom**
Feng Zhou, Lei Zhang, Yu Yan, Yuanping Wu, Yunfeng Yuan, Sufang Liu, Meilin Huang

85 **Analysis of the Clinical Efficacy and Safety of CT-Guided Precision Nerve Block for the Treatment of Lumbar Disc Herniation**
Pengfei Yao, Lu Cai

92 **Diagnosis and Treatment Report of Parkinson's Disease Complicated by Cerebrovascular Disease, Mood Disorder, and Gastrointestinal Dysfunction**
Haowen Zhang

99 **A Resting-state Functional Magnetic Resonance Imaging Study on Macroscale Topological Properties of Whole-brain Functional Networks in Patients with Post-traumatic Stress Disorder**
Yumei Zhang, Qi Chen, Jun Lu, Yuanyuan Hu, Chengwei Wang

107 **Effect of Sequential Therapy with Edaravone Dexborneol on Prognosis in Patients with Progressive Cerebral Infarction**
Yong Yang, Bing Wang, Fei Wu, Hao Wen, Mei Jin

114 **With a View to Fear Extinction and to Brain Functional Change: A Neurotheoretical Hypothesis About Traditional Health-Preserving Exercises as Treatments for Post-Aortic Dissection Kinesiophobia**
Xiangyang Hu, Jia Liu, Jieyu Cao, Zhengwen Lei

Clinical Neuroscience Research, 2026, Volume 4, Issue 3
http://ojs.bbwpublisher.com/index.php/CNR
Online ISSN: 2981-8133
Print ISSN: 3083-4899

Bidirectional Causal Relationship Between Sleep Duration, Insomnia, and Cerebral Infarction: A Two-Sample Mendelian Randomization Study

Jing Shi, Yanhua Zhao, Yangyang Wu, Jiangping Wang, Xuan Chen*

Department of Neurology, Taiyuan Central Hospital, Taiyuan 030000, Shanxi, China

***Corresponding author:** Xuan Chen, ccccxuanxuan@163.com

Copyright: © 2026 Author(s). This is an open-access article distributed under the terms of the Creative Commons Attribution License (CC BY 4.0), permitting distribution and reproduction in any medium, provided the original work is cited.

Abstract: *Objective:* Observational studies suggest that abnormal sleep duration and insomnia are associated with stroke, but residual confounding factors, reverse causal bias, and the nonlinear characteristics of exposure-response relationships limit precise causal inference. This study employed a two-sample Mendelian randomization (MR) approach to systematically investigate the bidirectional causal relationship between sleep duration, insomnia, and cerebral infarction, clarifying their genetic causal effects. *Methods:* Genome-wide association study (GWAS) summary statistics were retrieved from the IEU OpenGWAS platform for sleep duration (ieu-a-1088; 128,266 participants of European descent), insomnia (ukb-b-3957; 462,341 participants of European descent), and cerebral infarction (ukb-d-I63; 361,194 participants of European descent). The inverse variance weighted (IVW) method was used as the core analytical approach, combined with the maximum likelihood method, MR-Egger regression, weighted median method, and weighted mode method for sensitivity analysis. Cochran's Q test quantified heterogeneity across genetic instruments, while the MR-Egger intercept test was applied to detect directional horizontal pleiotropy. *Results:* After data harmonization, 26, 38, 24, and 128 genetic variants were included in the analyses of sleep duration → cerebral infarction, insomnia → cerebral infarction, cerebral infarction → sleep duration, and cerebral infarction → insomnia, respectively. IVW analysis revealed no significant causal effect of genetically predicted sleep duration on cerebral infarction [OR=1.002, 95% confidence interval (CI): 0.998-1.006, *P*=0.252], nor did genetic susceptibility to insomnia significantly affect the risk of cerebral infarction (OR=0.994, 95% CI: 0.988-1.001, *P*=0.100). In reverse analyses, genetic susceptibility to cerebral infarction showed no significant causal relationship with sleep duration (β=0.394, 95% CI: -1.620-2.408, *P*=0.701) or the insomnia phenotype (β=0.057 SD, 95% CI: -0.245-0.360, *P*=0.711). The results of various supplementary analyses were consistent with the core IVW results, demonstrating stable conclusions. Neither the Cochran's Q test nor the MR-Egger intercept test detected significant heterogeneity or directional horizontal pleiotropy. *Conclusion:* This bidirectional MR study indicates that there is currently no reliable genetic evidence supporting a bidirectional causal relationship between sleep duration, insomnia, and cerebral infarction. Their clinical correlation may be largely mediated by non-genetic confounding factors.

Keywords: Sleep duration; Insomnia; Cerebral infarction; Mendelian randomization; Bidirectional analysis

Online publication: August 5, 2026

1. Introduction

Cerebral infarction is a major cause of death and long-term neurological deficits in the population, imposing a heavy burden on the public health system. Its complex genetic architecture and subtype heterogeneity have been confirmed by multiple cross-ancestry genetic studies [1–2]. Identifying modifiable risk factors is crucial for primary prevention of cerebral infarction, but traditional behavioral risk factors are often confounded by vascular pathology, psychological state, and socioeconomic factors, making it difficult to establish independent causal relationships accurately. Abnormal sleep duration and insomnia are prevalent and modifiable lifestyle risk factors in the population that can participate in the cerebrovascular pathology process through various pathways, including autonomic nervous system dysfunction, increased blood pressure, metabolic abnormalities, chronic inflammation, and endothelial damage. Existing observational studies and meta-analyses indicate that both short and long sleep durations are associated with an increased risk of stroke incidence and mortality, often exhibiting U-shaped or J-shaped nonlinear exposure-response relationships. Persistent insomnia has also been shown to increase the risk of stroke incidence [3–7]. However, current studies suffer from methodological heterogeneity, with inconsistent sleep assessment methods, study populations, and outcome definitions. Moreover, sleep disturbances are often accompanied by confounding factors such as hypertension, obesity, depression, and sleep-disordered breathing, leading to observational associations susceptible to residual confounding, reverse causality, and subclinical disease interference [8]. The true causal relationship between sleep and cerebral infarction remains to be further validated.

Mendelian randomization, by selecting germline genetic variants stably associated with exposure phenotypes as instrumental variables, can effectively circumvent confounding bias and reverse causality issues inherent in traditional observational studies, providing reliable genetic evidence for causal inference of diseases [9–10]. Nevertheless, issues such as sample overlap, weak instrument bias, horizontal pleiotropy, and non-standardized analytical reporting can still affect the accuracy and stability of MR study conclusions [11–12]. Existing MR studies have not found a stable linear causal relationship between sleep duration and overall stroke risk and suggest potential heterogeneity between different sleep characteristics and stroke phenotypes, with no unified conclusion on their causal relationship [13].

Notably, most existing studies have focused on the unidirectional effect of sleep phenotypes on stroke, neglecting their bidirectional interaction effects. Clinical studies have confirmed that patients with cerebral infarction often experience sleep disturbances such as abnormal sleep duration, insomnia, and decreased sleep quality after onset, and these abnormal sleep states are closely related to neurological recovery, cognitive prognosis, and the risk of recurrent cardiovascular and cerebrovascular events in patients [14–15]. However, no study has yet determined whether genetic susceptibility to cerebral infarction can reversely regulate sleep duration and insomnia phenotypes at the population level. Based on this, this study employed a bidirectional two-sample MR analysis to clarify:

(1) the causal effect of genetically predicted sleep duration and insomnia on the risk of cerebral infarction incidence;

(2) the reverse causal impact of genetic susceptibility to cerebral infarction on sleep duration and insomnia phenotypes, providing genetic evidence to clarify the causal relationship between sleep and cerebral infarction and refine precise prevention strategies for cerebral infarction.

2. Methods

2.1. Study design and fundamental assumptions

This study employed a bidirectional two-sample Mendelian Randomization (MR) design based on publicly available GWAS summary statistics. The analysis was conducted in accordance with three core assumptions regarding instrumental variables: the selected genetic variants are associated with the exposure; the genetic variants are independent of confounding factors in the exposure-outcome relationship; and the genetic variants affect the outcome solely through the exposure, without exhibiting unbalanced horizontal pleiotropy [11]. The study design, analysis, and result reporting adhered to the recommendations of the STROBE-MR statement and recent quality studies on MR reporting [12]. This study evaluated four directions: sleep duration → cerebral infarction, insomnia → cerebral infarction, cerebral infarction → sleep duration, and cerebral infarction → insomnia.

2.2. GWAS data sources

Summary statistics were obtained from the IEU OpenGWAS platform. All datasets primarily consisted of participants of European ancestry to minimize bias caused by significant population stratification. For sleep duration, the ieu-a-1088 dataset was used, derived from 128,266 UK Biobank participants; for insomnia, the ukb-b-3957 dataset was utilized, representing an ordinal categorical phenotype from the UK Biobank with 462,341 participants; and for cerebral infarction, the ukb-d-I63 dataset was employed, based on ICD-10 I63 diagnoses from 361,194 UK Biobank participants, including 2,353 cases and 358,841 controls. The main characteristics of each dataset are presented in **Table 1**.

Table 1. GWAS datasets used in the bidirectional Mendelian randomization study

Trait	OpenGWAS ID	Role	Population	Sample size	Phenotype/scale	Year
Sleep duration	ieu-a-1088	Exposure and outcome	European	128,266	Self-reported; continuous; SD	2016
Insomnia symptoms	ukb-b-3957	Exposure and outcome	European	462,341	Ordered categorical phenotype; SD	2018
Cerebral infarction	ukb-d-I63	Exposure and outcome	European	361,194	ICD-10 I63; binary; 2,353 cases	2018

Abbreviations: GWAS, genome-wide association study; ICD-10, International Classification of Diseases, 10th Revision; SD, standard deviation

2.3. Selection of instrumental variables and data harmonization

To ensure the reliability and statistical power of the bidirectional Mendelian Randomization (MR) analysis, this study rigorously screened eligible single nucleotide polymorphisms (SNPs) as genetic instrumental variables. Independent SNPs associated with each exposure were selected using a genome-wide significance threshold of $P < 5 \times 10^{-8}$. Linkage disequilibrium pruning was performed using a European reference population, with parameters set at $r^2 < 0.001$ and a window distance of 10,000 kb. To mitigate weak instrument bias, variants with an F-statistic ≤ 10 were excluded. The effect alleles in the exposure and outcome data were harmonized to ensure that the SNP effects corresponded to the same effect allele. Palindromic SNPs with intermediate allele frequencies and indeterminate directions were excluded. When an exposure SNP was missing in the outcome data, it was handled according to the proxy SNP and allele alignment rules specified in the analytical protocol. Due to differences in variant availability and allele

compatibility, the number of instrumental variables ultimately included varied across the different analytical directions.

2.4. Mendelian randomization analysis

This study pre-specified the inverse variance weighted (IVW) method as the primary approach for estimating causal effects. This method combines the Wald ratios of each instrumental variable to estimate the overall effect size, providing precise and reliable causal effect estimates under the premise that all instrumental variables are valid or that sample-level pleiotropy cancels out. To verify the robustness of the results, multiple sensitivity analyses were conducted using the maximum likelihood method, MR-Egger regression, weighted median method, and weighted mode method [9–10].

2.5. Sensitivity analysis

Heterogeneity among SNP-specific estimates was assessed using the Cochran Q statistic from the IVW and MR-Egger models. Directional horizontal pleiotropy was examined using the MR-Egger intercept test. Statistical significance was set at $P < 0.05$. The analysis was performed using the TwoSampleMR framework in R software, and data sources, instrumental variable selection, primary analysis, and sensitivity analysis were transparently reported in accordance with STROBE-MR guidelines [16–17].

3. Results

3.1. Composition of instrumental variables

After data extraction and harmonization, 26 SNPs were retained for the sleep duration → cerebral infarction analysis, 38 SNPs for the insomnia → cerebral infarction analysis, 24 SNPs for the cerebral infarction → sleep duration analysis, and 128 SNPs for the cerebral infarction → insomnia analysis. The variation in the number of instrumental variables across different directions reflects the genetic architecture of each exposure GWAS and the number of variants that could be harmonized in the outcome dataset.

3.2. Effects of sleep duration and insomnia on cerebral infarction

The primary IVW analysis did not support a causal effect of genetically predicted sleep duration on cerebral infarction (OR = 1.002, 95% CI: 0.998-1.006, $P = 0.252$). Similar non-significant results were obtained using the maximum likelihood method, MR-Egger, weighted median method, and weighted mode method, with effect estimates closely clustered around the null value **(Table 2)**.

The IVW analysis also failed to detect an association between genetic susceptibility to insomnia and cerebral infarction (OR = 0.994, 95% CI: 0.988-1.001, $P = 0.100$). The maximum likelihood method yielded a similar estimate (OR = 0.994, 95% CI: 0.988-1.001, $P = 0.077$), and none of the other robust estimation methods reached statistical significance. Thus, the forward analysis provided no evidence to support that a linear increase in sleep duration or heightened genetic susceptibility to the insomnia phenotype leads to cerebral infarction.

Table 2. Bidirectional Mendelian randomization estimates

Direction	Method	SNPs	Effect scale	Estimate	95% CI	*P* value
Sleep duration → cerebral infarction	IVW	26	OR	1.002	0.998 to 1.006	0.252
	Maximum likelihood	26	OR	1.002	0.998 to 1.006	0.248
	MR-Egger	26	OR	1.005	0.992 to 1.019	0.419
	Weighted median	26	OR	1.001	0.996 to 1.006	0.666
	Weighted mode	26	OR	1.002	0.993 to 1.011	0.692
Insomnia symptoms → cerebral infarction	IVW	38	OR	0.994	0.988 to 1.001	0.100
	Maximum likelihood	38	OR	0.994	0.988 to 1.001	0.077
	MR-Egger	38	OR	0.991	0.969 to 1.012	0.397
	Weighted median	38	OR	0.997	0.987 to 1.006	0.487
	Weighted mode	38	OR	0.999	0.985 to 1.012	0.835
Cerebral infarction → sleep duration	IVW	24	β (SD)	0.394	−1.620 to 2.408	0.701
	Maximum likelihood	24	β (SD)	0.414	−1.474 to 2.303	0.667
	MR-Egger	24	β (SD)	1.389	−2.809 to 5.588	0.523
	Weighted median	24	β (SD)	1.045	−1.649 to 3.739	0.447
	Weighted mode	24	β (SD)	0.956	−3.600 to 5.512	0.685
Cerebral infarction → insomnia symptoms	IVW	128	β (SD)	0.057	−0.245 to 0.360	0.711
	Maximum likelihood	128	β (SD)	0.058	−0.253 to 0.368	0.715
	MR-Egger	128	β (SD)	−0.040	−0.662 to 0.582	0.901
	Weighted median	128	β (SD)	−0.007	−0.443 to 0.429	0.974
	Weighted mode	128	β (SD)	−0.014	−1.175 to 1.146	0.981

Note: Forward effects are expressed as odds ratios (ORs) for cerebral infarction per 1-SD increase in the genetically predicted sleep phenotype. Reverse effects are expressed as β coefficients in SD units for the standardized sleep phenotype per unit increase in genetic liability to cerebral infarction. Abbreviations: CI, confidence interval; IVW, inverse-variance weighted; OR, odds ratio; SD, standard deviation; SNP, single-nucleotide polymorphism.

3.3. Effects of genetic susceptibility to cerebral infarction on sleep phenotypes

The reverse analysis revealed no significant association between genetic susceptibility to cerebral infarction and sleep duration (IVW β = 0.394, 95% CI: -1.620-2.408, P = 0.701). Estimates from other methods were also non-significant. The wide confidence intervals suggest limited precision in the estimates, and a potentially clinically meaningful effect of genetic susceptibility to cerebral infarction on sleep duration cannot be excluded.

Similarly, no significant association was found between genetic susceptibility to cerebral infarction and insomnia (IVW β = 0.057, 95% CI: -0.245-0.360, P = 0.711). Consistent negative results were obtained using the maximum likelihood method, MR-Egger, weighted median method, and weighted mode method. As with the sleep duration analysis, this result reflects genetic susceptibility to cerebral infarction and does not exclude sleep disturbances caused by neurological impairment, psychological changes, or treatment consequences following the actual occurrence of cerebral infarction. The effect estimates from various methods in the bidirectional MR analysis of sleep phenotypes and cerebral infarction are shown in **Figure 1**.

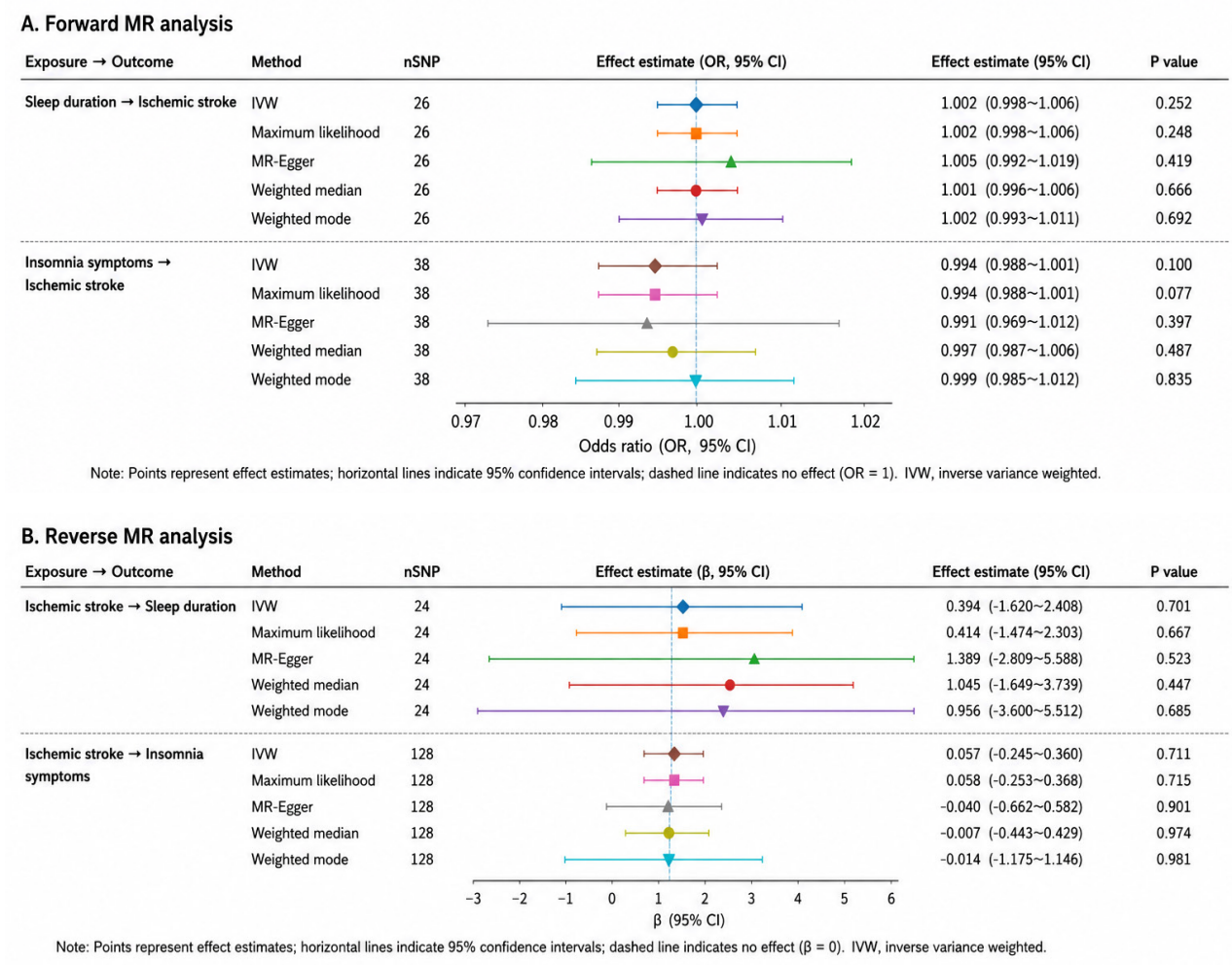

Figure 1. Forest plot of bidirectional Mendelian randomization (MR) analysis on sleep duration, insomnia, and cerebral infarction. (A) Forward MR analysis of the effects of sleep duration and insomnia on cerebral infarction, with effect sizes expressed as odds ratios (ORs) and 95% confidence intervals (CIs); (B) Reverse MR analysis of the effects of genetic predisposition to cerebral infarction on sleep duration and insomnia, with effect sizes expressed as β coefficients and 95% CIs. The dashed line represents the line of no effect, and the inverse-variance weighted (IVW) method was the primary analytical approach

3.4. Heterogeneity, pleiotropy, and directionality

No significant heterogeneity was indicated by the Cochran Q test in any of the analytical directions (**Table 3**). The *P*-values for the IVW Q test were as follows: sleep duration → cerebral infarction: 0.913, insomnia → cerebral infarction: 0.242, cerebral infarction → sleep duration: 0.223, cerebral infarction → insomnia: 0.665. The MR-Egger intercept test was also non-significant in all cases ($P = 0.600–0.727$), providing no statistical evidence of directional horizontal pleiotropy.

Table 3. Heterogeneity and directional pleiotropy analyses

Direction	Q-test method	Q statistic	df	Q-test P value	MR-Egger intercept	SE	Intercept *P* value
Sleep duration → cerebral infarction	IVW	16.055	25	0.913	−0.000084	0.000165	0.613
	MR-Egger	15.792	24	0.895			
Insomnia symptoms → cerebral infarction	IVW	42.613	37	0.242	0.000045	0.000126	0.721
	MR-Egger	42.460	36	0.213			
Cerebral infarction → sleep duration	IVW	27.803	23	0.223	−0.001708	0.003210	0.600
	MR-Egger	27.450	22	0.195			
Cerebral infarction → insomnia symptoms	IVW	119.679	127	0.665	0.000173	0.000494	0.727
	MR-Egger	119.556	126	0.645			

Note: The MR-Egger intercept is shown once for each analytical direction. A nonsignificant intercept test does not prove the absence of pleiotropy but indicates no statistical evidence of unbalanced directional horizontal pleiotropy. Abbreviations: df, degrees of freedom; IVW, inverse-variance weighted; SE, standard error.

4. Discussion

This bidirectional two-sample MR study found no clear evidence to support a causal effect of genetically predicted sleep duration or genetic predisposition to insomnia on cerebral infarction, nor did it find evidence that genetic predisposition to cerebral infarction alters sleep duration or insomnia. Consistent results across the IVW, maximum likelihood, MR-Egger, weighted median, and weighted mode methods reinforced the internal consistency of the negative findings. The Cochran Q test revealed no heterogeneity, and the MR-Egger intercept did not suggest directional pleiotropy.

Several observational studies and meta-analyses have indicated a U-shaped or J-shaped nonlinear relationship between sleep duration and stroke risk, with both insufficient and excessive sleep, as well as persistent insomnia, identified as potential risk factors for cardiovascular and cerebrovascular diseases [6, 18–21]. This genetic causal analysis found no linear causal association between sleep duration, insomnia, and cerebral infarction, consistent with recent studies combining observational cohorts with MR approaches, suggesting that observational correlations do not equate to genetic causal effects [22]. The discrepancies primarily stem from inherent limitations of observational research methods: observational studies are susceptible to confounding factors, reverse causation, and subclinical disease interference, revealing only association trends; in contrast, Mendelian randomization effectively circumvents postnatal confounding biases through germline genetic variations, making it more suitable for causal inference. Furthermore, previous studies have primarily focused on the stroke risk associated with extreme sleep durations and long-term insomnia trajectories, whereas conventional two-sample MR can only evaluate overall average linear effects and cannot capture nonlinear risk characteristics at both ends, which may be a significant reason for the absence of positive linear associations in this study. Additionally, the ukb-b-3957 insomnia phenotype used in this study is a self-reported genetic proxy phenotype in the population, differing phenotypically from clinically confirmed chronic insomnia, and does not differentiate stroke subtypes, potentially overlooking potential subtype-specific associations between the two.

Regarding sleep duration, multiple dose-response meta-analyses have confirmed a U-shaped nonlinear association with cardiovascular and cerebrovascular risk, with both short and long sleep durations exerting adverse vascular effects, although the risk intensities of these two extreme phenotypes differ [6, 23–31]. Conventional linear MR can only estimate overall average effects, with opposing risk effects at both extremes canceling each other out, resulting in an overall effect approaching null. Therefore, this negative result does not negate the cerebrovascular damage caused by extreme abnormal sleep. The negative result for insomnia is primarily attributed to phenotypic heterogeneity: the insomnia phenotype in this study is based on a population self-reported sleep disturbance scale, not clinically confirmed pathological insomnia, and its genetic predisposition may overlap with confounding genetic traits such as mood and neuroticism, representing only the population's sleep-related genetic load and not directly generalizable to clinical insomnia subtypes. The negative results of the reverse analysis do not contradict clinical post-stroke sleep disorders: sleep abnormalities after clinical cerebral infarction are mostly secondary to brain injury, neurological deficits, mood changes, and clinical interventions, whereas this MR analysis focuses on the impact of congenital genetic predisposition on basic sleep phenotypes, with different research dimensions. Additionally, the confidence interval for the effect of cerebral infarction on sleep duration is wide, and a weak potential clinical effect cannot be completely ruled out.

This study's methodological design offers significant advantages. First, the bidirectional MR design comprehensively validated the bidirectional causal hypotheses between sleep and cerebral infarction, addressing the limitations of previous unidirectional studies that could not distinguish causal sequences or ignore bidirectional interactions. Second, the study, based on large-sample public GWAS data from individuals of European ancestry, effectively controlled for population stratification bias, and the high consistency of results across multiple MR methods with different statistical assumptions ensured the robustness of the conclusions. Third, the study strictly differentiated between the OR effects of binary cerebral infarction outcomes and the β effects of continuous sleep phenotypes, providing differentiated interpretations of bidirectional outcomes and avoiding bias caused by mismatched effect dimensions. Finally, systematic quality control of instrumental variables, along with heterogeneity and pleiotropy tests, minimized common biases in MR analysis, ensuring the accuracy of causal inference.

However, this study also has several methodological limitations. First, the study data were mostly sourced from the UK Biobank cohort, with potential sample overlap, which could introduce slight estimation bias under conditions of weak instrumental variables. Second, although weak instrumental variables with $F \leq 10$ were excluded, the use of conventional genome-wide significance thresholds for instrumental variable selection could not completely eliminate weak instrumental variable interference. Third, sleep duration and insomnia were self-reported phenotypes, subject to subjective bias and not fully reflective of objective sleep structure or clinical sleep disorders. Fourth, the study, based on overall cerebral infarction outcomes (ICD-10 I63), did not differentiate ischemic stroke subtypes, making it impossible to rule out the possibility of specific causal associations between different subtypes and sleep phenotypes. Fifth, the linear MR model could not test for nonlinear and threshold effects between sleep and cerebral infarction, making it difficult to identify special risks associated with extreme sleep durations. Sixth, the study included only individuals of European ancestry, requiring caution when generalizing the conclusions to other ethnic groups.

5. Conclusion

In summary, this bidirectional two-sample Mendelian randomization study suggests that, at the level of genetic linear effects, there is no clear bidirectional causal association between sleep duration, genetic predisposition to insomnia, and cerebral infarction. The correlations between sleep abnormalities and cerebral infarction reported in previous observational studies are not attributable to congenital genetic linear causal effects but are more likely mediated by postnatal confounding factors, nonlinear dose effects, and secondary sleep disorders after cerebral infarction. Future research could leverage individual clinical data to conduct nonlinear MR analyses, further exploring the specific associations between extreme sleep durations, clinically confirmed insomnia subtypes, and different ischemic stroke subtypes, elucidating the causal mechanisms between sleep disorders and cerebral infarction, and providing a more comprehensive genetic basis for the precise prevention and control of sleep-related risk factors for cerebral infarction.

Funding

This study was supported by grants from the Taiyuan Bureau of Science and Technology, Science, Technology, and Innovation Program of National Regional Medical Center (202209) and the Taiyuan Bureau of Science and Technology, Science, Technology, and Innovation Program of National Regional Medical Center (202269).

Disclosure statement

The authors declare no conflict of interest.

References

[1] Mishra A, Malik R, Hachiya T, et al., 2022, Stroke Genetics Informs Drug Discovery and Risk Prediction Across Ancestries. Nature, 611(7934): 115–123.

[2] Ibanez L, Heitsch L, Carrera C, et al., 2022, Multi-ancestry GWAS Reveals Excitotoxicity Associated with Outcome after Ischaemic Stroke. Brain, 145(7): 2394–2406.

[3] Wang H, Sun J, Sun M, et al., 2022, Relationship of Sleep Duration with the Risk of Stroke incidence and Stroke Mortality: An Updated Systematic Review and Dose-response Meta-analysis of Prospective Cohort Studies. Sleep Medicine, 2022(90): 267–278.

[4] Huang YM, Xia W, Ge YJ, et al., 2022, Sleep Duration and Risk of Cardio-cerebrovascular Disease: A Dose-response Meta-analysis of Cohort Studies Comprising 3.8 million Participants. Frontiers in Cardiovascular Medicine, 2022(9): 907990.

[5] Ke J, Liu X, Ruan X, et al., 2023, Short Sleep Duration Associated with the Incidence of Cardio-cerebral Vascular Disease: A Prospective Cohort Study in Shanghai, China. BMC Cardiovascular Disorders, 2023(23): 177.

[6] Fang Y, He Y, Huang Y, et al., Sleep Duration, Daytime Napping, and Risk of Incident Stroke: Nuances by Metabolic Syndrome from the China Health and Retirement Longitudinal Study. Frontiers in Cardiovascular Medicine, 2022(9): 976537.

[7] Sawadogo W, Adera T, Alattar M, et al., 2023, Association between Insomnia Symptoms and Trajectory with the Risk of Stroke in the Health and Retirement Study. Neurology, 101(5): e475–e488.

[8] Haddad C, Sacre H, Tawil S, et al., 2025, The Triangulation of Multimorbidity: A Systematic Review of Primary Sleep Disorders, Hypertension, and Psychiatric Disorders. PLOS Global Public Health, 5(10): e0005216.

[9] Sanderson E, Glymour MM, Holmes MV, et al., 2022, Mendelian Randomization. Nature Reviews Methods Primers, 2022(2): 6.

[10] Richmond RC, Davey Smith G, 2022, Mendelian Randomization: Concepts and Scope. Cold Spring Harbor Perspectives in Medicine, 12(1): a040501.

[11] Woolf B, Di Cara N, Moreno-Stokoe C, et al., 2022, Investigating the Transparency of Reporting in Two-sample Summary Data Mendelian Randomization Studies using the MR-Base Platform. International Journal of Epidemiology, 51(6): 1943–1956.

[12] Skrivankova VW, Richmond RC, Woolf BAR, et al., 2021, Strengthening the Reporting of Observational Studies in Epidemiology using Mendelian Randomization: The STROBE-MR Statement. JAMA, 326(16): 1614–1621.

[13] Guo C, Harshfield EL, Markus HS, 2024, Sleep Characteristics and Risk of Stroke and Dementia: An Observational and Mendelian Randomization Study. Neurology, 2024(102): e209141.

[14] Duss SB, Bauer-Gambelli SA, Bernasconi C, et al., 2023, Frequency and Evolution of Sleep-wake Disturbances after Ischemic Stroke: A 2-year Prospective Study of 437 Patients. Sleep Medicine, 2023(101): 244–251.

[15] Yang J, Lin A, Tan Q, et al., 2024, Development of Insomnia in Patients with Stroke: A Systematic Review and Meta-analysis. PLoS One, 2024(19): e0297941.

[16] Minelli C, Del Greco MF, van der Plaat DA, et al., 2021, The Use of Two-sample Methods for Mendelian Randomization Analyses on Single Large Datasets. International Journal of Epidemiology, 50(5): 1651–1659.

[17] Gibson MJ, Spiga F, Campbell A, et al., 2023, Reporting and Methodological Quality of Studies that Use Mendelian Randomisation in UK Biobank: A Meta-Epidemiological Study. BMJ Evidence-Based Medicine, 28(2): 103–110.

[18] Zhou B, Jiang C, Zhang W, et al., 2023, Association of Sleep Duration and Napping with Stroke Mortality in Older Chinese: A 14-Year Prospective Cohort Study of the Guangzhou Biobank Cohort Study. Sleep Medicine, 2023(101): 384–391.

[19] Chen Y, Kartsonaki C, Clarke R, et al., 2023, Sleep Duration and Risk of Stroke and Coronary Heart Disease: A 9-year Community-Based Prospective Study of 0.5 million Chinese Adults. BMC Neurology, 2023(23): 327.

[20] Mc Carthy CE, Yusuf S, Judge C, et al., 2023, Sleep Patterns and the Risk of Acute Stroke: Results from the INTERSTROKE International Case-Control Study. Neurology, 100(21): e2191–e2203.

[21] Joundi RA, Patten SB, Williams JVA, et al., 2023, Association between Excess Sleep Duration and Risk of Stroke: A Population-Based Study. Canadian Journal of Neurological Sciences, 2023(50): 17–22.

[22] Ungvari Z, Fekete M, Lehoczki A, et al., 2025, Inadequate Sleep Increases Stroke Risk: Evidence from a Comprehensive Meta-analysis of Incidence and Mortality. GeroScience, 47(3): 4679–4695.

[23] Zhong Q, Qin Z, Wang X, et al., 2023, Healthy Sleep Pattern Reduce the Risk of Cardiovascular Disease: A 10-Year Prospective Cohort Study. Sleep Medicine, 2023(105): 53–60.

[24] Matas A, Amaral L, Patto AV, 2022, Is post-ischemic stroke insomnia related to a negative functional and cognitive outcome? Sleep Medicine, 2022(94): 1–7.

[25] Duss SB, Bernasconi C, Steck A, et al., 2023, Multiple Sleep-wake Disturbances after Stroke Predict an Increased Risk of Cardio-Cerebrovascular Events or Death: A Prospective Cohort Study. European Journal of Neurology, 30(6): 1696–1705.

[26] Hale E, Gottlieb E, Usseglio J, et al., 2023, Post-stroke Sleep Disturbance and Recurrent Cardiovascular and

Cerebrovascular Events: A Systematic Review and Meta-analysis. Sleep Medicine, 2023(104): 29–41.

[27] Luo Y, Yu G, Liu Y, et al., 2023, Sleep Quality After Stroke: A Systematic Review and Meta-analysis. Medicine (Baltimore), 2023(102): e33777.

[28] Sawadogo W, Adera T, Burch JB, et al., 2024, Sleep Duration and All-cause Mortality among Stroke Survivors. Journal of Stroke & Cerebrovascular Diseases, 33(4): 107615.

[29] McLaren DM, Evans J, Baylan S, et al., 2024, Assessing Insomnia after Stroke: A Diagnostic Validation of the Sleep Condition Indicator in Self-reported Stroke Survivors. BMJ Neurology Open, 6(2): e000768.

[30] Wang YY, Li JX, Liu YF, et al., 2025, Prevalence of Poor Sleep Quality among Stroke Survivors: A Meta-analysis and Systematic Review. Sleep Medicine Reviews, 2025(80): 102070.

[31] Zhang Y, Xia X, Zhang T, et al., 2023, Relation between Sleep Disorders and Post-stroke Cognitive Impairment. Frontiers in Aging Neuroscience, 2023(15): 1036994.

Publisher's note

Bio-Byword Scientific Publishing remains neutral with regard to jurisdictional claims in published maps and institutional affiliations.

Clinical Neuroscience Research, 2026, Volume 4, Issue 3
http://ojs.bbwpublisher.com/index.php/CNR
Online ISSN: 2981-8133
Print ISSN: 3083-4899

The Impact of Cerebral Small Vessel Disease on Hemorrhagic Transformation After Mechanical Thrombectomy in Acute Large Vessel Occlusion Ischemic Stroke

Yangyang Wu, Jing Shi, Xuan Chen*

Department of Neurology, Taiyuan Central Hospital, Taiyuan 030000, Shanxi, China

***Corresponding author:** Xuan Chen, ccccxuanxuan@163.com

Copyright: © 2026 Author(s). This is an open-access article distributed under the terms of the Creative Commons Attribution License (CC BY 4.0), permitting distribution and reproduction in any medium, provided the original work is cited.

Abstract: With the intensification of population aging and the rapid development of neuroimaging, cerebral small vessel disease (CSVD) has garnered increasing attention. Endovascular thrombectomy (EVT) can significantly improve functional outcomes in patients with intracranial large vessel occlusion and has become the standard treatment for acute large vessel occlusion ischemic stroke. Numerous studies suggest that pre-existing CSVD before acute ischemic stroke may increase the risk of hemorrhagic transformation (HT) after EVT, yet results remain controversial. This article primarily discusses the impact of different subtypes of CSVD and the total burden on magnetic resonance imaging on HT after EVT in patients with acute large vessel occlusion ischemic stroke, aiming to provide a clinical reference.

Keywords: Cerebral small vessel disease; Acute large vessel occlusion ischemic stroke; After endovascular thrombectomy; Hemorrhagic transformation

Online publication: August 5, 2026

1. Introduction

Approximately 17 million people worldwide suffer from acute ischemic stroke (AIS) each year, leading to around 6 million deaths. It is projected that by 2030, the number of new ischemic stroke patients could reach 77 million [1]. Ischemic stroke is the most common type of stroke, accounting for 69.6%–70.8% of all strokes, with AIS caused by large vessel occlusion being the most critical, accounting for approximately 28% to 46% of all AIS cases [2]. Current effective treatments for AIS aim to rapidly open occluded vessels, restore blood flow perfusion to ischemic regions, and salvage viable brain tissue. Intravenous thrombolysis with alteplase within 4.5 hours of onset is recommended as the first-line treatment for AIS patients. However, for patients with concurrent large vessel occlusion (LVO), the recanalization rate with intravenous thrombolysis

is low (13%–18%), with suboptimal efficacy, and fewer than 3% of patients truly benefit [3]. A series of randomized clinical trials have demonstrated that EVT can significantly improve functional outcomes in patients with intracranial large vessel occlusion and has become the standard treatment for AIS-LVO patients [4–5]. However, complications such as HT, vascular embolism, vasospasm, and contrast-induced nephropathy may occur postoperatively, with HT being the most severe complication [6]. HT can exacerbate brain tissue damage and even increase the risk of death in patients, making it crucial to identify factors influencing HT after EVT to guide targeted clinical prevention and control measures [7].

Cerebral small vessel disease (CSVD) refers to a series of clinical, imaging, and pathological syndromes affecting intracranial small arteries, arterioles, capillaries, venules, and small veins, as well as the surrounding brain parenchyma, caused by various etiologies [8]. It may be a risk factor for intracranial hemorrhage [9]. Some studies speculate that the reasons for poor prognosis after EVT may be related to chronic ischemia and cerebral hypoperfusion caused by arteriole, venule, and capillary lesions [10]. With the rapid development of neuroimaging technology, an increasing number of AIS patients undergoing vascular recanalization treatment are being detected with concurrent CSVD signs in clinical practice. CSVD patients may have an impact on HT after vascular recanalization treatment due to factors such as blood-brain barrier disruption, cerebral microcirculation disorders, poor microvascular reperfusion, and reduced effective connectivity in neural networks [11]. In light of this, domestic and foreign scholars have conducted a series of studies, and this article will provide an overview of the current research status in this field.

2. Hemorrhagic transformation (HT) after endovascular therapy (EVT) in patients with acute ischemic stroke with large vessel occlusion (AIS-LVO)

Hemorrhagic transformation refers to bleeding within or at remote sites from the ischemic focus due to multiple potential mechanisms during ischemic stroke. Its diagnosis primarily relies on imaging findings. Before endovascular treatment, cranial imaging in patients with AIS-LVO does not show hemorrhage. However, when cranial imaging is repeated within 24–72 hours after mechanical thrombectomy, hemorrhage found within the infarct area or at remote sites is termed hemorrhagic transformation after mechanical thrombectomy for acute large vessel occlusion stroke [12]. Depending on whether it is accompanied by neurological deterioration (i.e., an increase of ≥4 points on the National Institutes of Health Stroke Scale (NIHSS) or an increase of ≥ 2 points in specific NIHSS items), hemorrhagic transformation can be classified as symptomatic intracranial hemorrhage (sICH) and asymptomatic intracranial hemorrhage. Among these, sICH is a more severe type of hemorrhage, often leading to poor patient prognosis or even death. The incidence of asymptomatic intracranial hemorrhage after mechanical thrombectomy performed within 8 hours of onset is 51.4%, while the incidence of sICH is 4.5% [13]. As the time from onset increases, the incidence of hemorrhagic transformation may be higher. According to the Endovascular Treatment of Acute Anterior Circulation Ischemic Stroke (ACTUAL) study in China, the incidence of postoperative hemorrhagic transformation in patients undergoing mechanical thrombectomy within 6 hours of onset is 46.7%, with an sICH incidence of 15.5% [14]. By analyzing the Multicenter Randomized Clinical Trial of Endovascular Treatment for Acute Ischemic Stroke in the Netherlands (MR CLEAN-NO IV and MR CLEAN-MED), among 1017 cases, 331 (33%) had asymptomatic intracranial hemorrhage, and 90 (9%) had sICH. Both asymptomatic intracranial hemorrhage and sICH were associated with poorer functional outcomes [15]. Overall, the incidence of HT after EVT ranges from 26.0% to 58.0%, while the incidence of sICH ranges

from 2.0% to 20.89% [16–17]. The mechanisms underlying HT may include oxidative stress, inflammatory responses, and blood-brain barrier disruption [18–20]. Exploring the risk factors for hemorrhagic transformation after mechanical thrombectomy helps in better preoperative patient selection and optimizing perioperative management, thereby reducing the incidence of hemorrhagic transformation and maximizing treatment benefits. In recent years, the correlation between cerebral small vessel disease (CSVD) and HT after EVT has gradually attracted attention.

3. Overview of cerebral small vessel disease (CSVD)

CSVD refers to degenerative brain diseases caused by lesions in cerebral small arteries and their distal branches, arterioles, capillaries, venules, and small veins [8]. Age-related and hypertension-associated cerebral small vessel disease and amyloid angiopathy are the most common types. Depending on the affected brain regions, CSVD patients may exhibit various clinical manifestations, including lacunar syndromes, gait disturbances, depression, cognitive impairment, and urinary incontinence [21]. Current examination methods cannot evaluate CSVD damage, and clinical diagnosis relies entirely on the detection of brain tissue damage associated with cerebral small vessel disease. Therefore, cranial imaging is crucial for diagnosing cerebral small vessel disease. According to the 2013 Standards for Reporting Vascular Changes on Neuroimaging (STRIVE) criteria, CSVD imaging manifestations mainly include the following six subtypes: recent small subcortical infarct (RSSI), presumed vascular origin lacunar infarction (LI), presumed vascular origin white matter hyperintensity (WMH), perivascular space (PVS), cerebral microbleed (CMB), and brain atrophy [22]. With the publication of the second edition of STRIVE (STRIVE-2) in 2023, new imaging features such as cortical superficial siderosis, cortical cerebral microinfarcts, and incidental DWI-positive lesions have been incorporated, and imaging characteristics have been defined and updated [23]. Multiple studies have shown that different CSVD subtypes can have additive effects on the brain and interact with each other [24–25]. However, not every degree of damage from each CSVD subtype can reflect the severity of brain damage. A comprehensive assessment of all existing lesions helps in reaching more accurate conclusions, leading to the concept of total CSVD burden. The total CSVD burden incorporates WMH, LI, CMB, and PVS imaging markers into a scoring scale to comprehensively evaluate their impact on clinical diagnosis and treatment [26]. Studies have confirmed that CSVD may increase the risk of stroke onset, treatment complications, and poor prognosis, as well as the risk of stroke recurrence [27].

4. Cerebral small vessel disease (CSVD) and acute ischemic stroke with large vessel occlusion (AIS-LVO)

The intracranial large and small vessels together form the cerebral vascular tree. Although there are certain differences in structure and function, their anatomical structures are continuous, and they are both influenced by hemodynamics and exposed to similar risk factors. Therefore, intracranial large vessel disease often coexists with CSVD, and large vessel disease can further aggravate CSVD, which in turn affects the prognosis of patients with AIS-LVO [28]. Intracranial large artery atherosclerosis (LAA) is the most common cause of intracranial large vessel disease [28]. Imaging analysis shows that the coexistence rate of LAA and CSVD can reach 49.5% [29]. LAA may lead to the development and progression of CSVD through the following mechanisms: (1) Thickening of the vessel wall, stenosis, or even occlusion in LAA patients causes

chronic ischemia and hypoperfusion; (2) Microemboli generated from LAA plaque rupture block distal arterioles with blood flow; (3) Abnormal matrix metalloproteinase activity in LAA patients damages the blood-brain barrier, promoting the occurrence of CSVD; (4) Hemodynamic changes in LAA cause functional and structural disorders in small vessels, leading to CSVD [30–33].

For AIS patients with LAA complicated by CSVD, a high burden of WMH indicates a poorer neurological prognosis. Moreover, the correlation between WMH burden in different regions and post-stroke neurological status varies, with periventricular WMH burden appearing more relevant to poor post-stroke outcomes than deep WMH burden, possibly because periventricular white matter is more sensitive to decreases in cerebral blood flow [34]. In addition to WMH, LI and CMB also have potential impacts on the neurological prognosis of AIS. Due to aging and poor establishment of leptomeningeal collateral compensation, CSVD patients experience decreased cerebral metabolism and cerebrovascular reserve function, as well as reduced tolerance of local brain tissue to ischemia. When AIS occurs, the ischemic penumbra rapidly progresses to the core infarct area, leading to poor patient prognosis [35]. CSVD impairs the function of the neurovascular unit, increasing blood-brain barrier permeability. Vascular components leak into the perivascular space, causing local inflammatory responses and leading to poor prognosis in AIS patients [36]. CSVD patients have poor reperfusion of cerebral microvessels, and successful reperfusion of cerebral microvessels is a more effective predictor of functional outcomes than successful recanalization of occluded large vessels [37]. Additionally, patients with comorbid CSVD have an increased risk of postoperative complications after EVT, which also affects their prognosis [38]. With the widespread application of EVT in the treatment of AIS-LVO, the impact of CSVD on postoperative HT and clinical prognosis after EVT has become a research focus for scholars both domestically and internationally in recent years.

5. Different subtypes of CSVD and HT after EVT in AIS-LVO patients

Cerebral small vessel disease (CSVD) is a widely distributed cerebrovascular disease, primarily manifested as cerebral microbleeds (CMB), white matter hyperintensity (WMH), lacunar infarctions (LI), and perivascular spaces (PVS). Different subtypes of CSVD may have varying impacts on hemorrhagic transformation (HT) after endovascular therapy (EVT) in patients with acute ischemic stroke with large vessel occlusion (AIS-LVO), and different CSVD subtypes often coexist in the same AIS patient. Previous studies have suggested that CSVD may increase the risk of HT in EVT patients, but this has not been widely confirmed.

5.1. Relationship between WMH and HT after EVT

WMH is a parenchymal lesion caused by CSVD, commonly found in elderly patients who have a higher prevalence of stroke and transient ischemic attack (TIA) [39]. It is closely associated with an increased risk of stroke and vascular death [40]. As a marker of chronic hypoperfusion, WMH is strongly related to chronic endothelial dysfunction and disruption of the blood-brain barrier throughout the brain [41]. Cranial magnetic resonance imaging (MRI) indicates that as CSVD progresses, pathological changes in the white matter worsen, which is associated with early neurological deterioration and poor functional outcomes after AIS [42–43]. Studies have shown that severe WMH is associated with an increased risk of HT after vascular reperfusion in AIS. The incidence of symptomatic intracranial hemorrhage (sICH) is significantly higher in patients with moderate to severe leukoaraiosis in the deep white matter compared to those without or with mild leukoaraiosis [44]. Guo et al. conducted a multicenter retrospective analysis of 273 acute stroke patients

after EVT, evaluating early neurological improvement and deterioration based on the Van Swieten classification [45]. Multivariate analysis revealed that severe WMH was negatively correlated with early neurological improvement. Among patients with asymptomatic intracranial hemorrhage, severe WMH was an independent predictor of early neurological deterioration. A systematic review and meta-analysis of 1,296 patients after EVT across seven studies found unique differences in the risk factor profiles and clinical outcomes of ischemic stroke among patients with varying severities of WMH [46]. Patients with severe WMH may be associated with risk factors for cerebrovascular disease and have poorer outcomes. The severity of WMH is negatively correlated with the patency of collateral blood flow, indicating that chronic hypoperfusion associated with WMH may promote the development of cerebral collateral circulation [47]. Subjects with severe WMH also exhibit hypercoagulability, platelet activation, oxidative stress, and inflammation, which may facilitate the formation of microemboli leading to reperfusion failure [48]. Acute cerebral ischemia and reperfusion injury may exacerbate pre-existing blood-brain barrier disruption in patients with severe WMH [49]. Increased blood-brain barrier permeability will intensify the processes of edema, inflammation, and cytotoxicity, thereby promoting infarction and even HT [50]. Shi et al. retrospectively analyzed 105 patients with acute anterior circulation occlusion who underwent EVT and identified deep white matter and periventricular WMH on preoperative MRI images [51]. Patients were divided into a deep white matter (DWM) group and a non-DWM group. Comparison of the two groups revealed that moderate to severe WMH in the DWM group was an independent predictor of HT after EVT. Simone et al. graded the severity of WMH in 3,046 patients from the MR CLEAN study and found that more severe WMH was associated with poorer functional outcomes, a higher probability of ineffective recanalization, and a negative correlation with early neurological recovery, but not with the probability of successful reperfusion or sICH [42]. The results of the study by Kang-Ho Cho et al. also showed that WMH did not affect postoperative HT in AIS-LVO patients, which may be related to the use of a new stent retriever device in this study [52].

5.2. Relationship between CMB and HT after EVT

CMB is defined as the leakage of hemosiderin deposits (primarily macrophages) from cerebral small vessels around them, presenting as a hemorrhagic-prone pathological state, mainly attributed to cerebral amyloid angiopathy and hypertensive vasculopathy [53–54]. The prevalence of cerebral microbleeds increases with age, with a higher prevalence in males. Hypertension increases the risk of cerebral microbleeds, including those in deep and mixed locations [55]. Cerebral microbleeds have been confirmed to be associated with spontaneous cerebral hemorrhage and hemorrhagic recurrence [56]. The detection of cerebral microbleeds on susceptibility-weighted imaging (SWI) is a marker of hemorrhagic small vessel disease [57]. Study results indicate that an increased number of microbleeds is significantly associated with the risk of asymptomatic intracranial hemorrhage and sICH, introducing the concept of cerebral microvascular burden as a possible predictor of thrombolytic intracranial hemorrhage after AIS [58]. This risk is most pronounced in patients with >10 microbleeds, of whom 57% have experienced sICH. However, the impact of CMB on HT and clinical outcomes after EVT in AIS-LVO patients remains inconclusive. A subgroup analysis in the study by CHOI et al. showed that the presence of CMB has a greater impact on AIS-LVO patients, potentially increasing the risk of sICH and serving as an independent predictor of poor 3-month outcomes [52]. However, the study by Shi et al. suggested that a small number of CMBs do not increase the risk of HT and mortality after EVT, while the risk of HT in patients with extensive CMBs (≥ 5) requires further investigation [59].

5.3. Relationship between EPVS and HT after EVT

PVS are penetrating vessels surrounded by brain parenchyma. They are defined as round or tubular fluid-filled spaces that facilitate interstitial fluid drainage and the clearance of metabolites from the brain, with signal intensity similar to cerebrospinal fluid on all MRI sequences [60]. Typically, the diameter of PVS is less than 2 mm, while enlarged perivascular spaces (EPVS) can extend to a diameter range of 2–4 mm [61]. Initial pathological studies found that EPVS rarely cause damage to brain parenchyma and were therefore considered normal variants of limited clinical significance [62]. Recently, a study on elderly patients showed that EPVS are associated with an increased risk of stroke, dementia, and depression [27]. Furthermore, increasing evidence suggests that EPVS are more prevalent in stroke patients, and a high EPVS burden can predict poor outcomes after stroke [63–65]. However, there are few studies on the relationship between EPVS and HT after ischemic stroke. Whether EPVS play a role in HT remains uncertain. A study of 1,386 patients with AIS and TIA found that EPVS were associated with spontaneous intracranial hemorrhage during follow-up (mean follow-up period of 2.34 years) [66]. Evidence suggests that EPVS are more common in stroke patients and are associated with poor outcomes in AIS patients [67]. Increasing evidence indicates that EPVS are associated with intracerebral hemorrhage (ICH) [66, 68]. However, Song et al. found that EPVS are common in patients with ischemic stroke and are significantly correlated with other CSVD markers [69]. The presence or burden of EPVS is not associated with the risk of HT after ischemic stroke. In a population-based study, the presence of a large number of EPVS on MRI was significantly associated with an increased risk of subcortical infarction and CMBs, as well as more severe progression of WMH [70]. Whether EPVS increase the risk of HT after EVT and their role in HT remain uncertain. The sample sizes of the aforementioned studies are relatively small, and there are certain limitations in representing the stroke population. Therefore, the relationship between EPVS and HT after EVT requires further investigation.

5.4. Relationship between LI and HT after EVT

LI is defined as a round or oval small cavity with a diameter of approximately 3–15 mm, mostly caused by ischemic stroke, but can also result from the outcome of hemorrhagic stroke. It is commonly found in the basal ganglia region and the centrum semiovale. LI often presents without clinical symptoms. On MRI, LI shows signal intensity similar to cerebrospinal fluid on T1-weighted imaging (T1WI) and T2-weighted imaging (T2WI), with a central low signal and a peripheral high signal ring on fluid-attenuated inversion recovery (FLAIR) imaging. Studies on the relationship between LI and outcomes after EVT are extremely limited. An international multicenter large-scale randomized controlled trial indicated that lacunae have a predictive effect on sICH (OR=1.73) [71]. A study by Sillanpää et al. on the clinical outcomes of elderly AIS patients aged 60 and above who received EVT treatment showed that LI is correlated with poor prognosis after EVT [72]. That is, elderly AIS patients without LI lesions have a 3.7 times higher likelihood of achieving a good prognosis after EVT compared to those with LI lesions. However, Arba et al. argued that the presence and burden of LI are not associated with early or late clinical outcomes after EVT [73].

5.5. Relationship between total CSVD burden and HT after EVT

The academic community believes that CSVD is a dynamically progressive whole-brain disease, and it is difficult to comprehensively evaluate the impact on bodily functions using a single CSVD imaging marker. Therefore, the study of total CSVD burden has received increasing attention from the academic community. Studies have found that some pre-ischemic signs on cranial computed tomography (CT) in AIS

patients (tissue hypoattenuation, infarct size, swelling, and arterial hyperattenuation) and existing ischemic signs (old infarcts, WMHs, and atrophy) are associated with an increased risk of HT [71]. When multiple imaging markers are present simultaneously, the absolute risk of sICH increases. Wang et al. conducted a meta-analysis of 9,419 patients from 24 centers and found that CSVD is correlated with HT, sICH, and neurological outcomes at 3 months after intravenous thrombolysis [74]. Compared to patients without CSVD, the presence of CSVD is associated with an increased risk of HT (OR=1.81) and sICH (OR=2.42). Moreover, the heavier the total CSVD burden, the higher the risk of hemorrhage. SOHN et al. explored the association between CSVD burden and infarct growth rate in AIS-LVO patients receiving EVT treatment and conducted a retrospective analysis of 495 patients with anterior circulation stroke who received EVT [75]. After adjusting for confounding factors, a higher CSVD burden was significantly associated with a faster infarct growth rate. A high CSVD burden also independently predicted stroke progression and poor functional outcomes. Furthermore, the total CSVD burden reflects the decline in whole-brain reserve and compensatory capacity and may provide an overall reflection of the brain's functional reserve [76]. Poor brain reserve and compensatory capacity have adverse effects on stroke recovery [77]. Hooper et al. conducted a cohort analysis of AIS-LVO patients receiving EVT treatment and found that patients with severe CSVD burden had poorer functional outcomes and increased mortality at 90 days [10]. As an imaging marker of cerebral vascular reserve, CSVD burden, used alone or in combination with established quantitative imaging scores, can serve as an independent predictor of successful EVT. However, some studies have failed to find a correlation between the severity of CSVD and postoperative hemorrhagic transformation in AIS-LVO patients with poor EVT outcomes [78]. The impact of CSVD on HT after EVT in AIS-LVO patients may be influenced by multiple factors and exhibit individual differences. Therefore, the value of total CSVD burden in evaluating the prognosis of AIS-LVO patients still requires further verification.

6. Summary and outlook

In summary, assessing the severity of a single subtype of CSVD alone cannot accurately represent the overall brain damage caused by CSVD. The total CSVD burden score provides a more comprehensive and accurate evaluation of the impact of CSVD on the brain, offering a simple and practical approach. In clinical practice, it aids in further risk stratification for patients undergoing vascular recanalization therapy and assists in predicting HT and clinical outcomes. Although the relationship between CSVD and post-EVT HT in patients with AIS-LVO remains inconclusive, studies both domestically and internationally have indicated a certain correlation between the presence of severe WMH or CMB and HT following vascular recanalization therapy. Future research requires extensive multicenter prospective studies to validate the impact of CSVD on post-EVT HT in patients with AIS-LVO, providing a reference basis for clinical treatment decisions.

Funding

This study was supported by grants from the Taiyuan Bureau of Science and Technology, Science, Technology, and Innovation Program of National Regional Medical Center (202209) and the Taiyuan Bureau of Science and Technology, Science, Technology, and Innovation Program of National Regional Medical Center (202269).

Disclosure statement

The authors declare no conflict of interest.

References

[1] Paul S, Candelario-Jalil E, 2021, Emerging Neuroprotective Strategies for the Treatment of Ischemic Stroke: An Overview of Clinical and Preclinical Studies. Experimental Neurology, 2021(335): 113518.

[2] Report on Stroke Center in China Writing Group, 2024, Summary of the "China Stroke Center Report 2022". Chinese Journal of Cerebrovascular Diseases, 21(8): 565–576.

[3] Huo XC, Gao F, 2023, Chinese Guidelines for Endovascular Treatment of Acute Ischemic Stroke 2023. Chinese Stroke Journal, 18(6): 684–711.

[4] Nogueira RG, Jadhav AP, Haussen DC, et al., 2018, DAWN Trial Investigators. Thrombectomy 6 to 24 Hours after Stroke with a Mismatch between Deficit and Infarct. The New England Journal of Medicine, 378(1): 11–21.

[5] Albers GW, Marks MP, Kemp S, et al., 2018, DEFUSE 3 Investigators. Thrombectomy for Stroke at 6 to 16 Hours with Selection by Perfusion Imaging. The New England Journal of Medicine, 378(8): 708–718.

[6] Duarte AR, Vilela P, 2020, Acute Ischemic Stroke Hemorrhagic Transformation at Angiography before Mechanical Thrombectomy: A Neurointerventional Dilemma. Clinical Neuroradiology, 2020(30): 875–878.

[7] Li W, Xing X, Wen C, et al., 2023, Risk Factors and Functional Outcome were Associated with Hemorrhagic Transformation after Mechanical Thrombectomy for Acute Large Vessel Occlusion Stroke. Journal of Neurosurgical Sciences, 67(5): 585–590.

[8] Hu WL, Yang L, Li XT, et al., 2021, Chinese Expert Consensus on the Diagnosis and Treatment of Cerebral Small Vessel Diseases 2021. Chinese Stroke Journal, 16(7): 716–726.

[9] Pang J, Zhang JH, Jiang Y, 2019, Delayed Recanalization in Acute Ischemic Stroke Patients: Late is Better than Never? Journal of Cerebral Blood Flow & Metabolism, 39(12): 2536–2538.

[10] Hooper D, Nisar T, McCane D, et al., 2021, Severe Cerebral Small Vessel Disease Burden is Associated with Poor Outcomes after Endovascular Thrombectomy in Acute Ischemic Stroke with Large Vessel Occlusion. Cureus, 13(2): e13122.

[11] Duan YX, Zhao Y, Pei HL, et al., 2021, Cerebral Small Vessel Disease and Outcomes After Endovascular Thrombectomy in Patients with Acute Ischemic Stroke. International Journal of Cerebrovascular Diseases, 29(8): 602–607.

[12] von Kummer R, Broderick JP, Campbell BC, et al., 2015, The Heidelberg Bleeding Classification: Classification of Bleeding Events After Ischemic Stroke and Reperfusion Therapy. Stroke, 46(10): 2981–2986.

[13] Martins SO, Mont'Alverne F, Rebello LC, et al., 2020, Thrombectomy for Stroke in the Public Health Care System of Brazil. The New England Journal of Medicine, 382(24): 2316–2326.

[14] Zi W, Wang H, Yang D, et al., 2017, Clinical Effectiveness and Safety Outcomes of Endovascular Treatment for Acute Anterior Circulation Ischemic Stroke in China. Cerebrovascular Disease, 44(5–6): 248–258.

[15] vander Steen W, van der Ende NAM, Luijten SPR, et al., 2023, MR CLEAN-NO IV, MR CLEAN-MED, and CONTRAST investigators. Type of Intracranial Hemorrhage after Endovascular Stroke Treatment: Association with Functional Outcome. Journal of NeuroInterventional Surgery, 15(10): 971–976.

[16] Jovin TG, Nogueira RG, Lansberg MG, et al., 2022, Thrombectomy for Anterior Circulation Stroke beyond 6 h from Time last Known Well (AURORA): A Systematic Review and Individual Patient Data Meta-analysis. Lancet, 399(10321): 249–258.

[17] Neurology Branch of the Chinese Medical Association, Cerebrovascular Disease Group of the Neurology Branch of the Chinese Medical Association, 2019, Chinese Expert Consensus on the Diagnosis and Treatment of Hemorrhagic Transformation after Acute Cerebral Infarction 2019. Chinese Journal of Neurology, 52(4): 252–265.

[18] Jurcau A, Ardelean AI, 2022, Oxidative Stress in Ischemia/Reperfusion Injuries following Acute Ischemic Stroke. Biomedicines, 10(3): 574.

[19] Candelario-Jalil E, Dijkhuizen RM, Magnus T, 2022, Neuroinflammation, Stroke, Blood-Brain Barrier Dysfunction, and Imaging Modalities. Stroke, 53(5): 1473–1486.

[20] Zhang X, Xie Y, Wang H, et al., 2020, Symptomatic Intracranial Hemorrhage After Mechanical Thrombectomy in Chinese Ischemic Stroke Patients: The ASIAN Score. Stroke, 51(9): 2690–2696.

[21] Wardlaw JM, Smith C, Dichgans M, 2019, Small Vessel Disease: Mechanisms and Clinical Implications. Lancet Neurology, 18(7): 684–696.

[22] Wardlaw JM, Smith EE, Biessels GJ, et al., 2013, Standards for Reporting Vascular Changes on Neuroimaging (STRIVE v1). Neuroimaging Standards for Research into Small Vessel Disease and its Contribution to Ageing and neurodegeneration. Lancet Neurology, 12(8): 822–838.

[23] Duering M, Biessels GJ, Brodtmann A, et al., 2023, Neuroimaging Standards for Research into Small Vessel Disease-advances since 2013. Lancet Neurology, 22(7): 602–618.

[24] Gao Z, Wang W, Wang Z, et al., 2014, Cerebral Microbleeds are Associated with Deep White Matter Hyperintensities, but only in Hypertensive Patients. PLoS One, 9(3): e91637.

[25] Zhu YC, Tzourio C, Soumaré A, et al., 2010, Severity of Dilated Virchow-Robin Spaces is Associated with Age, Blood Pressure, and MRI Markers of Small Vessel Disease: A Population-based Study. Stroke, 41(11): 2483–2490.

[26] Staals J, Makin SD, Doubal FN, et al., 2014, Stroke Subtype, Vascular Risk Factors, and Total MRI Brain Small-vessel Disease Burden. Neurology, 83(14): 1228–1234.

[27] Debette S, Schilling S, Duperron MG, et al., 2019, Clinical Significance of Magnetic Resonance Imaging Markers of Vascular Brain Injury: A Systematic Review and Meta-analysis. JAMA Neurology, 76(1): 81–94.

[28] Yang YY, Wang YJ, Wang YL, 2019, Research Progress on the Relationship Between Cerebral Small Vessel Disease and Intracranial Large Artery Disease. Chinese Stroke Journal, 14(11): 1135–1139.

[29] Kwon HM, Lynn MJ, Turan TN, et al., 2016, SAMMPRIS Investigators. Frequency, Risk Factors, and Outcome of Coexistent Small Vessel Disease and Intracranial Arterial Stenosis: Results From the Stenting and Aggressive Medical Management for Preventing Recurrent Stroke in Intracranial Stenosis (SAMMPRIS) Trial. JAMA Neurology, 73(1): 36–42.

[30] Hori S, Hori E, Shibata T, et al., 2019, Correlation Between Cerebral Microbleeds and Vulnerable Plaque in Patients with Severe Carotid Artery Stenosis; Comparative Magnetic Resonance Imaging Study. Journal of Stroke and Cerebrovascular Diseases, 28(10): 104300.

[31] Lu T, Liang J, Wei N, et al., Extracranial Artery Stenosis is Associated with Total MRI Burden of Cerebral Small Vessel Disease in Ischemic Stroke Patients of Suspected Small or Large Artery Origins. Frontiers in Neurology, 2019(10): 243.

[32] Sun Z, Gao C, Gao D, et al., 2021, Reduction in Pericyte Coverage Leads to Blood-brain Barrier Dysfunction via Endothelial Transcytosis Following Chronic Cerebral Hypoperfusion. Fluids and Barriers of the CNS, 18(1): 21.

[33] Kerkhofs D, Wong SM, Zhang E, et al., 2021, Blood-brain Barrier Leakage at Baseline and Cognitive Decline in Cerebral Small Vessel Disease: A 2-Year Follow-Up Study. Geroscience, 43(4): 1643–1652.

[34] Huo YC, Li Q, Zhang WY, et al., 2019, Total Small Vessel Disease Burden Predicts Functional Outcome in

Patients with Acute Ischemic Stroke. Frontiers in Neurology, 2019(10): 808.

[35] Zhang J, Puri AS, Khan MA, et al., 2014, Leukoaraiosis Predicts a Poor 90-day Outcome after Endovascular Stroke Therapy. American Journal of Neuroradiology, 35(11): 2070–2075.

[36] Fladt J, Kronlage C, De Marchis GM, 2018, Cerebral White Matter Hyperintensities and Microbleeds in Acute Ischemic Stroke: Impact on Recanalization Therapies. A Review of the Literature. Neuroscience Letters, 2018(687): 55–64.

[37] Eilaghi A, Brooks J, d'Esterre C, et al., 2013, Reperfusion is a Stronger Predictor of Good Clinical Outcome Than Recanalization in Ischemic Stroke. Radiology, 269(1): 240–248.

[38] Kumral E, Güllüoğlu H, Alakbarova N, et al., 2015, Cognitive Decline in Patients with Leukoaraiosis within 5 Years after Initial Stroke. Journal of Stroke and Cerebrovascular Diseases, 24(10): 2338–2347.

[39] Deng G, Xiao J, Yu H, et al., 2022, Predictors of Futile Recanalization after Endovascular Treatment in Acute Ischemic Stroke: A Meta-analysis. Journal of NeuroInterventional Surgery, 14(9): 881–885.

[40] Demchuk AM, Khan F, Hill MD, et al., 2008, Importance of Leukoaraiosis on CT for Tissue Plasminogen Activator Decision Making: Evaluation of the NINDS rt-PA Stroke Study. Cerebrovascular Disease, 26(2): 120–125.

[41] Kongbunkiat K, Wilson D, Kasemsap N, et al., 2017, Leukoaraiosis, Intracerebral Hemorrhage, and Functional Outcomes after Thrombolysis for Acute Stroke. Neurology, 88(7): 638–645.

[42] Uniken Venema SM, Postma AA, van den Wijngaard IR, et al., 2021, White Matter Lesions and Outcomes after Endovascular Treatment for Acute Ischemic Stroke: Results from the MR CLEAN Registry. Stroke, 52(9): 2849–2857.

[43] Xu T, Wang Y, Yuan J, et al., 2021, The Burden of Small Vessel Disease and Outcomes of Mechanical Thrombectomy in Ischemic Stroke: A Systematic Review and Meta-analysis. Frontiers in Neurology, 2021(12): 602037.

[44] Neumann-Haefelin T, Hoelig S, Berkefeld J, et al., 2006, Leukoaraiosis is a Risk Factor for Symptomatic Intracerebral Hemorrhage after Thrombolysis for Acute Stroke. Stroke, 37(10): 2463–2466.

[45] Guo Y, Zhang S, Li M, et al., 2020, Leukoaraiosis and Early Neurological Outcomes after Mechanical Thrombectomy in Acute Ischemic Stroke. Journal of Neuroradiology, 47(6): 428–432.

[46] Huo L, Chen P, Wang Z, et al., The Impact of Leukoaraiosis Severity on the Outcomes of Mechanical Thrombectomy for Acute Ischemic Stroke: A Systematic Review and Meta-analysis. Journal of Neuroradiology, 268(11): 4108–4116.

[47] Henninger N, Lin E, Haussen DC, et al., 2013, Leukoaraiosis and Sex Predict the Hyperacute Ischemic Core Volume. Stroke, 44(1): 61–67.

[48] Xu H, Stamova B, Jickling G, et al., 2010, Distinctive RNA Expression Profiles in Blood Associated with White Matter Hyperintensities in the Brain. Stroke, 41(12): 2744–2749.

[49] Warach S, Latour LL, 2004, Evidence of Reperfusion Injury, Exacerbated by Thrombolytic Therapy, in Human Focal Brain Ischemia using a Novel Imaging Marker of Early Blood-brain Barrier Disruption. Stroke, 35(11 Suppl 1): 2659–2661.

[50] Chen B, Friedman B, Cheng Q, et al., 2009, Severe Blood-Brain Barrier Disruption and Surrounding Tissue Injury. Stroke, 40(12): e666–e674.

[51] Shi ZS, Loh Y, Liebeskind DS, et al., 2012, Leukoaraiosis Predicts Parenchymal Hematoma after Mechanical Thrombectomy in Acute Ischemic Stroke. Stroke, 43(7): 1806–1811.

[52] Choi KH, Kim JH, Kang KW, et al., 2019, Impact of Microbleeds on Outcomes Following Recanalization in Patients with Acute Ischemic Stroke. Stroke, 50(1): 127–134.

[53] Charidimou A, Kakar P, Fox Z, et al., 2013, Cerebral Microbleeds and Recurrent Stroke Risk: A Systematic Review and Meta-Analysis of Prospective Ischemic Stroke and Transient Ischemic Attack Cohorts. Stroke, 44(4): 995–1001.

[54] Graff-Radford J, Simino J, Kantarci K, et al., 2017, Neuroimaging Correlates of Cerebral Microbleeds: The ARIC Study (Atherosclerosis Risk in Communities). Stroke, 48(11): 2964–2972.

[55] Romero JR, Preis SR, Beiser A, et al., Risk Factors, Stroke Prevention Treatments, and Prevalence of Cerebral Microbleeds in the Framingham Heart Study. Stroke, 45(5): 1492–1494.

[56] Cordonnier C, Al-Shahi Salman R, Wardlaw J, 2007, Spontaneous Brain Microbleeds: Systematic Review, Subgroup Analyses, and Standards for Study Design and Reporting. Brain, 130(Pt 8): 1988–2003.

[57] Greenberg SM, Vernooij MW, Cordonnier C, et al., 2009, Cerebral microbleeds: A Guide to Detection and Interpretation. Lancet Neurology, 8(2): 165–174.

[58] Shoamanesh A, Kwok CS, Lim PA, et al., 2013, Risk of Postthrombolysis Intracranial Hemorrhage in Acute Stroke Patients with Cerebral Microbleeds: A Systematic Review and Meta-analysis. International Journal of Stroke, 8(5): 348–356.

[59] Shi ZS, Duckwiler GR, Jahan R, et al., 2016, Mechanical Thrombectomy for Acute Ischemic Stroke with Cerebral Microbleeds. Journal of NeuroInterventional Surgery, 8(6): 563–567.

[60] Brown R, Benveniste H, Black SE, et al., 2018, Understanding the Role of the Perivascular Space in Cerebral Small Vessel Disease. Cardiovascular Research, 114(11): 1462–1473.

[61] Chen X, Wang J, Shan Y, et al., 2019, Cerebral Small Vessel Disease: Neuroimaging Markers and Clinical Implications. Journal of Neurology, 266(10): 2347–2362.

[62] Jungreis CA, Kanal E, Hirsch WL, et al., 1988, Normal Perivascular Spaces Mimicking Lacunar Infarction: MR Imaging. Radiology, 169(1): 101–104.

[63] Wang X, Feng H, Wang Y, et al., 2019, Enlarged Perivascular Spaces and Cerebral Small Vessel Disease in Patients with Spontaneous Intracerebral Hemorrhage. Frontiers in Neurology, 14(10): 881.

[64] Liang Y, Chan YL, Deng M, et al., 2018, Enlarged Perivascular Spaces in the Centrum Semiovale are Associated with Poststroke Depression: A 3-month Prospective study. Journal of Affective Disorders, 2018(228): 166–172.

[65] Liang Y, Deng M, Chen YK, et al., 2017, Enlarged Perivascular Spaces are Associated with Health-related Quality of Life in Patients with Acute Ischemic Stroke. CNS Neuroscience & Therapeutics, 23(12): 973–979.

[66] Best JG, Barbato C, Ambler G, et al., 2020, Association of Enlarged Perivascular Spaces and Anticoagulant-related Intracranial Hemorrhage. Neurology, 95(16) :e2192–e2199.

[67] Lau KK, Li L, Lovelock CE, et al., 2017, Clinical Correlates, Ethnic Differences, and Prognostic Implications of Perivascular Spaces in Transient Ischemic Attack and Ischemic Stroke. Stroke, 48(6): 1470–1477.

[68] Charidimou A, Boulouis G, Pasi M, et al., 2017, MRI-visible Perivascular Spaces in Cerebral Amyloid Angiopathy and Hypertensive Arteriopathy. Neurology, 88(12): 1157–1164.

[69] Song Q, Cheng Y, Wang Y, et al., 2021, Enlarged Perivascular Spaces and Hemorrhagic Transformation after Acute Ischemic Stroke. Annals of Translational Medicine, 9(14): 1126.

[70] Ding J, Sigurðsson S, Jónsson PV, et al., 2017, Large Perivascular Spaces Visible on Magnetic Resonance Imaging, Progression of Cerebral Small Vessel Disease, and Risk of Dementia: The Age, Gene/Environment Susceptibility-Reykjavik Study. JAMA Neurology, 74(9): 1105–1112.

[71] ST-3 Collaborative Group, 2015, Association between Brain Imaging Signs, Early and Late Outcomes, and Response to Intravenous Alteplase after Acute Ischaemic Stroke in the Third International Stroke Trial (IST-3): Secondary Analysis of a Randomised Controlled Trial. Lancet Neurology, 14(5): 485–496.

[72] Sillanpää N, Pienimäki JP, Protto S, et al., 2018, Chronic Infarcts Predict Poor Clinical Outcomes in Mechanical Thrombectomy for Patients Aged Sixty and above. Journal of Stroke and Cerebrovascular Diseases, 27(7): 1789–1795.

[73] Arba F, Testa GD, Limbucci N, et al., 2019, Small Vessel Disease and Clinical Outcomes after Endovascular Treatment in Acute Ischemic Stroke. Neurological Sciences, 40(6): 1227–1235.

[74] Wang Y, Yan X, Zhan J, et al., 2021, Neuroimaging Markers of Cerebral Small Vessel Disease and their Impact on Hemorrhagic Transformation and Functional Outcomes after Intravenous Thrombolysis in Patients with Acute Ischemic Stroke: A Systematic Review and Meta-analysis. Frontiers in Aging Neuroscience, 2021(13): 692942.

[75] Sohn JH, Kim Y, Kim C, et al., 2023, Effect of Cerebral Small Vessel Disease Burden on Infarct Growth Rate and Stroke Outcomes in Large Vessel Occlusion Stroke Receiving Endovascular Treatment. Biomedicines, 11(11): 3102.

[76] Ter Telgte A, van Leijsen EMC, Wiegertjes K, et al., 2018, Cerebral Small Vessel Disease: From A Focal to a Global Perspective. Nature Reviews Neurology, 14(7): 387–398.

[77] Backhouse EV, McHutchison CA, et al., 2017, Early Life Risk Factors for Cerebrovascular Disease: A Systematic Review and Meta-analysis. Neurology, 88(10): 976–984.

[78] Wu X, Yan J, Ye H, et al., 2020, Pre-treatment Cerebral Microbleeds and Intracranial Hemorrhage in Patients with Ischemic Stroke Receiving Endovascular Therapy: A Systematic Review and Meta-analysis. Journal of Neurology, 267(5): 1227–1232.

Publisher's note

Bio-Byword Scientific Publishing remains neutral with regard to jurisdictional claims in published maps and institutional affiliations.

Clinical Neuroscience Research, 2026, Volume 4, Issue 3
https://bbwpublisher.com/journal/CNR
Online ISSN: 2981-8133
Print ISSN: 3083-4899

Development and Validation of a Machine Learning Model Integrating Stress Hyperglycemia for Predicting Early Neurological Deterioration in Acute Mild-to-Moderate Ischemic Stroke

Zhihui Chen, Zhixin Huang*, Kaili Huang

Department of Neurology, The Affiliated Guangdong Second Provincial General Hospital of Jinan University, Guangzhou 510317, Guangdong, China

***Corresponding author:** Zhixin Huang, huangjamie@126.com

Copyright: © 2026 Author(s). This is an open-access article distributed under the terms of the Creative Commons Attribution License (CC BY 4.0), permitting distribution and reproduction in any medium, provided the original work is cited.

Abstract: *Objective*: To investigate the predictive value of stress hyperglycemia and various machine learning models for early neurological deterioration (END) in patients with acute mild-to-moderate ischemic stroke, and to provide a quantitative reference for early clinical identification of high-risk patients and formulation of individualized intervention strategies. *Methods*: In this retrospective study, a total of 1,169 patients with acute mild-to-moderate ischemic stroke who met the inclusion criteria were enrolled from Guangdong Second Provincial General Hospital between January 2017 and June 2023. After applying the predefined exclusion criteria, 933 eligible subjects were finally included. *Results*: Among the 933 enrolled patients, the END incidence was 18.97%. Baseline data showed that the END group had higher body mass index (BMI), admission blood pressure, baseline National Institutes of Health Stroke Scale (NIHSS) score, admission blood glucose, glycated hemoglobin, and stress hyperglycemia ratio (SHR), while Alberta Stroke Program Early CT Score (ASPECTS) and Activities of Daily Living (ADL) scores were lower. Stress hyperglycemia was also more frequent in the END group. A history of hypertension was significantly more common in the END group, whereas the difference in diabetes mellitus history was not statistically significant ($P = 0.064$). Four machine learning prediction models were constructed based on the dataset divided at a 7:3 ratio. XGBoost may have potential utility for sensitivity-oriented screening, although the current findings do not demonstrate its overall superiority over the other models. *Conclusion*: Four machine learning models integrating stress hyperglycemia can effectively predict the risk of early neurological deterioration in patients with acute mild-to-moderate ischemic stroke. Among the evaluated models, XGBoost showed potential utility for sensitivity-oriented screening and may support risk stratification.

Keywords: Stress hyperglycemia; Acute mild-to-moderate ischemic stroke; Early neurological deterioration; Machine learning; Prediction model

Online publication: October 19, 2026

1. Introduction

Acute ischemic stroke is a leading cause of mortality and disability among Chinese residents, with mild-to-moderate ischemic stroke accounting for nearly half of all ischemic stroke cases [1]. Although the overall prognosis for mild-to-moderate ischemic stroke is generally considered favorable, 10% to 30% of patients nevertheless experience early neurological deterioration within days of onset, resulting in poor outcomes, disability, or death [2-5]. Early identification of high-risk individuals and timely clinical intervention are therefore critical to improving prognosis. Recent studies have shown that stress hyperglycemia is associated with poor prognosis in acute ischemic stroke [6-8]. Even in non-diabetic patients, elevated post-onset blood glucose levels increase the risk of neurological deterioration. However, few studies have integrated stress hyperglycemia into prediction models for END risk assessment in this population. Machine learning algorithms can efficiently integrate multidimensional clinical features, improving the accuracy and efficiency of disease risk prediction, and have been increasingly applied to cerebrovascular prognostic research. This study aimed to develop and validate machine learning prediction models integrating stress hyperglycemia indicators based on clinical data from patients with acute mild-to-moderate ischemic stroke, and to evaluate the predictive performance of different models to support early clinical identification of high-risk patients.

2. Materials and methods

2.1. Study design and population

A retrospective study design was adopted. A total of 1,169 patients with acute mild-to-moderate ischemic stroke who met the inclusion criteria were enrolled from a hospital between January 2017 and June 2023. The study protocol was approved by the institutional ethics committee (No. 2025-KY-KZ-310-01) and was conducted in accordance with the Declaration of Helsinki. According to the predefined exclusion criteria, 4 patients with a pre-stroke modified Rankin Scale (mRS) score >2, 28 with recent severe infection, 25 with thyroid disorders, 8 with hematological diseases (e.g., moderate-to-severe anemia), 12 with severe cardiac, hepatic, or renal dysfunction, 5 with malignant tumors, and 154 with incomplete clinical data were sequentially excluded. A total of 933 eligible subjects were finally included. Patients were divided into END and non-END groups according to the occurrence of END after onset, with 177 cases (18.97%) and 756 cases, respectively. The baseline characteristics of the two groups are summarized in **Table 1**.

The 933 included patients ranged in age from 18 to 99 years, with a mean of 59.28 ± 11.85 years and a median (interquartile range) of 58 (51–67) years. In the non-END group (n = 756), ages ranged from 18 to 99 years, with a mean of 59.60 ± 11.96 years and a median of 59 (51–68) years. In the END group (n = 177), ages ranged from 22 to 85 years, with a mean of 57.93 ± 11.34 years and a median of 56 (50–66) years. The difference in age between the two groups was not statistically significant ($P > 0.05$).

2.1.1. Inclusion criteria

(1) Diagnosis of acute mild-to-moderate ischemic stroke conforming to the relevant criteria in the Chinese Guidelines for the Diagnosis and Treatment of Acute Ischemic Stroke [9], confirmed by cranial CT or MRI;
(2) Admission within 72 hours of onset;
(3) National Institutes of Health Stroke Scale (NIHSS) score ≤15 after onset;
(4) Informed consent signed by the patient or family members.

2.1.2. Exclusion criteria

(1) Pre-stroke modified Rankin Scale (mRS) score ≥3, indicating pre-existing neurological deficits that could affect prognostic assessment;
(2) Severe infection within 4 weeks before onset or ongoing immunosuppressive therapy;
(3) Thyroid dysfunction, active bleeding, moderate-to-severe anemia, or other hematological diseases;
(4) Severe cardiac, hepatic, or renal insufficiency;
(5) Malignant tumors or other diseases with an expected survival of less than 1 year;
(6) Incomplete clinical or laboratory data precluding the required analyses.

2.2. Methods

2.2.1. Data collection

2.2.1.1. Baseline characteristic collection

A total of 62 research indicators were collected and categorized into 11 major dimensions, comprehensively covering baseline data, clinical assessments, laboratory tests, and personal history. The specific classifications were as follows:

(1) Demographic characteristics: age, sex, onset time, height, weight, and body mass index (BMI) (6 items).
(2) Vital signs and functional scores: admission systolic BP, admission diastolic blood pressure, and Activities of Daily Living (ADL) score (3 items).
(3) Past medical history: history of hypertension, diabetes mellitus, atrial fibrillation, prior cerebral infarction, and coronary heart disease (5 categorical items).
(4) Medication history: glucose-lowering medication use, antihypertensive medication use, anticoagulant use, antiplatelet use, and statin use (5 categorical items).
(5) Lifestyle habits: smoking history and drinking history (2 categorical items).
(6) Neurological and treatment-related characteristics: admission National Institutes of Health Stroke Scale (NIHSS) score, Alberta Stroke Program Early CT Score (ASPECTS), infarct location, Trial of Org 10172 in Acute Stroke Treatment (TOAST) classification, and treatment modality (5 items).
(7) Routine blood tests: white blood cell count, absolute neutrophil count, absolute monocyte count, absolute eosinophil count, absolute basophil count, absolute lymphocyte count, red blood cell count, hemoglobin, and platelet count (9 items).
(8) Thyroid function: thyroid-stimulating hormone, free T3 and free T4 (3 items).
(9) Coagulation function: prothrombin time, thrombin time, international normalized ratio, D-dimer, activated partial thromboplastin time, and fibrin degradation products (6 items).
(10) Blood biochemistry: total cholesterol, triglycerides, high-density lipoprotein cholesterol, low-density lipoprotein cholesterol, alanine aminotransferase, aspartate aminotransferase, homocysteine, C-reactive protein, creatinine, uric acid, admission blood glucose, creatine kinase, creatine kinase-MB, total protein, and albumin (15 items).
(11) Glucose metabolism indicators: glycated hemoglobin, stress hyperglycemia ratio, and stress hyperglycemia (3 items).

These indicators collectively cover patients' baseline personal information, past medical history and medication use, lifestyle habits, neurological functional status, core organ function, and various biochemical, coagulation, and metabolic laboratory tests. The comprehensive data dimensions and complete content provide sufficient support for subsequent statistical analyses.

2.2.1.2. Definition of key indicators

Stress hyperglycemia (SHG) was defined as follows: for patients without a history of diabetes mellitus, admission random blood glucose ≥7.8 mmol/L; for patients with a history of diabetes mellitus, blood glucose elevated by ≥2.5 mmol/L above the baseline level [10-14]. SHG was coded as 1 if present and 0 if absent.

The stress hyperglycemia ratio (SHR) was calculated using the following formula:

$$SHR=\frac{\text{Admission blood glucose}}{1.59\times \text{HbA1c-2.59}}$$

where SHR is calculated as admission random blood glucose divided by the estimated average glucose derived from glycated hemoglobin, i.e., 1.59 × HbA1c − 2.59. SHR was analyzed as a continuous indicator and was not used to define stress hyperglycemia. Stress hyperglycemia classification was based only on the admission glucose criteria described above. All laboratory tests were performed by professional technicians using standardized equipment. All clinical assessments were independently scored by two neurologists who had received unified training. In cases of disagreement, a third senior neurologist performed a review to confirm the final score, ensuring the accuracy and reliability of all data included in the study. All raw data were compiled by researchers, entered into a dedicated database, verified through double data entry, and locked for subsequent model development and validation analysis.

2.2.1.3. Outcome definition

Early neurological deterioration was defined as an increase in the total NIHSS score of ≥2 points from baseline, or an increase of ≥1 point in the motor item score, at any repeated NIHSS assessment within 72 hours of admission.

2.3. Data preprocessing and feature engineering

The collected raw data were cleaned and organized. Features with missing proportions exceeding 30% were excluded. The remaining missing data were imputed using multiple imputation methods. All continuous features were standardized to eliminate the influence of different units and scales on model training. Categorical features were transformed using one-hot encoding. All subjects were randomly divided into a training set and a test set at a 7:3 ratio. The training set was used for model training and feature selection, while the test set was used for independent performance evaluation. The least absolute shrinkage and selection operator (LASSO) algorithm was applied to the 62 original features in the training set to eliminate redundant features with low contribution, retain core features with high predictive value, reduce overfitting risk, and improve model efficiency.

2.4. Model construction and validation

Four machine learning prediction models were constructed: Logistic regression, support vector machine (SVM), random forest, and extreme gradient boosting (XGBoost). Model training and parameter tuning were completed on the training set, with Logistic regression serving as a baseline reference. The area under the receiver operating characteristic curve (AUC), accuracy, sensitivity, specificity, positive predictive value, and negative predictive value were used to evaluate model performance in both the training and test sets. Calibration curves combined with the Hosmer-Lemeshow test were used to assess calibration. Feature

importance analysis was performed to determine the contribution of each feature. Decision curve analysis (DCA) was used to calculate the net benefit of the models at various threshold probabilities.

2.5. Statistical analysis

All statistical analyses were performed using R language and Python software. Continuous variables following a normal distribution were expressed as mean ± standard deviation, and between-group comparisons using independent sample *t*-tests. Non-normally distributed variables were expressed as median (interquartile range), and between-group comparisons using rank-sum tests. Categorical variables were expressed as counts (percentages), and between-group comparisons using chi-square or Fisher's exact tests. All tests were two-sided, and $P < 0.05$ was considered statistically significant.

3. Results

3.1. Baseline characteristics of the study population

A total of 933 subjects were included, of whom 177 developed END (18.97%) and 756 did not. Compared with the non-END group, the END group had significantly higher height, weight, BMI, admission systolic and diastolic blood pressures, admission NIHSS score, white blood cell count, absolute neutrophil count, red blood cell count, hemoglobin, total protein, admission blood glucose, glycated hemoglobin, and SHR, while admission ADL score, ASPECTS, and absolute eosinophil count were significantly lower (all $P < 0.05$). A history of hypertension and antihypertensive medication use were more common in the END group, and stress hyperglycemia was also more frequent (all $P < 0.05$). The distributions of TOAST classification and treatment modality differed significantly between groups (both $P < 0.001$). By contrast, the difference in diabetes mellitus history did not reach statistical significance ($P = 0.064$), and infarct location also showed no significant between-group comparisons ($P = 0.075$). The remaining indicators showed no statistically significant differences ($P > 0.05$).

Table 1. Baseline characteristics of the study population

Variable	Total (n=933)	Non-END (n=756)	END (n=177)	Test Statistic	*P* value
Demographic characteristics					
Sex (male)	685 (73.4%)	556 (73.5%)	129 (72.9%)	0.03	0.857
Age(year)	58.00 (51.00, 67.00)	59.00 (51.00, 68.00)	56.00 (50.00, 66.00)	1.55	0.121
Onset time (h)	13.00 (4.00, 31.00)	13.00 (4.00, 30.65)	12.00 (4.50, 32.00)	-0.41	0.685
Height (m)	1.65 (1.60, 1.70)	1.65 (1.60, 1.70)	1.66 (1.60, 1.70)	-1.98	0.047
Weight (kg)	65.00 (60.00, 75.00)	65.00 (60.00, 74.00)	68.00 (62.00, 75.00)	-3.12	0.002
BMI (kg/m²)	24.22 (22.38, 26.57)	24.22 (22.09, 26.42)	24.49 (23.44, 27.34)	-2.99	0.003
Admission systolic BP(mmHg)	151.00 (135.00, 167.00)	149.50 (134.00, 165.00)	157.00 (139.00, 177.00)	-3.79	<0.001
Admission diastolic BP(mmHg)	89.00 (80.00, 100.00)	88.00 (79.00, 100.00)	92.00 (85.00, 102.00)	-3.27	0.001
Admission ADL score	75.00 (50.00, 95.00)	75.00 (55.00, 95.00)	55.00 (35.00, 85.00)	7.23	<0.001
History of hypertension	587 (62.9%)	464 (61.4%)	123 (69.5%)	4.05	0.044
History of diabetes mellitus	229 (24.5%)	176 (23.3%)	53 (29.9%)	3.44	0.064
History of atrial fibrillation	11 (1.2%)	9 (1.2%)	2 (1.1%)	—	>0.999

Variable	Total (n=933)	Non-END (n=756)	END (n=177)	Test Statistic	*P* value
Demographic characteristics					
Prior cerebral infarction	129 (13.8%)	107 (14.2%)	22 (12.4%)	0.36	0.550
History of coronary heart disease	54 (5.8%)	45 (6.0%)	9 (5.1%)	0.20	0.656
History of antihypertensive medication use	422 (45.2%)	327 (43.3%)	95 (53.7%)	6.28	0.012
History of glucose-lowering medication use	177 (19.0%)	137 (18.1%)	40 (22.6%)	1.87	0.171
History of anticoagulant use	7 (0.8%)	7 (0.9%)	0 (0.0%)	—	0.358
History of antiplatelet use	90 (9.6%)	74 (9.8%)	16 (9.0%)	0.09	0.761
History of statin use	87 (9.3%)	72 (9.5%)	15 (8.5%)	0.19	0.666
Smoking history	461 (49.4%)	374 (49.5%)	87 (49.2%)	0.01	0.939
Drinking history	272 (29.2%)	221 (29.2%)	51 (28.8%)	0.01	0.912
Admission NIHSS score	3.00 (2.00, 5.00)	3.00 (2.00, 4.00)	4.00 (2.00, 6.00)	-4.56	<0.001
ASPECTS	9.00 (8.00, 9.00)	9.00 (8.00, 9.00)	8.00 (7.00, 9.00)	8.07	<0.001
Infarct location				5.18	0.075
1	641 (68.7%)	531 (70.2%)	110 (62.1%)		
2	187 (20.0%)	147 (19.4%)	40 (22.6%)		
3	105 (11.3%)	78 (10.3%)	27 (15.3%)		
TOAST classification				—	<0.001
1	434 (46.5%)	321 (42.5%)	113 (63.8%)		
2	26 (2.8%)	21 (2.8%)	5 (2.8%)		
3	451 (48.3%)	394 (52.1%)	57 (32.2%)		
4	17 (1.8%)	15 (2.0%)	2 (1.1%)		
5	5 (0.5%)	5 (0.7%)	0 (0.0%)		
Treatment modality				59.57	<0.001
1	637 (68.3%)	539 (71.3%)	98 (55.4%)		
2	127 (13.6%)	75 (9.9%)	52 (29.4%)		
3	27 (2.9%)	19 (2.5%)	8 (4.5%)		
4	41 (4.4%)	29 (3.8%)	12 (6.8%)		
5	101 (10.8%)	94 (12.4%)	7 (4.0%)		
White blood cell count	8.04 (6.60, 9.65)	7.96 (6.60, 9.44)	8.54 (6.88, 10.09)	-2.09	0.036
Absolute neutrophil count	5.30 (4.10, 6.97)	5.26 (4.09, 6.75)	5.91 (4.45, 7.64)	-3.00	0.003
Absolute monocyte count	0.46 (0.36, 0.58)	0.46 (0.36, 0.58)	0.46 (0.36, 0.58)	0.04	0.965
Absolute eosinophil count	0.10 (0.04, 0.18)	0.10 (0.05, 0.20)	0.08 (0.04, 0.14)	2.66	0.008
Absolute basophil count	0.03 (0.02, 0.04)	0.03 (0.02, 0.04)	0.03 (0.02, 0.04)	-0.93	0.351
Absolute lymphocyte count	1.81 (1.34, 2.31)	1.82 (1.34, 2.33)	1.79 (1.34, 2.22)	1.26	0.209
Red blood cell count	4.79 (4.41, 5.18)	4.78 (4.40, 5.13)	4.94 (4.55, 5.29)	-2.89	0.004
Hemoglobin	144.00 (131.00, 155.00)	143.00 (131.00, 154.00)	148.00 (135.00, 157.00)	-2.19	0.029
Platelet count	238.00 (201.00, 281.00)	237.50 (200.00, 278.50)	243.00 (203.00, 288.00)	-1.33	0.185
Thyroid-stimulating hormone	1.39 (0.87, 2.06)	1.44 (0.87, 2.09)	1.26 (0.87, 1.74)	1.94	0.052
Free triiodothyronine	4.39 (3.97, 4.86)	4.39 (3.97, 4.83)	4.43 (3.97, 5.07)	-0.93	0.353
Free thyroxine	15.98 (14.60, 17.30)	15.95 (14.60, 17.21)	16.04 (14.64, 17.63)	-0.61	0.543
Prothrombin time	12.90 (12.40, 13.50)	12.90 (12.40, 13.50)	12.90 (12.60, 13.40)	-0.74	0.458

Variable	Total (n=933)	Non-END (n=756)	END (n=177)	Test Statistic	*P* value
Demographic characteristics					
Thrombin time	16.20 (15.60, 16.80)	16.20 (15.60, 16.80)	16.20 (15.60, 16.90)	-0.03	0.978
International normalized ratio	0.99 (0.94, 1.03)	0.99 (0.94, 1.04)	0.99 (0.95, 1.03)	-0.57	0.566
D-dimer	0.29 (0.22, 0.49)	0.29 (0.22, 0.49)	0.30 (0.22, 0.53)	-1.12	0.261
Activated partial thromboplastin time	35.70 (32.80, 38.50)	35.70 (32.80, 38.65)	35.40 (32.80, 37.50)	1.00	0.319
Fibrin degradation products (mg/L)	13.80 (12.00, 15.80)	13.80 (11.90, 15.85)	13.80 (12.10, 15.80)	-0.39	0.699
Total cholesterol	4.95 (4.28, 5.66)	4.95 (4.26, 5.62)	5.00 (4.40, 5.78)	-1.56	0.119
Triglycerides	1.44 (1.05, 2.17)	1.43 (1.03, 2.17)	1.48 (1.12, 2.22)	-1.70	0.089
High-density lipoprotein cholesterol	1.09 (0.92, 1.30)	1.09 (0.92, 1.30)	1.09 (0.92, 1.29)	0.18	0.859
Low-density lipoprotein cholesterol	2.98 (2.40, 3.62)	2.98 (2.40, 3.62)	2.98 (2.43, 3.72)	-0.43	0.667
Alanine aminotransferase	21.00 (16.00, 30.00)	21.00 (16.00, 29.00)	23.00 (17.00, 30.00)	-1.55	0.122
Aspartate aminotransferase	19.00 (16.00, 23.00)	19.00 (16.00, 23.00)	19.00 (16.00, 23.00)	0.46	0.645
Homocysteine	12.70 (10.30, 15.30)	12.80 (10.23, 15.30)	12.57 (10.30, 15.32)	0.25	0.799
C-reactive protein	2.80 (0.30, 6.74)	2.72 (0.20, 6.70)	3.30 (0.50, 7.00)	-1.10	0.269
Creatinine	83.00 (68.00, 101.00)	83.00 (68.10, 101.00)	81.00 (67.10, 99.00)	0.65	0.514
Uric acid	370.00 (304.00, 443.00)	371.00 (304.00, 440.50)	368.00 (301.00, 456.00)	-0.39	0.693
Admission blood glucose	6.38 (5.27, 8.59)	6.23 (5.21, 8.24)	7.06 (5.73, 10.02)	-4.06	<0.001
Creatine kinase	94.00 (68.00, 134.00)	94.00 (68.00, 132.00)	94.00 (74.00, 145.00)	-0.97	0.330
Creatine kinase-MB	8.20 (3.41, 12.30)	8.20 (3.50, 12.55)	7.20 (3.10, 10.90)	1.79	0.074
Total protein	71.80 (66.90, 76.90)	71.80 (66.60, 76.70)	72.90 (68.10, 78.60)	-2.70	0.007
Albumin	40.60 (37.60, 43.80)	40.60 (37.45, 43.60)	41.00 (38.50, 44.10)	-1.60	0.110
Glycated hemoglobin	6.00 (5.60, 6.80)	6.00 (5.60, 6.70)	6.10 (5.70, 7.30)	-2.03	0.042
Stress hyperglycemia	192 (20.6%)	145 (19.2%)	47 (26.6%)	4.77	0.029
Stress hyperglycemia ratio	0.91 (0.77, 1.09)	0.89 (0.76, 1.08)	0.96 (0.83, 1.13)	-3.05	0.002

[1]Median (Q1, Q3); n (%)

[2]Wilcoxon rank-sum test (standardized Z); Pearson's Chi-squared test; Fisher's exact test

3.2. Model performance comparison

All 933 subjects were randomly divided into a training set and a test set at a 7:3 ratio. The test set included 280 patients, of whom 53 were END-positive. Four machine learning models were constructed based on admission baseline indicators. ROC curves for each model in the test set are shown in **Figure 1**.

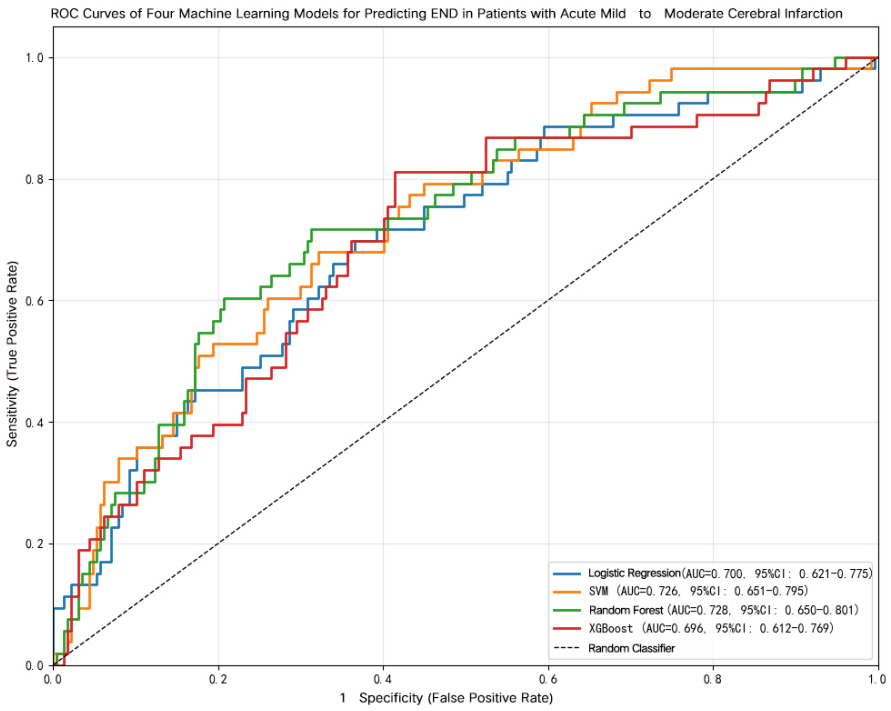

Figure 1. ROC curves of the four models on the test set

The AUC values, in descending order, were: random forest, 0.728 (95% CI: 0.650–0.801); SVM, 0.726 (95% CI: 0.651–0.795); Logistic regression, 0.700 (95% CI: 0.621–0.775); and XGBoost, 0.696 (95% CI: 0.612–0.769). All four models demonstrated moderate predictive performance for END.

Using the XGBoost model as the reference for the DeLong test, pairwise comparisons of AUC between the XGBoost model and the Logistic regression, SVM, and random forest models showed no statistically significant differences ($P = 0.9105$, 0.3079, and 0.1422, respectively; all $P > 0.05$).

After determining the optimal cutoff values based on the Youden index, sensitivity, specificity, accuracy, positive predictive value, negative predictive value, and F1 score were calculated. The random forest model achieved the highest F1 score (0.469) and the highest specificity (0.687), with a sensitivity of 0.717 and an accuracy of 0.693. The XGBoost model demonstrated the highest sensitivity (0.811), making it potentially useful for initial screening of high-risk populations, although its specificity was relatively low (0.586). The Logistic regression model had a specificity of 0.634, while the SVM model exhibited relatively balanced performance across the evaluated indicators. The negative predictive values of all four models exceeded 0.90, indicating potential clinical utility for excluding low-risk patients.

3.3. Feature importance analysis based on SHapley Additive exPlanations (SHAP)

To explore the contribution of each clinical indicator to the prediction of early neurological deterioration (END) in patients with acute mild-to-moderate ischemic stroke, this study applied the SHapley Additive exPlanations (SHAP) algorithm to the XGBoost prediction model for feature analysis, quantifying the contribution of each variable to the risk of END occurrence. The features, ranked in descending order by mean absolute SHAP value, were: ASPECTS (0.5806), BMI (0.3898), admission diastolic blood pressure (0.3509), admission systolic BP (0.3287), admission NIHSS score (0.3247), age (0.2900), stress hyperglycemia ratio (SHR, 0.2608), onset time (0.2081), admission blood glucose (0.1899), and sex (0.0314), as shown in **Figure 2**.

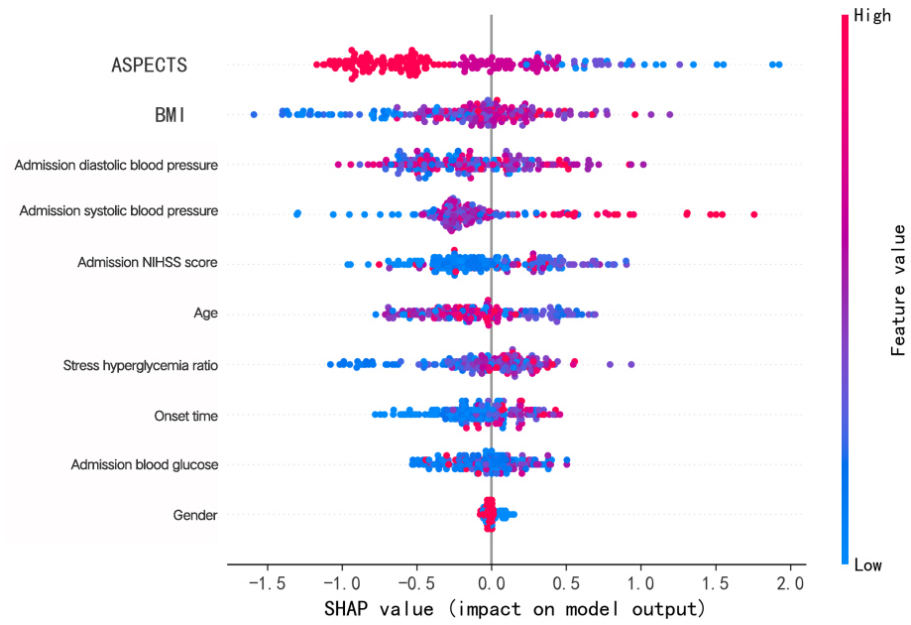

Figure 2. SHAP summary plot of the XGBoost model

As shown in **Figure 2**, the magnitude of predictive contribution of each feature and the direction of influence of feature values on the prediction results can be observed. Among all features, ASPECTS was the strongest predictor of END risk, with lower scores indicating larger infarct extent and higher risk of END. BMI, admission blood pressure, and baseline neurological deficit severity (admission NIHSS score) were also key predictors of END. SHAP values demonstrated that SHR ranked seventh with respect to predictive contribution. The predominance of positive SHAP values indicated that higher SHR was linked to increased predicted probability of END within the model. It should be noted that SHAP quantifies feature-level contribution to model-based prediction, which does not constitute evidence for SHR as an independent risk factor derived from conventional regression.

The nonlinear positive correlation between SHR and the predicted probability is shown in **Figure 3**.

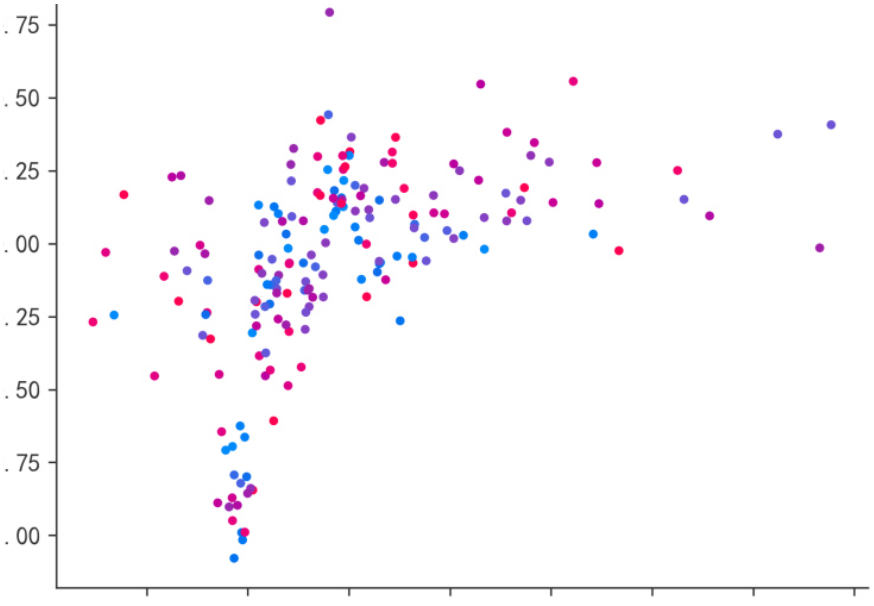

Figure 3. SHAP dependence plot for SHR

As shown in **Figure 3**, the SHAP dependence plot for the stress hyperglycemia ratio intuitively reflects the nonlinear relationship between SHR and the predicted risk of END: as SHR values increased, the corresponding SHAP values showed an overall upward trend, and the predicted probability of END gradually increased, suggesting that stress hyperglycemia may contribute to END risk prediction. Sex had the lowest predictive contribution, with a mean absolute SHAP value of only 0.0314, indicating a relatively weak impact on model predictive performance.

3.4. Decision curve analysis

In this study, Logistic regression and XGBoost prediction models were selected for decision curve analysis, with the risk threshold range limited to the clinically common interval of 0 to 0.6 in order to evaluate the clinical net benefit of the two models in screening high-risk populations for early neurological deterioration (END) in patients with acute mild-to-moderate ischemic stroke.

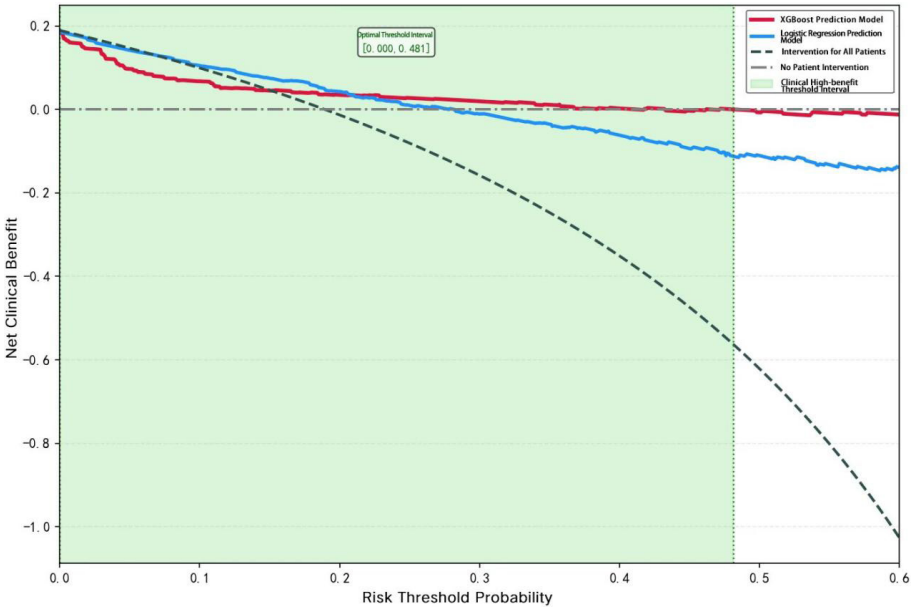

Figure 4. Decision curve analysis

As shown in **Figure 4**, the net benefit curves did not remain above the “treat all” and “treat none” reference strategies across the entire 0 to 0.6 threshold range. The Logistic regression curve approached and crossed the zero-net-benefit line at approximately 0.27, whereas the XGBoost curve retained positive net benefit over a wider interval, extending to approximately 0.481, which corresponds to the threshold interval marked in **Figure 4**. Beyond these ranges, net benefit declined, and neither model maintained a positive advantage throughout the full evaluated interval. Therefore, the DCA findings support potential clinical utility within selected threshold ranges rather than across all thresholds from 0 to 0.6. DeLong comparisons among the four models showed no statistically significant differences in AUC (all $P > 0.05$). The negative predictive values of both Logistic regression and XGBoost exceeded 0.90, suggesting potential value for excluding low-risk END patients.

4. Discussion

4.1. Analysis of baseline risk factors for END in patients with acute mild-to-moderate ischemic stroke

A total of 933 patients were included, with an END incidence of 18.97%, consistent with the 17%–20% range reported in recent studies. Between-group comparisons using showed that the END group had significantly higher BMI, admission blood pressure, admission NIHSS score, admission blood glucose, glycated hemoglobin, white blood cell count, neutrophil count, red blood cell count, hemoglobin, total protein, and SHR, and significantly lower ASPECTS, ADL score, and eosinophil count. Height and weight were also higher in the END group, while stress hyperglycemia was more frequent. A history of hypertension and antihypertensive medication use were significantly more common in the END group. In contrast, diabetes mellitus history was numerically more frequent but did not reach statistical significance ($P = 0.064$), and infarct location did not differ significantly between groups ($P = 0.075$). TOAST classification and treatment modality showed significant differences in distribution rather than ordinal " higher" or "lower" scores.

Obesity and hypertension are classic modifiable risk factors for stroke. Elevated BMI may aggravate vascular endothelial dysfunction and low-grade systemic inflammation, while abnormally elevated admission blood pressure may contribute to hemodynamic instability around the infarct and worsen ischemic penumbral injury. Higher baseline NIHSS and lower ASPECTS indicate greater initial neurological deficit and ischemic burden. Elevated admission blood glucose, glycated hemoglobin, stress hyperglycemia, and SHR in the END group suggest that acute metabolic stress is closely associated with early neurological worsening. Differences in leukocyte and neutrophil counts are also consistent with an inflammatory contribution. The marked between-group comparisons in treatment modality ($P < 0.001$) requires particular caution because treatment selection is related to baseline severity, onset-to-admission time, imaging findings, and treatment eligibility and may itself influence the early neurological course. Treatment modality was included among the candidate variables during feature selection, but residual confounding by indication cannot be fully excluded in this retrospective analysis. Future external validation should further stratify or adjust for treatment categories when assessing END risk.

4.2. Predictive performance of the four machine learning models for END in patients with acute mild-to-moderate ischemic stroke

Four models (Logistic regression, SVM, random forest, and XGBoost) were constructed based on admission baseline indicators. All achieved AUC values between 0.696 and 0.728, indicating moderate predictive performance. DeLong tests showed no significant differences in AUC among the four models, suggesting comparable overall predictive ability.

The Logistic regression model, as a classical approach, allows intuitive access to regression coefficients for each variable and offers strong interpretability. Its specificity was 0.634. The SVM model demonstrated balanced and stable performance with good generalization under small-sample, high-dimensional data. The random forest model achieved both the highest F1 score (0.469) and the highest specificity (0.687), supporting a comparatively balanced trade-off between sensitivity and specificity. The XGBoost model had the highest sensitivity (0.811), which may be useful when minimizing missed high-risk patients is prioritized, although its lower specificity results in more false-positive classifications. Traditional regression models can be presented as visualized nomograms, whereas ensemble machine learning models have advantages in handling nonlinear features and variable interactions. The negative predictive values of all four models

exceeded 0.90, supporting their potential value for identifying patients at relatively low predicted risk. The absence of statistically significant AUC differences in the DeLong comparisons indicates that these performance differences should be interpreted as model-specific operating characteristics rather than evidence of overall superiority.

4.3. Feature importance based on SHAP algorithm and the predictive value of stress hyperglycemia

The SHAP algorithm was applied to the XGBoost model to quantify feature contributions, addressing the interpretability limitation of black-box models. The top five predictors were ASPECTS, BMI, admission diastolic blood pressure, admission systolic BP, and baseline NIHSS. The stress hyperglycemia ratio ranked seventh and was the primary predictor of interest in this study.

ASPECTS is a well-established quantitative CT-based indicator of early ischemic burden that allows rapid assessment of the extent of early ischemic brain tissue injury. Lower scores indicate larger infarct extent and higher risk of penumbral injury, consistent with its highest predictive weight in this study. Elevated BMI and abnormal admission blood pressure increase END risk through vascular endothelial injury, chronic inflammation, and hemodynamic disturbances, corroborating the baseline differences observed. Baseline NIHSS directly reflects initial deficit severity; greater deficits are associated with higher rates of thrombus extension, cerebral edema, and hemorrhagic transformation.

This study innovatively incorporated the stress hyperglycemia ratio as a predictive feature. The SHAP dependence plot confirmed a significant nonlinear positive correlation with END risk. As SHR increased, oxidative stress, blood-brain barrier disruption, and systemic inflammation progressively intensified, elevating END risk. Compared with a single blood glucose measurement, SHR better reflects the overall post-stroke stress metabolic state and avoids prediction bias from isolated glucose fluctuations. Sex had the lowest predictive contribution, suggesting that after adjustment for confounders, sex was not an independent predictor. The SHAP analysis not only clarified the predictive weights and directions of risk factors but also validated the clinical rationale for incorporating stress hyperglycemia, providing a theoretical basis for future mechanistic studies and model optimization.

4.4. Clinical decision-making value of the two prediction models: insights from decision curve analysis

Decision curve analysis was performed within the 0 to 0.6 risk threshold range to evaluate the net clinical benefit of the Logistic regression and XGBoost models. The clinical utility was threshold-dependent rather than uniform across the entire interval. The Logistic regression curve declined to approximately the zero-net-benefit line at a threshold of about 0.27, whereas the XGBoost curve remained positive over a wider portion of the range and extended to approximately 0.481, consistent with the interval annotated in **Figure 4**. Beyond these points, the corresponding net benefit decreased, so neither model should be interpreted as providing positive net benefit throughout the full 0 to 0.6 range.

These DCA findings suggest that XGBoost may retain clinical net benefit over a broader portion of the evaluated threshold range than Logistic regression, but they do not support a claim of uniformly higher net benefit or superiority across all thresholds. This distinction is consistent with the DeLong analysis, which detected no statistically significant AUC differences among the four models. In practice, model choice should therefore depend on the intended operating point: XGBoost may be useful when sensitivity is prioritized,

whereas the comparatively simple Logistic regression model may remain attractive when interpretability is important. Both models had negative predictive values above 0.90, indicating potential value for identifying patients at relatively low predicted risk. The DCA results support further evaluation of these models as threshold-dependent decision-support tools; prospective external validation is still required before broad clinical implementation.

5. Conclusion

In summary, the risk of END in patients with acute mild-to-moderate ischemic stroke can be predicted using machine learning models constructed from routine admission baseline characteristics. All four models demonstrated moderate discriminative performance, with no statistically significant AUC differences detected by the DeLong test. XGBoost showed the highest sensitivity and retained positive net benefit over a broader portion of the evaluated DCA threshold range, extending to approximately 0.481, whereas this benefit did not persist across the entire 0 to 0.6 interval. ASPECTS showed the highest SHAP importance for END prediction, while the stress hyperglycemia ratio exhibited a nonlinear positive association with the model-predicted risk of END and contributed meaningfully to prediction. These findings support the potential use of machine learning for risk stratification, while external prospective validation and careful consideration of treatment-related confounding are needed before wider clinical application.

Disclosure statement

The authors declare no conflict of interest.

References

[1] Lin L, Jiang LJ, Wang XG, et al., 2023, Effect of Leukoaraiosis on Intravenous Thrombolysis Efficacy in Acute Mild-to-moderate Cerebral Infarction. Cardiovascular and Cerebrovascular Disease Prevention and Treatment, 23(7): 32-36.

[2] Yang W, Kim KY, Lee JK, et al., 2026, Abstract DP329: Impact of White Matter Hyperintensity Burden on Response to Induced Hypertension Therapy in Small Vessel Occlusion Stroke with Early Neurological Deterioration, Stroke, 57(Suppl_1).

[3] Khasiyev F, Pandit M, Jumani S, et al., 2026, Abstract WP118: Exploring Intracranial Arterial Variants and Early Neurological Deterioration in Lacunar Stroke, Stroke, 57(Suppl_1).

[4] Wang N, Lin H, Deng B, et al., 2026, Comparative the Predictive Value of Neutrophil-to-HDL Ratio and Monocyte-to-HDL Ratio for Early Neurological Deterioration in Acute Ischemic Stroke Patients Following Intravenous Thrombolysis. Neurological Sciences, 47(5):431.

[5] Zhong X, Yang J, Xu R, et al., 2026, Anticoagulant or Antithrombotic Therapy after Early Neurological Deterioration in Patients with Branch Atheromatous Disease Receiving Dual Antiplatelet Therapy, International Journal of Clinical Practice, 8636214, 7 pages.

[6] Zhong X, Chen Z, Cao T, et al., 2026, Development and Validation of a Nomogram to Predict Early Neurological Deterioration in Patients with Acute Ischemic Stroke and Type 2 Diabetes Mellitus: the Pivotal Role of Glycemic Variability and Thrombo-inflammation, Neurological Sciences, 47(6):544.

[7] Font MN, García-Sánchez SM, Catalan Stroke Code and Reperfusion Consortium, 2026, Impact of Arterial Occlusion Location on Early Neurological Deterioration in Patients with Minor Stroke Treated with Intravenous Thrombolysis, The MINORCAT-END Study. Neurological Sciences, 47(1): 12.

[8] Xu S, Jiang Z, Zhou Y, et al., 2026, The Effect of Indobufen and Aspirin on Platelet Function in Acute Ischemic Stroke Patients with Early Neurological Deterioration, European Journal of Pharmacology, 1011: 178439.

[9] Neurology Branch and Cerebrovascular Diseases Group of the Chinese Medical Association, 2026, Chinese Guidelines for the Diagnosis and Treatment of Acute Ischemic Stroke 2023: Stroke Recognition, Management, and Transfer. Practical Journal of Cardiac Cerebral Pneumal and Vascular Disease, 34(4): 24.

[10] Writing Group of the Clinical Guidelines for the Prevention and Treatment of Type 2 Diabetes Mellitus in the Elderly in China, Geriatric Endocrinology and Metabolism Branch of the Chinese Geriatrics Society, Geriatric Endocrinology and Metabolism Branch of the Chinese Association of Geriatric Research, et al., 2026, Clinical Guidelines for the Prevention and Treatment of Type 2 Diabetes Mellitus in the Elderly in China (2026 edition) Released in Beijing, Diabetes Friend, (5): 7.

[11] Huang S, Zou DJ., 2025, Treatment of Type 2 Diabetes Mellitus: Should Metformin Step Down to Second-line? Reflections on the Glucose-lowering Pathway of the Chinese Guidelines for Diabetes Prevention and Treatment (2024 edition). Chinese Journal of Diabetes Mellitus, 17(10): 1261-1266.

[12] Zhou XY, 2025, Dietary Habits Survey of Patients with Type 2 Diabetes Mellitus Complicated with Cardiovascular Disease: Based on the Chinese Guidelines for Prevention and Treatment of Type 2 Diabetes (2020 edition), Xi'an Medical University.

[13] Khasiyev F, Pandit M, Jumani S, et al., 2026, Abstract DP320: Elevated Neutrophil-to-lymphocyte Ratio Does Not Predict Early Neurological Deterioration in Patients with Acute Lacunar Infarct. Stroke, 57(Suppl_1).

[14] Stutz A, Borei K, Pan A, et al., 2026, Abstract DP382: Increased Blood Pressure Variability over the First 24 Hours of Admission is Independently Associated with Neurological Deterioration among Patients with Acute Ischemic Stroke. Stroke, 57(Suppl_1).

Publisher's note

Bio-Byword Scientific Publishing remains neutral with regard to jurisdictional claims in published maps and institutional affiliations.

Clinical Neuroscience Research, 2026, Volume 4, Issue 3
https://bbwpublisher.com/journal/CNR
Online ISSN: 2981-8133
Print ISSN: 3083-4899

Combined Laminotomy and Spinal Endoscopic-Assisted Decompression for Gouty Tophi Involving the Lumbar Epidural Space and Multi-level Paravertebral Regions: A Case Report

Yaolei Chen[1], Shaojun Kang[1], Zhi Hou[2], Chenglong Luo[3], Xin He[4]*

[1]Department of Neurosurgery, Chonggang General Hospital, Chongqing 400000, China
[2]Department of Neurosurgery, The Second Affiliated Hospital of Army Medical University, Chongqing 400000, China
[3]Department of Radiology, Chonggang General Hospital, Chongqing 400000, China
[4]Department of Pediatrics, Chonggang General Hospital, Chongqing 400000, China

***Corresponding author:** Xin He, 327368246@qq.com

Copyright: © 2026 Author(s). This is an open-access article distributed under the terms of the Creative Commons Attribution License (CC BY 4.0), permitting distribution and reproduction in any medium, provided the original work is cited.

Abstract: Tophaceous gout involving the spinal canal is a rare but potentially debilitating condition. The study reports the case of a 41-year-old man with chronic gout who developed severe lumbar radiculopathy from extensive intraspinal epidural and multi-level paravertebral tophaceous deposits. The patient was treated with a combined procedure involving open L3–4 laminotomy and spinal endoscopic-assisted decompression to remove both intraspinal and extraspinal tophi. This strategy enabled thorough neural decompression and tophus excision while minimizing tissue disruption. Postoperatively, the patient's neurological symptoms improved significantly. The study examines the technical nuances and benefits of integrating open and endoscopic methods for managing complex spinal gout, particularly in cases where the lesion involves multiple segments of the paravertebral region.

Keywords: Gouty tophus; Spinal gout; Lumbar posterior elements; Spinal endoscopic-assisted; Laminotomy

Online publication: October 19, 2026

1. Introduction

Gout is a metabolic disorder characterized by the deposition of monosodium urate crystals in joints and periarticular soft tissues. Spinal involvement occurs only rarely, with fewer than 200 cases reported in the literature [1]. Clinical manifestations range from axial back pain to radiculopathy or myelopathy resulting from nerve root or spinal cord compression [2–3]. Diagnosis is often delayed due to nonspecific imaging features and a low index of clinical suspicion [4]. The study presents a case of gouty tophi in the L3/L4 spinal canal epidural space and paravertebral regions from L1 to L3, which was successfully treated with a combined surgical approach.

2. Case presentation

A 41-year-old male presented with a one-year history of low back pain and right lower extremity radiculopathy, which had acutely worsened over the preceding week and was accompanied by neurogenic claudication. He also reported a ten-year history of gouty arthritis, with a peak serum uric acid level of 950 μmol/L (reference range 202–420 μmol/L), managed intermittently with colchicine, febuxostat, celecoxib, and dexamethasone. Physical examination revealed multiple gouty tophi in the hands, knees, and toes, resulting in joint deformities, and right lower extremity motor weakness graded at 3/5.

Imaging studies included:

X-ray: patchy high-density shadow at L3–4 (**Figure 1**).

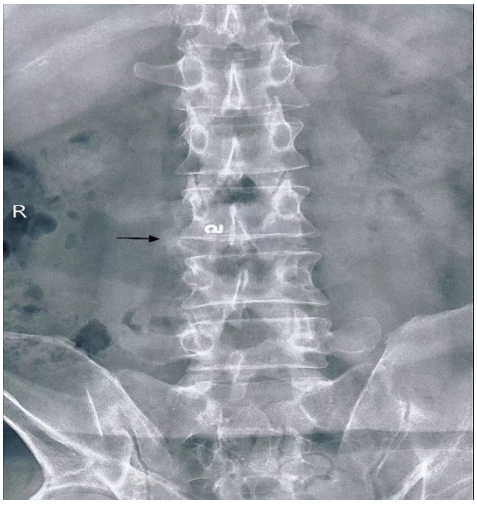

Figure 1. X-ray: Flocculent paraspinal opacity at L3/4

CT: Erosive changes in L1–4 vertebral appendages and paravertebral soft tissues, with a mass in the L3–4 spinal canal causing stenosis (**Figure 2**).

MRI: Intraspinal epidural and multi-level paravertebral tophaceous deposits compressing the thecal sac and nerve roots at L3–4 (**Figure 3**).

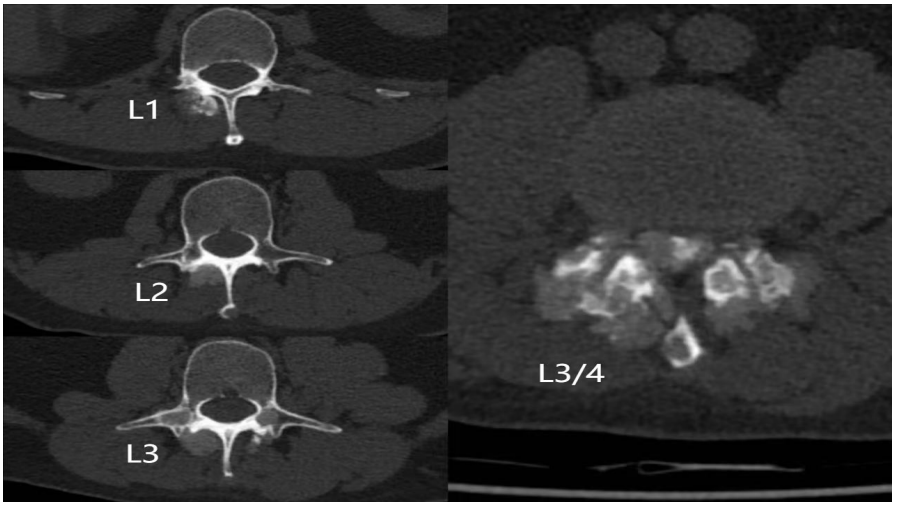

Figure 2. CT: Multiple slightly hyperdense lesions external to L1-L3 laminae and at L3/4 (intraspinal & extraspinal), accompanied by significant bony destruction

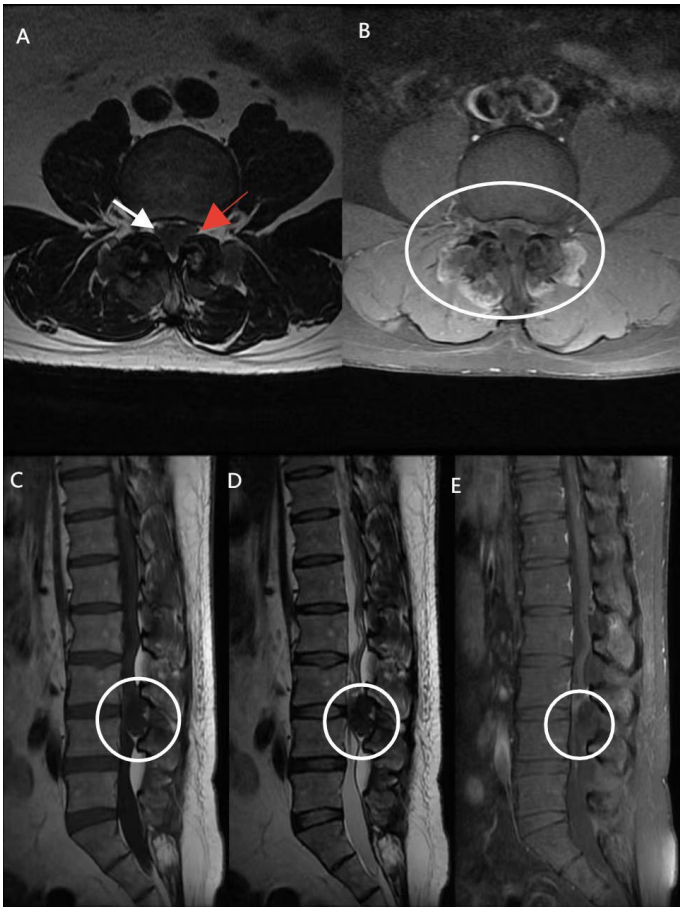

Figure 3. (A) Axial T2-weighted MRI: Red arrow, normal left nerve root; white arrow, compressed and deformed right nerve root. (B) Contrast-enhanced axial T1-weighted MRI: A slightly hyperintense, heterogeneous space-occupying lesion at L3/4, with both intraspinal and extraspinal components. (C) Sagittal T1-weighted MRI: A hypointense intraspinal space-occupying lesion at L3/4 with significant thecal sac compression. (D) Sagittal T2-weighted MRI: Persistent hypointense space-occupying lesion. (E) Contrast-enhanced sagittal T1-weighted MRI: Non-enhancing intraspinal space-occupying lesion

3. Surgical management

The patient underwent a two-part procedure:

3.1. Open L3–4 laminotomy

Extensive chalky white deposits were found eroding the lamina and compressing the thecal sac and right L4 nerve root. These were meticulously removed (**Figure 4**).

3.2. Spinal endoscopic-assisted decompression

To prevent further destruction of the vertebral lamina, under endoscopic guidance, paravertebral tophi at L1 to L3 were removed through a minimally invasive approach (**Figure 5**).

No spinal instrumentation was required as the facet joints were preserved.

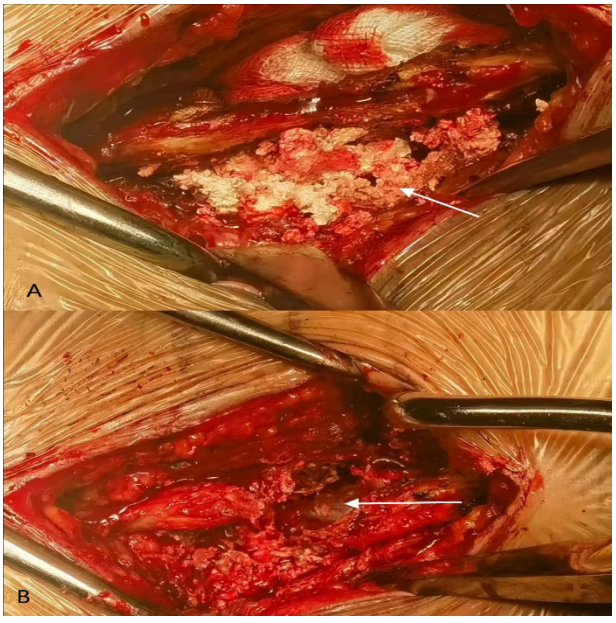

Figure 4. (A) Chalky, paste-like gouty tophus exterior to the vertebral lamina. (B) Gouty tophus eroding the right lamina with intracanalicular extension and significant thecal sac compression (arrow points to thecal sac post-removal)

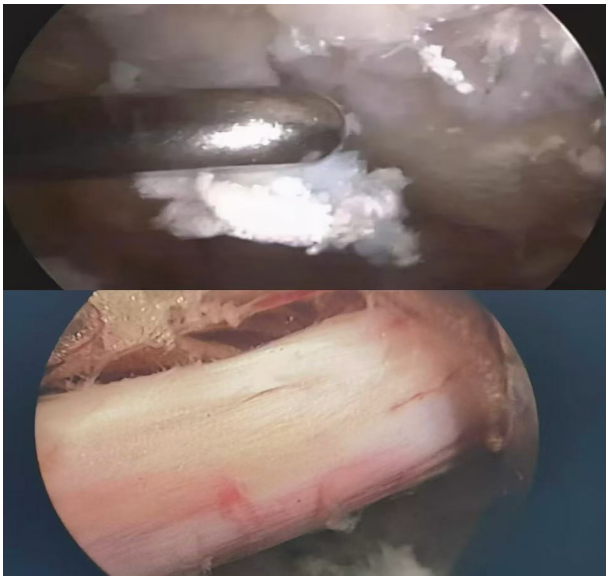

Figure 5. Endoscopic view of gouty tophi and an exposed nerve root

4. Outcome

Postoperatively, the patient's radiculopathy resolved, and motor strength improved significantly. Histopathological analysis confirmed the diagnosis of tophaceous gout (**Figure 6**). No recurrence was observed at the one-year follow-up.

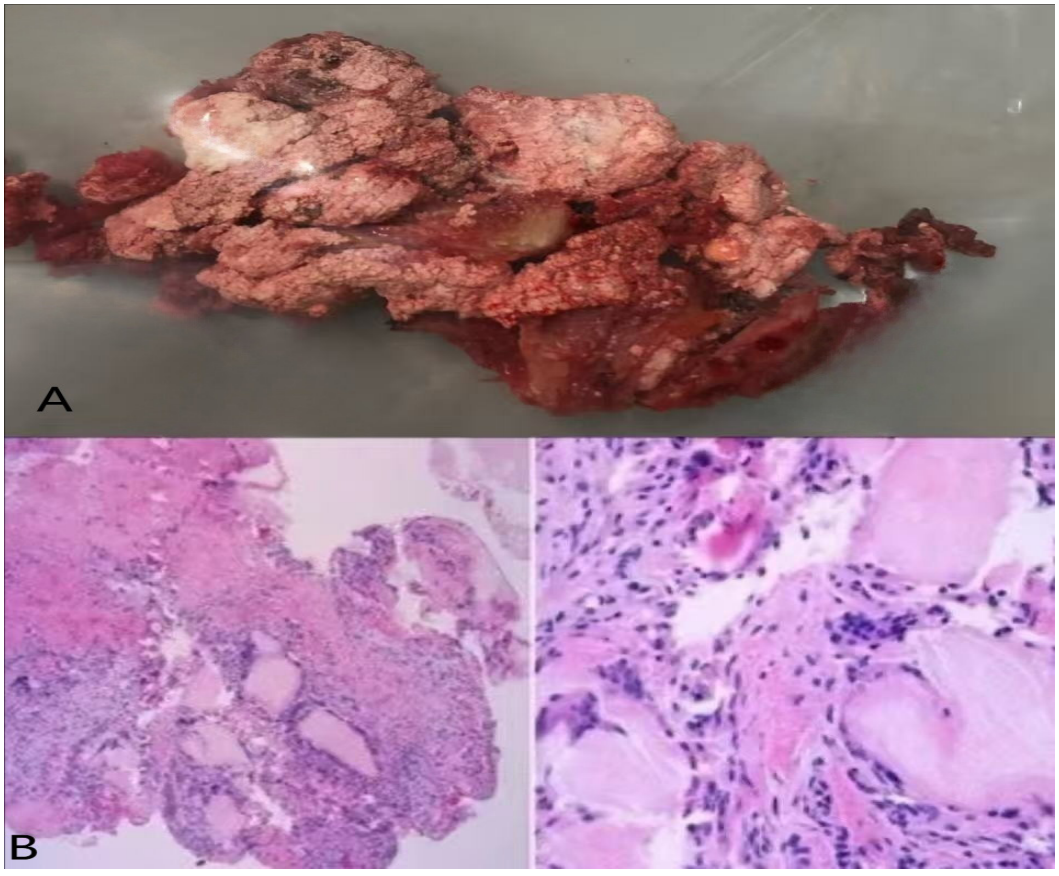

Figure 6. (A) Chalky, paste-like gouty tophus. (B) The pathological findings confirmed the lesion as a gouty tophus

5. Discussion

Spinal gout is often misdiagnosed as infection, tumor, or degenerative disease [5–6]. Imaging findings are nonspecific, and serum uric acid may be normal in up to 30% of cases [7]. Definitive diagnosis requires histopathological confirmation [8].

The case highlights several key points:

Combined Surgical Approach: The use of open laminotomy for direct intraspinal epidural decompression and endoscopic techniques for multi-level paravertebral tophi represents a novel and tailored strategy [9–10]. This combination minimizes soft tissue damage, reduces postoperative pain, and accelerates recovery compared to extensive open procedures alone [11].

Technical Considerations: Endoscopic visualization allows for precise identification and removal of paravertebral deposits without extensive muscular dissection [12–13]. Open surgery remains essential for safe and complete decompression of significant intraspinal lesions, especially those causing severe canal stenosis and nerve compression [14].

Literature Context: Previous reports have primarily described open laminectomy or, more recently, fully endoscopic surgery for spinal gout [15–18]. This integrated approach addresses the challenge of disease involving both the spinal canal and multiple paravertebral levels, which is technically difficult to manage with a single technique. This is supported by growing evidence for the efficacy of minimally invasive spine techniques in managing various pathologies [19–20].

6. Conclusion

Combined open laminotomy and spinal endoscopic-assisted decompression proves safe, effective, and technically feasible for managing extensive lumbar spinal epidural and multi-level paravertebral tophaceous gout. This technique enables thorough decompression and tophus removal without compromising spinal stability. Early surgical intervention is warranted for patients presenting with neurological deficits [21–22]. Gouty tophi should also be considered in the differential diagnosis of spinal masses, particularly in individuals with a known history of hyperuricemia [23-25].

Disclosure statement

The authors declare no conflict of interest.

References

[1] Toprover M, Krasnokutsky S, Pillinger MH, 2015, Gout in the Spine: Imaging, Diagnosis, and Outcomes. Current Rheumatology Reports, 2015(17): 70.

[2] Wu Z, Liu C, Dai K, et al., 2022, Intraspinal Extradural Gout Tophus in the Lumbar Vertebral Canal: Case Reports. Medicine, 2022(101): e28418.

[3] Mishra R, Panigrahi VP, Adsul N, et al., 2020, Tophaceous Gout in Thoracic Spine Mimicking Meningioma. Surgical Neurology International, 2020(11): 364.

[4] Barrett K, Miller ML, Wilson JT, 2001, Tophaceous Gout of the Spine Mimicking Epidural Infection. Neurosurgery. 2001(48): 1170–1173.

[5] Bonaldi VM, Duong H, Starr MR, et al., 1996, Tophaceous Gout of the Lumbar Spine Mimicking an Epidural Abscess. American Journal of Neuroradiology, 1996(17): 1949–1952.

[6] Si M, Cong M, Wang D, et al., 2020, Intraspinal Gouty Tophus. Neurology, 2020(95): e356–e358.

[7] Chen X, Xu G, Hu Q, et al., 2020, Percutaneous Transforminal Endoscopic Decompression for Intraspinal Tophaceous Gout. Medicine, 2020(99): e20125.

[8] Beier CP, Hartmann A, Woertgen C, et al., 2005, A Large, Erosive Intraspinal and Paravertebral Gout Tophus. Journal of Neurosurgery: Spine, 2005(3): 485–487.

[9] Chen J, Li M, Zhao F, et al., 2025, Tophaceous Gout in the Lumbar Spinal Canal Mimicking Epidural Spinal Tumor in a Male Adolescent. Medicine, 2025(104): e43661.

[10] Chang IC, 2005, Surgical Versus Pharmacologic Treatment of Intraspinal Gout. Clinical Orthopaedics and Related Research, 2005(433): 106–110.

[11] Yeung AT, Tsou PM, 2002, Posterolateral Endoscopic Excision for Lumbar Disc Herniation: Surgical Technique, Outcome, and Complications in 307 Consecutive Cases. Spine, 2002(27): 722–731.

[12] Ruettens S, Komp M, Merk H, et al., 2008, Full-endoscopic Interlaminar and Transforminal Lumbar Discectomy Versus Conventional Microsurgical Technique: A Prospective, Randomized, Controlled Study. Spine, 2008(33): 931–939.

[13] Xie L, Zhang X, Xi Z, et al., 2019, Percutaneous Endoscopic Treatment for Cervical Ligamentum Flavum Gouty Tophus. Medicine, 2019(98): e15665.

[14] Fenton P, Young S, Prutis K, 1995, Gout of the Spine. The Journal of Bone & Joint Surgery, 1995(77): 767–771.

[15] King JC, Nicholas C, 1997, Gouty Arthropathy of the Lumbar Spine. Spine, 1997(22): 2309–2312.

[16] Yasuhara K, Tomita Y, Takayama A, et al., 1994, Thoracic Myelopathy due to Compression by the Epidural Tophus. Journal of Spinal Disorders, 1994(7): 82–85.

[17] Kim T, Kim RJ, Kim SH, et al., 2017, Tophaceous Gout in the Lumbar Spinal Canal Mimicking Epidural Spinal Tumor. Journal of Korean Society of Spine Surgery, 2017(14): 50–52.

[18] Hoogland T, Schubert M, Miklitz B, et al., 2006, Transforminal Posterolateral Endoscopic Discectomy with or without the Combination of a Low-Dose Chymopapain: A Prospective Randomized Study in 280 Consecutive Cases. Spine, 2006(31): 890–897.

[19] Ahn SS, Kim SH, Kim DW, et al., 2016, Comparison of Outcomes of Percutaneous Endoscopic Lumbar Discectomy and Open Lumbar Microdiscectomy for Young Adults: A Retrospective Matched Cohort Study. World Neurosurgery, 2016(86): 250–258.

[20] Liu C, Zhou Y, 2018, Comparison between Percutaneous Endoscopic Lumbar Discectomy and Minimally Invasive Transforminal Lumbar Interbody Fusion for Lumbar Disc Herniation with Biradicular Symptoms. World Neurosurgery, 2018(120): e72–79.

[21] Chang P, Rogowski BC, Aziz KA, et al., 2023, Foraminal Stenosis and Radiculopathy Secondary to Tophaceous Gout. Journal of Neurosurgery: Case Lessons, 2023(6): CASE23298.

[22] Elgafy H, Liu X, Herron J, 2016, Spinal Gout: A Review with Case Illustration. World Journal of Orthopedics, 2016(7): 766–775.

[23] Dalbeth N, Choi HK, Joosten LAB, et al., 2002, Gout. Nature Reviews Disease Primers, 2019(5): 69.

[24] Hsu CY, Shih TT, Huang KM, et al. Tophaceous Gout of the Spine: MR Imaging Features. Clinical Radiology, 2002(57): 919–925.

[25] Harlianto NI, Harlianto ZN, 2023, Patient Characteristics, Surgical Treatment, and Outcomes in Spinal Gout: A Systematic Review of 315 Cases. European Spine Journal, 2023(32): 3697–3710.

Publisher's note

Bio-Byword Scientific Publishing remains neutral with regard to jurisdictional claims in published maps and institutional affiliations.

Clinical Neuroscience Research, 2026, Volume 4, Issue 3
https://bbwpublisher.com/journal/CNR
Online ISSN: 2981-8133
Print ISSN: 3083-4899

Study on Stress Response of Propofol Combined with Sevoflurane Combined IntravenousInhalation General Anesthesia in Laparoscopic Cholecystectomy

Wenyuan Zhang, Zhiyang Sun, Yunfang Wan

Department of Anesthesiology, Lianshui County Hospital of Traditional Chinese Medicine, Huai'an 223400, Jiangsu, China

Copyright: © 2026 Author(s). This is an open-access article distributed under the terms of the Creative Commons Attribution License (CC BY 4.0), permitting distribution and reproduction in any medium, provided the original work is cited.

Abstract: *Objective*: To investigate the effect of propofol combined with sevoflurane combined intravenousinhalation general anesthesia on stress response in laparoscopic cholecystectomy. *Methods*: A total of 60 patients scheduled for elective laparoscopic cholecystectomy in the hospital from January 2023 to June 2025 were enrolled and randomly divided into two groups using a random number table method: the control group (30 cases) received total intravenous anesthesia with propofol for maintenance; the observation group (30 cases) received combined intravenousinhalation anesthesia with propofol and sevoflurane for maintenance. The anesthetic effects were compared between the two groups. *Results*: The observation group showed superior values compared to the control group in terms of mean arterial pressure (MAP) and heart rate (HR) during surgery and at the end of surgery, serum cortisol (Cor), norepinephrine (NE), and blood glucose (Glu) levels at 24 h postoperatively, as well as eyeopening time, spontaneous respiration recovery time, extubation time, and orientation recovery time (all $P < 0.05$). There was no statistically significant difference in the total incidence of adverse reactions between the two groups ($P > 0.05$). *Conclusion*: The application of propofol combined with sevoflurane combined intravenousinhalation general anesthesia in laparoscopic cholecystectomy can effectively maintain perioperative hemodynamic stability, inhibit stress responses induced by surgical trauma, and provide better recovery quality with good safety, thus warranting clinical promotion.

Keywords: Laparoscopic cholecystectomy; Propofol; Sevoflurane; Combined intravenousinhalation general anesthesia; Stress response

Online publication: October 19, 2026

1. Introduction

In laparoscopic cholecystectomy, the establishment of CO_2 pneumoperitoneum, tracheal intubation, and surgical trauma can activate the hypothalamicpituitaryadrenal (HPA) axis and the sympatheticadrenal

medullary system, leading to elevated levels of cortisol, catecholamines, and other hormones, which in turn cause hemodynamic fluctuations, hyperglycemia, and immune dysfunction, thereby affecting patient prognosis. Therefore, selecting an appropriate anesthesia method to reduce perioperative stress response is an urgent clinical issue to be addressed [1]. Propofol is a commonly used shortacting intravenous anesthetic with advantages including rapid onset, quick recovery, and good controllability of anesthetic depth, making it a core agent for total intravenous anesthesia. However, highdose administration may cause adverse effects such as circulatory depression and injection pain. Sevoflurane is a widely used inhalational anesthetic with a low bloodgas partition coefficient, providing smooth induction and emergence, minimal impact on circulatory function, and enhanced effects of neuromuscular blockers. Combined intravenousinhalation anesthesia can integrate the advantages of both intravenous and inhalational anesthetics, exerting synergistic drug effects, maintaining adequate anesthetic depth while reducing the dosage of every single agent and lowering the risk of associated adverse reactions. This approach has attracted considerable attention in recent years and has achieved favorable outcomes. Therefore, this study focuses on analyzing the effect of propofol combined with sevoflurane combined intravenousinhalation general anesthesia on stress response in laparoscopic cholecystectomy, as detailed below.

2. General data and methods

2.1. General data

A total of 60 patients scheduled for elective laparoscopic cholecystectomy in the hospital from January 2023 to June 2025 were enrolled and randomly divided into two groups using a random number table method, with 30 cases in each group. In the observation group, there were 17 males and 13 females; age ranged from 32 to 64 years, with a mean of (47.25 ± 8.63) years; body mass index (BMI) ranged from 21.3 to 27.8 kg/m², with a mean of (24.16 ± 2.35) kg/m². In the control group, there were 16 males and 14 females; age ranged from 30 to 65 years, with a mean of (46.83 ± 9.12) years; BMI ranged from 20.8 to 28.1 kg/m², with a mean of (24.39 ± 2.51) kg/m². There were no significant differences in baseline data between the two groups ($P > 0.05$). This study complied with the requirements of the Declaration of Helsinki.

2.1.1. Inclusion criteria

(1) Diagnosed with benign lesions such as cholelithiasis or gallbladder polyps by abdominal ultrasound or CT, meeting the indications for laparoscopic cholecystectomy;
(2) Aged 18–65 years;
(3) No significant abnormalities in preoperative liver and kidney function, coagulation function, or electrocardiogram;
(4) Written informed consent obtained from patients and their families.

2.1.2. Exclusion criteria

(1) Severe cardiac or pulmonary insufficiency, endocrine system diseases, or psychiatric/neurological disorders;
(2) Longterm use of opioids, glucocorticoids, or antidepressants;
(3) Allergy to propofol, sevoflurane, or other anesthetic agents;
(4) Previous upper abdominal surgery;

(5) Conversion to open surgery during the procedure or operation time exceeding 2 hours.

2.2. Methods

All patients underwent routine preoperative fasting for 8 h and fluid restriction for 4 h. After entering the operating room, an upper extremity venous line was established, and normal saline was infused. Routine monitoring included electrocardiogram (ECG), noninvasive blood pressure (NIBP), pulse oximetry (SpO_2), and bispectral index (BIS).

Anesthesia induction: Both groups received intravenous midazolam 0.05 mg/kg, sufentanil 0.4 μg/kg, propofol 2.0 mg/kg, and cisatracurium 0.15 mg/kg. After loss of consciousness and adequate muscle relaxation, tracheal intubation and mechanical ventilation were performed. Tidal volume was set at 8–10 ml/kg, respiratory rate at 12–14 breaths/min, and endtidal carbon dioxide partial pressure ($PETCO_2$) was maintained at 35–45 mmHg.

Anesthesia maintenance: In the control group, propofol was continuously infused at 4–8 mg/(kg·h) via a pump, with intermittent boluses of sufentanil and cisatracurium, and BIS was maintained at 40–60. In the observation group, sevoflurane was inhaled at 1.0%–2.0%, and the propofol infusion rate was adjusted according to BIS values and hemodynamic changes to maintain BIS at 40–60. During surgery, vasoactive agents were used as needed based on blood pressure and heart rate, and pneumoperitoneum pressure was maintained at 12–14 mmHg. At the end of surgery, all anesthetics were discontinued. After spontaneous respiration resumed, consciousness returned, and the swallowing reflex recovered, the tracheal tube was removed, and the patient was transferred to the postanesthesia care unit for monitoring.

2.3. Observation indicators

(1 Mean arterial pressure (MAP) and heart rate (HR) were recorded and compared before surgery, during surgery (5 min after pneumoperitoneum establishment), and at the end of surgery.

(2) Serum cortisol (Cor) levels were measured by chemiluminescence, norepinephrine (NE) concentrations by highperformance liquid chromatography, and blood glucose (Glu) levels by the glucose oxidase method before surgery and 24 h after surgery.

(3) Eyeopening time, spontaneous respiration recovery time, extubation time, and orientation recovery time were recorded and compared.

(4) The incidence of adverse reactions within 24 h postoperatively, including nausea and vomiting, dizziness, agitation, and cough, was recorded and compared.

2.4. Statistical analysis

Data were processed using SPSS version 24.0. Continuous variables were analyzed using the ttest and presented as mean ± standard deviation (Mean ± SD); categorical variables were analyzed using the x^2 test and presented as percentages (%). A *P*value < 0.05 was considered statistically significant.

3. Results

3.1. Comparison of MAP and HR at different time points between the two groups

At the time points during surgery and at the end of surgery, MAP and HR in the observation group were significantly lower than those in the control group ($P < 0.05$), as shown in **Table 1**.

Table 1. Comparison of MAP and HR at different time points between the two groups (*n*, Mean ± SD)

Group	n	MAP (mmHg)			HR (beats/min)		
		Preoperative	Intraoperative	End of surgery	Preoperative	Intraoperative	End of surgery
Observation group	30	86.34±7.52	94.27±8.13	95.16±8.34	76.28±6.43	84.36±7.25	85.62±7.58
Control group	30	87.15±7.86	102.56±9.45	104.72±9.86	77.05±6.71	93.47±8.62	95.18±9.03
t		0.408	3.642	4.055	0.454	4.430	4.441
P		0.685	0.001	0.000	0.652	0.000	0.000

3.2. Comparison of stress indicators between the two groups at different time points

At 24 hours postoperatively, the levels of cortisol (Cor), norepinephrine (NE), and glucose (Glu) in the observation group were lower than those in the control group ($P < 0.05$), as shown in **Table 2**.

Table 2. Comparison of stress indicators between the two groups at different time points (*n*, Mean ± SD)

Group	n	Cor (nmol/L)		NE (pg/ml)		Glu (mmol/L)	
		Before surgery	24 h after surgery	Before surgery	24 h after surgery	Before surgery	24 h after surgery
Observation group	30	287.46±35.72	368.25±42.39	152.37±24.65	205.63±28.74	5.12±0.64	6.03±0.76
Control group	30	291.38±37.15	457.63±54.28	156.82±26.13	274.39±36.52	5.20±0.68	6.95±0.92
t		0.417	7.108	0.679	8.104	0.469	4.223
P		0.679	0.000	0.500	0.000	0.640	0.000

3.3. Comparison of recovery quality indicators between the two groups

In terms of recovery quality, the observation group demonstrated more prominent advantages compared with the control group ($P < 0.05$), as shown in **Table 3**.

Table 3. Comparison of recovery quality indicators between the two groups (*n*, Mean ± SD, min)

Group	n	Eye opening time	Spontaneous breathing recovery time	Extubation time	Orientation recovery time
Observation group	30	5.24±1.13	4.86±1.05	7.35±1.42	9.68±1.76
Control group	30	7.15±1.48	6.52±1.37	9.84±1.89	13.57±2.34
t		5.618	5.268	5.769	7.277
P		0.000	0.000	0.000	0.000

3.4. Comparison of adverse reactions between the two groups

There was no statistically significant difference in the incidence of adverse reactions between the two groups ($P > 0.05$), as shown in **Table 4**.

Table 4. Comparison of adverse reactions between the two groups (*n*, %)

Group	n	Nausea and vomiting	Dizziness	Agitation	Choking cough	Total incidence
Observation group	30	2 (6.67)	1 (3.33)	0 (0.00)	0 (0.00)	3 (10.00)
Control group	30	3 (10.00)	0 (0.00)	1 (3.33)	1 (3.33)	5 (16.67)

x^2	0.577
P	0.448

4. Discussion

Although laparoscopic cholecystectomy is a minimally invasive procedure, factors such as endotracheal intubation stimulation, increased intraabdominal pressure due to CO_2 pneumoperitoneum, and peritoneal traction can promote the secretion of stress hormones including catecholamines and cortisol, which in turn trigger a series of pathophysiological changes—such as elevated blood pressure, increased heart rate, and hyperglycemia—and increase the risk of perioperative cardiovascular events [2]. An ideal anesthetic approach should effectively inhibit perioperative stress responses while meeting the requirements for surgical sedation and analgesia, and maintaining hemodynamic stability [3].

Propofol is the most widely used intravenous general anesthetic in clinical practice. It primarily exerts its central inhibitory effects by enhancing the function of γaminobutyric acid type A (GABAA) receptors, and offers advantages including rapid onset, swift metabolic clearance, and negligible accumulation in the body. However, a largedose single injection can easily induce adverse reactions such as circulatory depression and injection pain [4]. Sevoflurane is a novel halogenated inhalational anesthetic that provides smooth induction and emergence, causes minimal airway irritation, allows mask induction, has a mild impact on hemodynamics, and can potentiate the effects of muscle relaxants. Combined intravenousinhalational anesthesia, by coadministering intravenous and inhalational agents to maintain anesthetic depth, can exploit drug synergies, reduce the dosage of individual drugs, and lower the risk of adverse effects associated with a single agent [5].

The results of this study showed that during surgery, both groups experienced fluctuations in MAP and HR; however, the MAP and HR levels at each time point were lower in the observation group than in the control group, indicating that propofol combined with sevoflurane intravenousinhalational anesthesia can more effectively inhibit sympathetic excitation and maintain more stable hemodynamics. Mechanistically, sevoflurane can reduce blood pressure by inhibiting myocardial contractility and dilating peripheral vessels, thereby attenuating the cardiovascular responses induced by endotracheal intubation and extubation, while propofol exerts circulatory effects through direct peripheral vasodilation and mild inhibition of myocardial contractility. The combined application of the two agents thus provides clear complementary effects [6].

Cortisol is a core endocrine indicator reflecting the degree of systemic stress, and norepinephrine is an important marker of sympathetic nervous system activation. Both are significantly elevated under surgical stress, and the magnitude of elevation is positively correlated with the intensity of stress [7]. Hyperglycemia is also an important manifestation of the stress response, and its mechanism is closely related to cortisol and catecholaminepromoted glycogenolysis and inhibition of insulin secretion [8]. The results of this study showed that at 24 hours postoperatively, the levels of Cor, NE, and Glu increased in both groups compared with preoperative values, but the levels of these stress indicators were lower in the observation group than in the control group, suggesting that propofol combined with sevoflurane intravenousinhalational anesthesia can more effectively attenuate the neuroendocrine stress response induced by surgical trauma [9]. This may be attributed to sevoflurane's action on the adrenal cortex and sympathetic ganglia, as well as its modulation of neuroendocrine activity in the hypothalamic paraventricular nucleus, thereby exerting synergistic antistress

effects with propofol [10].

Quality of recovery is an important indicator for evaluating anesthetic efficacy and directly affects the efficiency of postoperative patient recovery [11]. The results of this study showed that the observation group had shorter eyeopening time, spontaneous breathing recovery time, extubation time, and orientation recovery time than the control group, indicating that combined intravenousinhalational anesthesia can accelerate and improve the completeness of patient emergence. The underlying reasons include the low bloodgas partition coefficient of sevoflurane, which allows rapid pulmonary clearance after discontinuation with minimal residual accumulation in the body; simultaneously, combined anesthesia reduces the total propofol dosage, decreasing drug accumulation effects and thereby accelerating emergence and cognitive function recovery [12]. Sevoflurane can easily cause agitation during the emergence period, whereas propofol possesses good sedative and anxiolytic properties; their combination can reduce the risk of emergence agitation and improve recovery quality [13].

In terms of safety, the incidence of adverse reactions showed no statistically significant difference between the two groups ($P > 0.05$), and the reactions were mainly mild nausea, vomiting, and dizziness, all of which resolved after symptomatic treatment. This suggests that propofol combined with sevoflurane intravenousinhalational anesthesia does not increase the risk of adverse reactions and demonstrates good clinical safety [14]. Some studies have pointed out that sevoflurane can react with soda lime to produce compound A, and prolonged highconcentration inhalation carries a potential risk of nephrotoxicity; however, laparoscopic cholecystectomy is relatively short in duration, and lowconcentration inhalation generally does not cause significant organ damage [15].

5. Conclusion

In summary, for laparoscopic cholecystectomy, the administration of propofol combined with sevoflurane intravenousinhalational general anesthesia can effectively maintain perioperative hemodynamic stability, inhibit the stress response induced by surgical trauma, and provide better recovery quality with favorable safety, making it worthy of clinical promotion.

Disclosure statement

The authors declare no conflict of interest.

References

[1] Hu GK, 2026, Evaluation of the Clinical Anesthetic Efficacy of Sevoflurane or Propofol Combined with Dexmedetomidine in Laparoscopic Cholecystectomy. Primary Medical Forum, 30(17): 95–97.

[2] Li MX, Li XY, Wang J, 2026, Effects of SevofluraneRemifentanil Intravenousinhalational Combined Anesthesia on Hemodynamics, Stress Response, and Recovery Quality in Patients Undergoing Laparoscopic Cholecystectomy. Chinese Journal of Medicine, 61(1): 50–53.

[3] Jiang FF, Cao J, 2025, Clinical Anesthetic Efficacy of Propofol Combined with Cisatracurium Besylate in Laparoscopic Cholecystectomy. Journal of Rare and Uncommon Diseases, 32(12): 94–96.

[4] Wei SS, Mei JX, 2025, Value of Dexmedetomidine in Preventing Emergence Agitation during Sevoflurane

Anesthesia in Patients Undergoing Laparoscopic Cholecystectomy. Primary Medical Forum, 29(33): 96–98 + 102.

[5] Du L, Hao W, Wang Y, 2025, Observation of Anesthetic Effects of Dexmedetomidine Combined with Propofol in Patients with Gallstones Undergoing Laparoscopic Cholecystectomy. Modern Medicine and Health Research Electronic Journal, 9(22): 76–79.

[6] Liang DL, Tang ZR, Yao J, et al., 2025, Observation of the Efficacy of Remimazolam Besylate Total Intravenous Anesthesia in Laparoscopic Cholecystectomy. Modern Medicine, 53(11): 1769–1773.

[7] Bai T, Zheng SP, Song Z, et al., 2025, Analysis of Anesthetic Efficacy of Propofol Combined with Dexmedetomidine in Laparoscopic Cholecystectomy. China Practical Medicine, 20(21): 11–15.

[8] Huo YH, Pan CY, Zhang AP, et al., 2025, Observation of the Efficacy of Esketamine Combined with Propofol in Laparoscopic Cholecystectomy. Chief Physician, 10(21): 13–16.

[9] Qin Y, Sun R, Pan QY, 2025, Effects of Remifentanil Combined with Propofol Anesthesia on Cognitive Function and Hemodynamics in Patients after Laparoscopic Cholecystectomy. Journal of Harbin Medical University, 59(5): 541–546.

[10] Jin CC, Li CM, Su C, et al., 2025, Application of Different Concentrations of Sevoflurane Combined with Propofol for Maintenance of General Anesthesia in Laparoscopic Cholecystectomy in Elderly Patients with Gallstones. Clinical Misdiagnosis and Mistreatment, 38(20): 51–59.

[11] Yang Y, 2025, Analgesic Efficacy of Dexmedetomidine Combined with Propofol Anesthesia in Patients Undergoing Laparoscopic Cholecystectomy. Famous Doctor, 2025(17): 168–170.

[12] Wu DY, Li DD, 2022, Effects of Continuous Infusion of Dexmedetomidine after Sevoflurane Inhalation General Anesthesia on Analgesic Efficacy and Sleep in Patients Undergoing Laparoscopic Cholecystectomy. World Journal of Sleep Medicine, 9(6): 1019–1022.

[13] Huang H, Du Y, Chen Q, 2025, Effect of Sevoflurane Combined with Oxycodone on Postoperative Agitation in Patients with Gallstones Undergoing Laparoscopic Cholecystectomy. Clinical Rational Drug Use, 18(9): 75–78.

[14] Wang LJ, Cao J, Jia HP, et al., 2025, Impact of Sevoflurane Combined with Propofol and Remifentanil Intravenousinhalational Combined Anesthesia on Patients Undergoing Laparoscopic Cholecystectomy. Harbin Medicine, 45(1): 14–17.

[15] Qian Y, 2025, Analysis of the Impact of Sevoflurane or Propofol Combined with Remifentanil Clinical Anesthesia on Hemodynamics in Elderly Patients Undergoing Laparoscopic Cholecystectomy. Systems Medicine, 10(1): 76–79.

Publisher's note

Bio-Byword Scientific Publishing remains neutral with regard to jurisdictional claims in published maps and institutional affiliations.

Clinical Neuroscience Research, 2026, Volume 4, Issue 3
https://bbwpublisher.com/journal/CNR
Online ISSN: 2981-8133
Print ISSN: 3083-4899

The Global, Regional, and National Patterns of Change in the Burden of Skull Fractures from 1990 to 2021 and the Forecast for 2036: A Global Burden of Disease Study

Yuhang Gu†, Xiaoyu Ji†, Siyuan Yang†, Zhengquan Yu*

Department of Neurosurgery, The First Affiliated Hospital of Soochow University, Suzhou 215006, Jiangsu, China
†These authors contributed equally to this work and share the first authorship.

***Corresponding author:** Zhengquan Yu, zhengquan.yu@neurosci.com.cn

Copyright: © 2026 Author(s). This is an open-access article distributed under the terms of the Creative Commons Attribution License (CC BY 4.0), permitting distribution and reproduction in any medium, provided the original work is cited.

Abstract: *Background*: Skull fractures are a significant public health concern worldwide. The study aimed to measure the incidence, prevalence, and years of life lived with disability (YLDs) for skull fractures from all causes of injury in every country, to describe how these measures have changed and provide crucial information for the development of targeted prevention and treatment strategies. *Methods*: Data from the Global Health Data 2021 were used to measure the global, regional, and national burden of skull fractures by country, region, age, gender, and sociodemographic index (SDI). Age-period-cohort modeling, the AutoRegressive Integrated Moving Average (ARIMA) model, and joinpoint regression analysis were also carried out. *Results*: The global prevalence and YLDs of skull fractures increased from 1990 to 2021, marking a 20% and 18% increase. However, the global prevalence and YLDs rates of skull fractures declined from 1990 to 2021, with an EAPC of −1.37 (95% CI: −1.41 to −1.33) and −1.38 (95% CI: −1.42 to −1.34). The global incidence of skull fractures declined from 1990 to 2021, marking a 3% reduction. Skull fracture incidence rates, prevalence rates, and YLDs rates increased, followed by the rise of the SDI value. In 2021, the high SDI regions reported the highest absolute numbers of incident and YLD cases of skull fractures. The age effect across global and SDI regions demonstrates a downward trend with advancing age, except in the 80+ age groups. There were 5 major causes of skull fractures, including falls, road injuries, exposure to mechanical forces, interpersonal violence, and physical violence by other means. Falls were the most important cause of skull fractures. The ARIMA model predicts a global fall in the age-standardized rates (ASR) of prevalence, incidence, and YLDs from 2021 to 2036. *Conclusion*: Drawing on global epidemiological data, this work investigates trends for skull-fracture-related disease burden. While age-standardized rates (ASR) have fallen, worldwide prevalence and total years lived with disability keep going up. This mismatch between trends implies that one-size-fits-all approaches will not work; local context-adapted interventions are therefore required to tackle the expanding burden of such injuries. Even so, aggregate population burden from skull fractures is forecast to decline in the coming 15-year period.

Keywords: Skull fractures; Epidemiology; Global burden of disease; Prevalence

Online publication: October 19, 2026

1. Introduction

Neurological disorders rank as the top source of disability and the second-largest cause of death around the world. A broad spectrum of illnesses falls within this category of central nervous system (CNS) pathologies: infectious conditions, stroke, primary and secondary CNS malignancies, traumatic brain injuries (TBIs), alongside spinal cord injuries. Substantial disease burden also stems from neurodegenerative pathologies, including Alzheimer's disease and other dementia subtypes, Parkinson's disease, multiple sclerosis, and motor neuron disease. Idiopathic epilepsy, migraine, tension-type headache, plus a collection of rare neurological conditions further add to this public-health toll [1]. On a global scale, TBIs — among which skull fractures represent an important subgroup — are responsible for considerable morbidity and mortality [2]. According to World Health Organization (WHO) estimates, TBIs stand out as a major driver of death and long-term disability; roughly 69 million individuals sustain TBI each year, and a large proportion of these patients present with concurrent skull fractures [3–6].

Skull fractures constitute a major public-health issue across the globe, especially in settings where road traffic crashes, falls, and interpersonal violence occur frequently. Clinical presentations cover a wide severity spectrum, ranging from uncomplicated linear fractures to severe comminuted or depressed skull injuries [7–8]. Patients with skull fractures may develop multiple adverse sequelae such as intracranial hemorrhage, cerebrospinal fluid leak, secondary infection and seizure episodes [9]. The real-world incidence of skull fractures shows marked geographical heterogeneity. Low- and middle-income countries tend to bear higher incidence rates, partly attributable to insufficient road safety regulation, workplace injury risks and limited healthcare accessibility. One Danish registry reported a cranial fracture incidence of 1.2 per 100 000 following head trauma [10]. By contrast, in high-income nations, fall-related skull fractures predominate among older adults, whereas younger groups mostly incur such injuries through motor-vehicle collisions and sports activities. Available medical resources, prompt clinical intervention, and concomitant associated injuries collectively shape patient management and final prognosis. Even so, existing literature still lacks a clear picture regarding the regional and socioeconomic distribution of skull fracture incidence. Shifting focus toward preventive strategies to curb skull fracture occurrence has become a promising direction for mitigating its long-term societal burden.

2. Materials and methods

2.1. Data source

Epidemiological datasets analyzed in the present work were retrieved from the Global Burden of Disease Study 2021 (GBD 2021). This dataset supplies uptodate burden estimates covering 371 disease and injury conditions for 204 countries and territories grouped into 21 geographical GBD regions, with analytical timeframes ranging from 1990 through to 2021 [11]. Comprehensive source metadata can be accessed at https://ghdx.healthdata.org/gbd2021/sources.

The research was performed in compliance with the Guidelines for Accurate and Transparent Health Estimates Reporting (GATHER) [12]. Raw datasets alongside processing and modeling code associated with GBD 2021 are publicly accessible via the Global Health Data Exchange (GHDx) platform. Moreover, the STROCSS guideline checklist was supplemented for this investigation [13].

2.2. Disease definition

Within the GBD analytical framework, fractures are classified by injury nature instead of underlying etiology. The operational definition for skull fractures adopted by GBD draws upon codes from the International Classification of Diseases and Injuries (ICD) [14].

2.3. Socio-demographic index (SDI)

Developed by the Institute for Health Metrics and Evaluation (IHME) in 2015, the socio-demographic index (SDI) functions as a composite metric for evaluating regional and national developmental status, and it characterizes how social advancement correlates with population-level health performance. SDI values correspond to the geometric mean of three normalized indicators (each rescaled between 0 and 1): total fertility rate among women younger than 25 years, mean years of schooling for the population aged 15 years and older, and lag-distributed per-capita income. In GBD 2021, all 204 included countries and territories were stratified into five SDI tiers: low (0–0.2), low-middle (0.2-0.4), middle (0.4-0.6), high-middle (0.6-0.8), and high (0.8–1.0) [15].

2.4. Age-standardized prevalence rate (ASPR), age-standardized incidence rate (ASIR) and age-standardized YLDs rate (ASYR)

The ASIR and ASPR denote the number of cases per 100,000 individuals, adjusted for variations in population age. In contrast, the ASYR reflects the number of life years lived with disability per 100,000 people. The study calculated the ASR, including ASIR, ASPR, and ASYR, to assess the global burden of skull fractures using the following formula:

$$ASR=\frac{\sum_{i=1}^{A} a_i w_i}{\sum_{i=1}^{A} w_i} \times 100{,}000$$

where a_i denotes the age-specific rate in the age subgroup and w_i represents the number of individuals in the same age class of the GBD world age-standard population, which came from the GBD Study 2021 Population Estimates 1950-2021 [15–16].

2.5. Estimated annual percentage change (EAPC) and percentage change

The estimated annual percentage change (EAPC) serves as a well-validated statistical metric widely adopted to track temporal shifts in incidence, prevalence, and other health-related rates over a given time frame [17–18]. In this work, EAPC was applied to quantify how skull fracture prevalence, incidence, and years lived with disability (YLDs) evolved between 1990 and 2021. EAPC values were derived by fitting a linear regression to the natural logarithm of rates, with calendar year treated as the independent variable. After log-transforming each rate observation, the slope coefficient from this fitted linear model was used to compute final EAPC estimates [18–19].

$$y=\alpha+\beta x+\varepsilon$$

$$EAPC=100\times(\exp(\beta)-1)$$

The regression formula is specified as: $y=\alpha+\beta x+\varepsilon$, where x denotes the calendar year, y represents the logtransformed rate (prevalence or incidence), a is the intercept term, β stands for the regression slope, and å corresponds to random error. Modelgenerated 95% confidence intervals (CIs) were

obtained for each EAPC estimate. A statistically significant upward trend was identified when the lower bound of the 95% CI exceeded zero; conversely, a significant downward trend occurred if the upper bound of the 95% CI fell below zero. Trends were regarded as nonsignificant whenever zero fell within the 95% CI range. Besides EAPC calculations, simple percentage change was calculated to reflect absolute shifts in case counts for prevalence, incidence, and YLDs across 1990–2021, following the formula: Percentage change = (2021 cases − 1990 cases) / 1990 cases.

2.6. Correlation analysis

This study used correlation analysis to assess linear relationships between variables, with correlation coefficients used to judge the strength and direction of pairwise associations. Using the cor.test function in R, the study analyzed the correlation between age-standardized skull fracture rates (ASR) and socio-demographic index (SDI) across 21 GBD regions and 204 countries and territories. Scatter plots with fitted trend lines were constructed to intuitively visualize the correlation results [19–20].

2.7. Age-period-cohort model

The study adopted an age-period-cohort (APC) model to disaggregate temporal variations in skull fracture burden into three independent effect components: age, period, and cohort. Age effects refer to outcome changes related to individual aging. Period effects reflect broad societal and medical changes, including diagnostic updates and treatment improvements, that influence all age groups concurrently. Cohort effects represent differences in fracture risk across successive birth populations. A sum-to-zero constraint was applied during model fitting to resolve collinearity between the three dimensions. This approach enabled the calculation of net drift and local drift to describe long-term secular trends and periodic trend fluctuations, respectively. All age, period, and cohort data were organized into 5-year intervals for consistent APC analysis [21–22].

2.8. Joinpoint regression analysis

Characterizing long-term time-series patterns is essential for interpreting skull fracture incidence, prevalence, and YLDs. The study ran joinpoint regression using Joinpoint Regression Program version 4.9.1.0 (National Cancer Institute, Rockville, MD, USA) to detect inflection points and characterize changing epidemiological patterns. Annual percentage change (APC) for each segmented time interval and overall average annual percentage change (AAPC), together with their corresponding 95% CIs, were computed. Rising burden was indicated when APC and AAPC point estimates plus their entire 95% CI lay above zero, whereas declining burden was observed when these values fell entirely below zero. *P*-values greater than 0.05 suggested no statistically meaningful shift in rates within the evaluated time segment [23–24].

2.9. Forecasting the skull fractures over the next 15 years using the autoregressive integrated moving average (ARIMA) model

Future skull fracture incidence and mortality rates spanning 2022–2036 were predicted with the autoregressive integrated moving average (ARIMA) timeseries model. Modeling procedures were completed in R utilizing the forecast and tseries packages. ARIMA converts nonstationary raw timeseries data into stationary sequences via differencing operations and is defined by three core parameters: autoregressive order (p), differencing order (d), and movingaverage order (q). Autocorrelation and partial autocorrelation function outputs guide parameter selection for model configuration. Such timeseries forecasting supplies evidence

supporting publichealth planning and targeted intervention deployment [25–26].

2.10. Data processing and visualization

All data cleaning, computational procedures and plot generation were performed in R software (version 4.3.1). GBD injury aetiologies are organized into four hierarchical levels; source datasets mainly draw upon hospital admission records, injury surveillance registries, civil registration systems and vital-statistics archives. Fracture causes were classified according to external event types, including road-traffic collisions and falls. Clinical records informed calculations for proportional distributions of different causes and associated injury subtypes. When individuals sustained multiple-site fractures, the most severely disabling injury site was selected guided by disability weights derived from household and web-based population surveys. Multinomial regression ensured that summed proportions for all injury outcomes equaled one. Global skull-fracture burden patterns were stratified by sex and predefined age brackets: < 5, 5–10, 10–15, 15–19, 20–24, 25–29, 30–34, 35–39, 40–44, 45–49, 50–54, 55–59, 60–64, 65–69, 70–74, 75–79, 80–84, 85–89, 90–94, and > 95 years.

Figures were plotted with the "ggplot2" package, and final graphic adjustments were completed in Adobe Illustrator (version CS5). Study design, analytical execution, and result reporting followed the Strengthening the Reporting of Cohort Studies in Surgery (STROCSS) guidelines for observational surgical-related research.

3. Results

3.1. Global level

Globally, skull-fracture incident cases decreased moderately from 5 563.8 thousand (95% UI: 4415.9–7124.1 thousand) in 1990 down to 5424.3 thousand (95% UI: 4212.9–7235.1 thousand) by 2021, corresponding to an overall 3% reduction. Meanwhile, the global age-standardized incidence rate (ASIR) dropped from 98.6 per 100000 persons (95% UI: 78.3–126.8) in 1990 to 70.1 per 100000 persons (95% UI: 54.6–93) in 2021, with an EAPC of −1.15 (95% CI: −1.19 to −1.11).

By contrast, worldwide prevalent skull-fracture cases rose from 2005.3 thousand (95% UI: 1 818.6–2 242.3 thousand) in 1990 to 2399 thousand (95% UI: 2 184.6–2 677.2 thousand) in 2021, representing a 20% increase. Nonetheless, global age-standardized prevalence rates fell from 43 per 100000 (95% UI: 39.3–47.4) in 1990 to 29 per 100000 (95% UI: 26.4–32.5) in 2021; EAPC was −1.37 (95% CI: −1.41 to −1.33).

Total global YLDs attributable to skull fractures increased from 136.7 thousand (95% UI: 90.1–191 thousand) in 1990 to 161.2 thousand (95% UI: 108.1–224.6 thousand) in 2021, equivalent to an 18% rise. The corresponding age-standardized YLD rate declined from 2.9 per 100 000 (95% UI: 1.9–4) to 2 per 100000 (95% UI: 1.3–2.7), with an EAPC of −1.38 (95% CI: −1.42 to −1.34) (**Figure 1**).

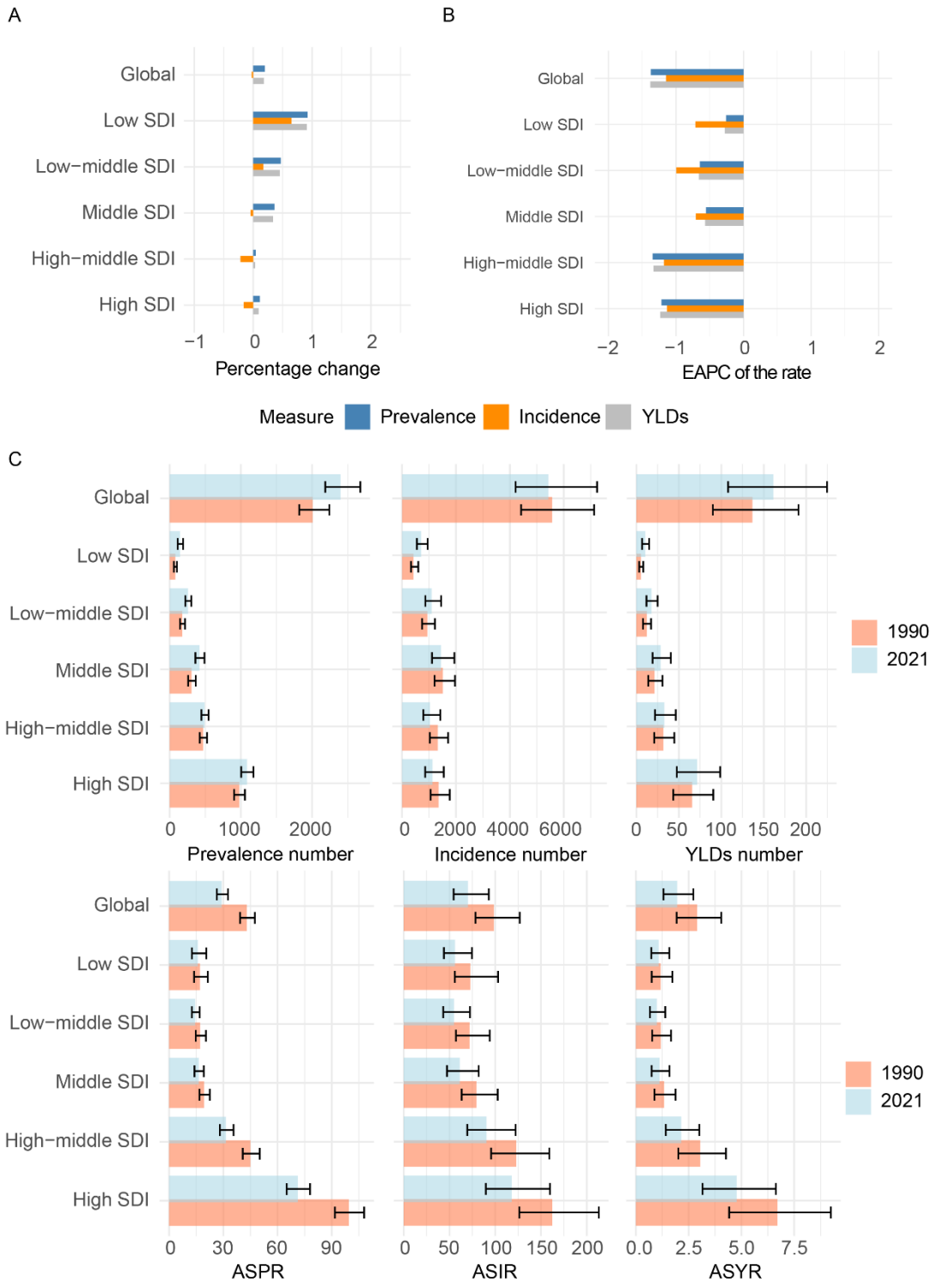

Figure 1. Temporal trend of skull fracture burden in global and 5 SDI regions. (A) Percentage change in cases of prevalent, incident, and YLDs in 1990 and 2021. (B) The EAPC of prevalence, incidence, and YLDs rates from 1990 to 2021. (C) Prevalence, incidence, and YLDs cases and rates in 1990 and 2021. SDI = Socio-demographic index, EAPC = Estimated Annual Percentage Change, YLDs = Years lived with disability

3.2. SDI regional level

In 2021, the high SDI regions reported the highest absolute numbers of incident and YLDs cases of skull fractures, with 1086.7 thousand (95% UI: 1003.1 to 1175.9) and 71.6 thousand (95% UI: 47.7 to 98.7). However, the middle SDI regions reported the highest absolute numbers of prevalent cases of skull fractures, with 1443.8 thousand (95% UI: 1108.7 to 1943.5) (**Figure 1**). The low SDI regions show the largest percentage change (incidence: 65%; prevalence: 92%; YLDs: 92%) from 1990 to 2021. In contrast, the high-middle SDI regions exhibited the smallest percentage change (incidence: -22%; prevalence: 4%, YLDs: 3%) (**Figure 1**). However, from 1990 to 2021, the EAPC in disease prevalence, incidence, and YLD rates exhibited a declining trend in all five SDI regions, and the high-middle SDI regions reported the highest EAPC rates for prevalence, incidence, and YLDs.

3.3. GBD regional level

In 2021, the Australasia regions reported the highest incident, prevalent, and YLDs rates of skull fractures, with 199.7 (140.6–281.3)/105,111 (99.8–123.4)/105, and 7.5 (4.9–10.5)/105, respectively **Figure 2** and **Figure 3**). Over the past 32 years, decreases in prevalence rates and YLDs rates have been observed in more than half of the regions, except the Caribbean and Oceania, while decreases in incident rates have been observed in more than half of the regions, except the Caribbean (**Figure 2** and **Figure 3**).

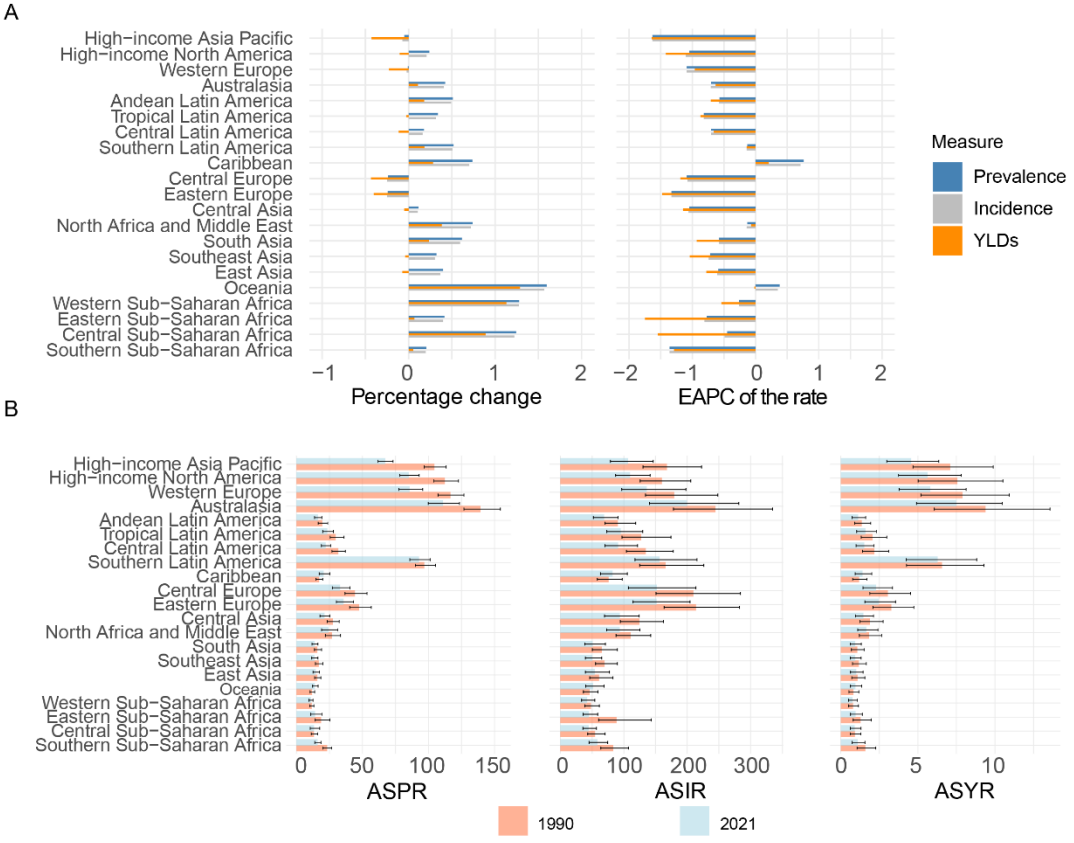

Figure 2. Temporal trend of skull fracture burden in 21 regions. (A) Percentage change in cases of prevalent, incident, and YLDs in 1990 and 2021. (B) The EAPC of prevalence, incidence, and YLDs rates from 1990 to 2021. SDI = Socio-demographic index, EAPC = Estimated Annual Percentage Change, YLDs = Years lived with disability

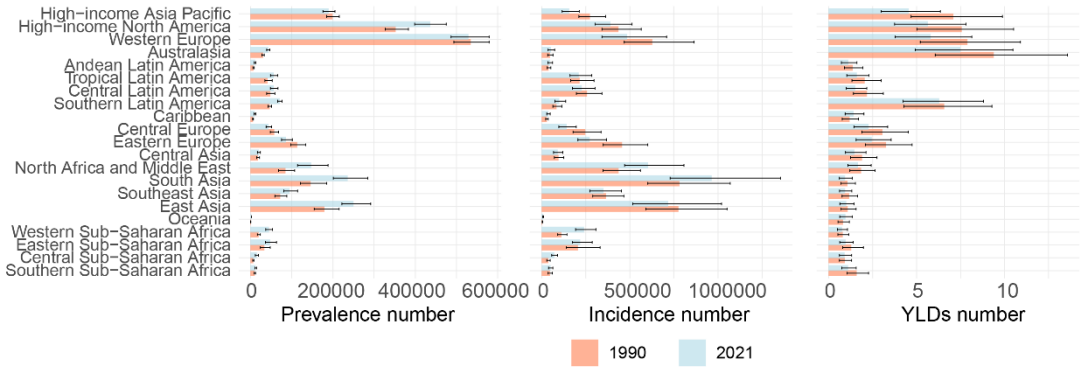

Figure 3. Prevalence, incidence, and YLDs cases across 21 regions in 1990 and 2021

3.4. Countries level

In 2021, the ASIR across the 204 countries was highest in Afghanistan (233.7 per 105, 95% UI: 138 to 425.9 per 105), followed by New Zealand (233 per 105, 95% UI: 165.9 to 324.9 per 105) while lowest in Tonga (29.3 per 105, 95% UI: 22.9 to 38.9 per 105) (**Figure 4**). The three highest countries in EAPC for the incidence rates were the Syrian Arab Republic (incidence: 5.3), Yemen (incidence: 2.21), and Libya (incidence: 2.05). The three lowest countries in EAPC for the incidence rates were Timor-Leste (incidence: -5.83), Burundi (incidence: -4.94), and Liberia (incidence: -4.8).

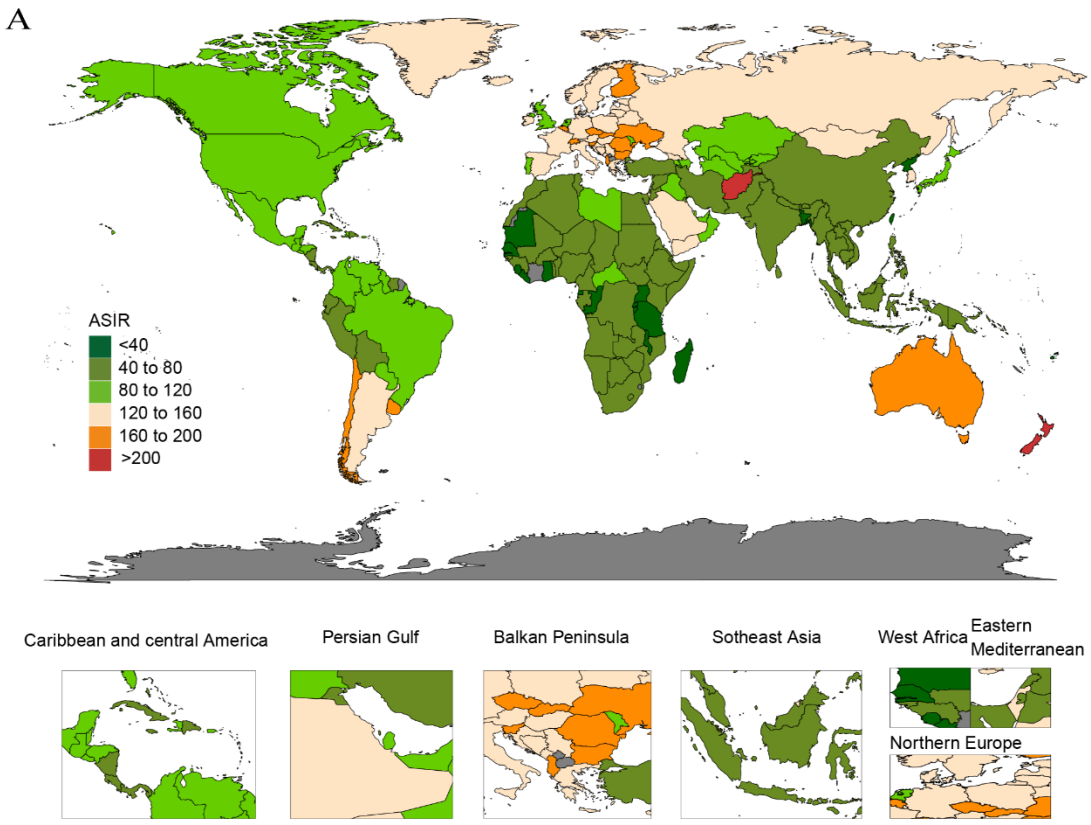
A
ASIR
<40
40 to 80
80 to 120
120 to 160
160 to 200
>200
Caribbean and central America
Persian Gulf
Balkan Peninsula
Sotheast Asia
West Africa
Eastern Mediterranean
Northern Europe
B
EAPC of the rate
<-4
-4 to -2
-2 to 0
0 to 2
2 to 4
>6
Caribbean and central America
Persian Gulf
Balkan Peninsula
Sotheast Asia
West Africa
Eastern Mediterranean
Northern Europe

Figure 4. Temporal trend of skull fracture burden at the country level. (A) ASR in incidence cases across 204 countries in 2021. (B) EAPC in incidence rates across 204 countries from 1990 to 2021. EAPC = Estimated Annual Percentage Change

In 2021, the ASPR and ASYR across the 204 countries was highest in New Zealand (ASPR: 126.9 per 105, 95% UI: 114.9 to 141.8 per 105; ASYR: 8.6 per 105, 95% UI: 5.1 to 11.2 per 105), followed by Andorra (ASPR: 116.3 per 105, 95% UI: 104.8 to 128.1 per 105; ASYR: 8.6 per 105, 95% UI: 5.5 to 12.1 per 105) while lowest in Tonga (ASPR: 7.3 per 105, 95% UI: 6.4 to 8.7 per 105; ASYR: 0.5 per 105, 95% UI: 0.3 to 0.7 per 105) (**Figure 5**, **Figure 6**). The highest countries in EAPC for the prevalence and YLDs rates were Syrian Arab Republic (prevalence: 5.28, YLDs: 5.23), Haiti (prevalence: 2.27, YLDs: 2.1), Libya (prevalence: 1.94, YLDs: 1.9). The lowest countries in EAPC for the incident rates were Taiwan (Province of China) (prevalence: -2.49, YLDs: -2.47), Portugal (prevalence: -2.48, YLDs: -2.48), Lebanon (prevalence: -2.33, YLDs: -2.36) (**Figure 5** and **Figure 6**).

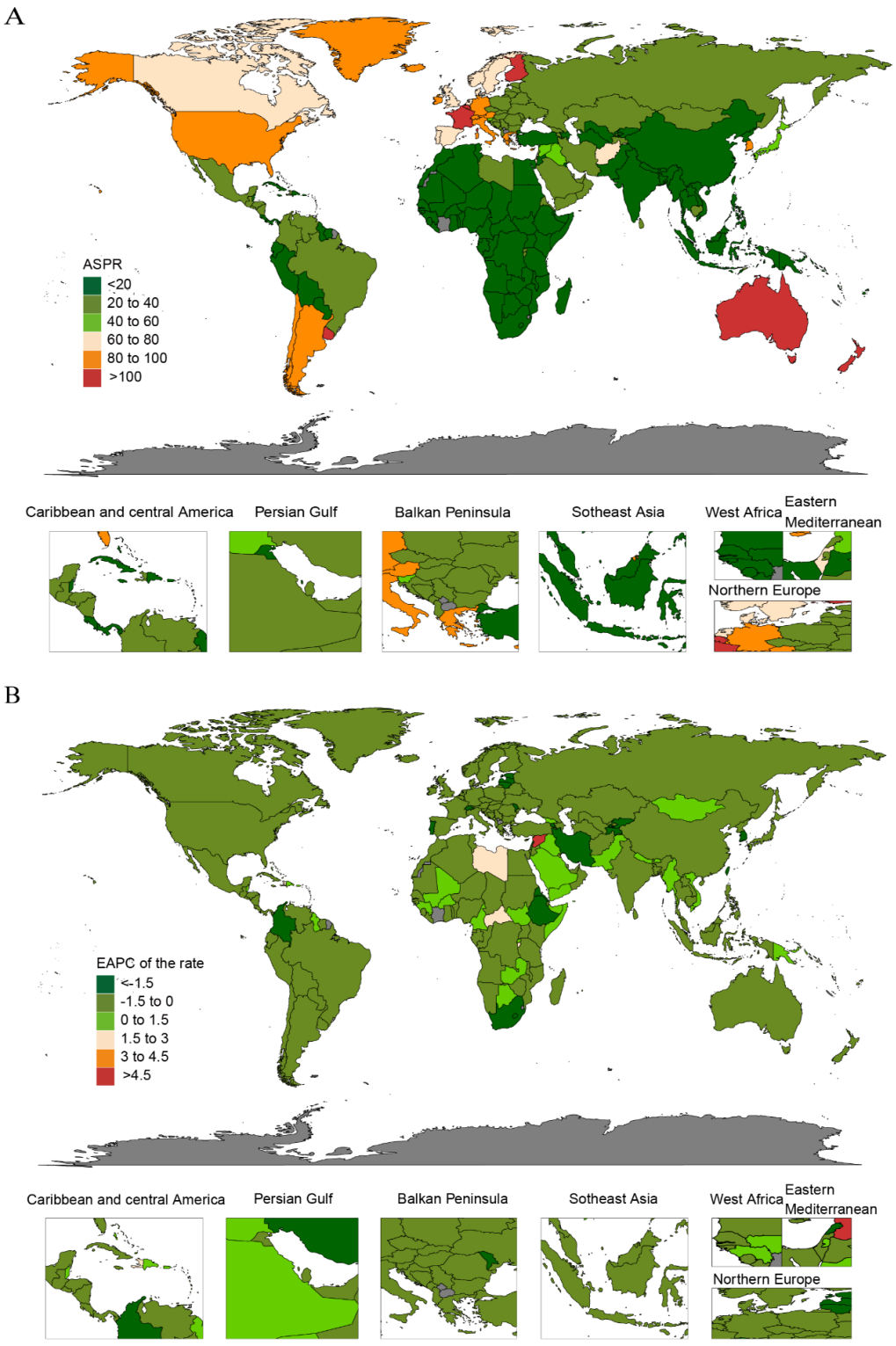

Figure 5. Temporal trend of skull fracture burden at the country level. (A) ASR in prevalent, incidence (Figure 4A), and YLDs (Figure 6A) cases across 204 countries in 2021. (B) EAPC in prevalent, incidence (Figure 4B), and YLDs (Figure 6B) rates across 204 countries from 1990 to 2021. EAPC = Estimated Annual Percentage Change, YLDs = Years lived with disability

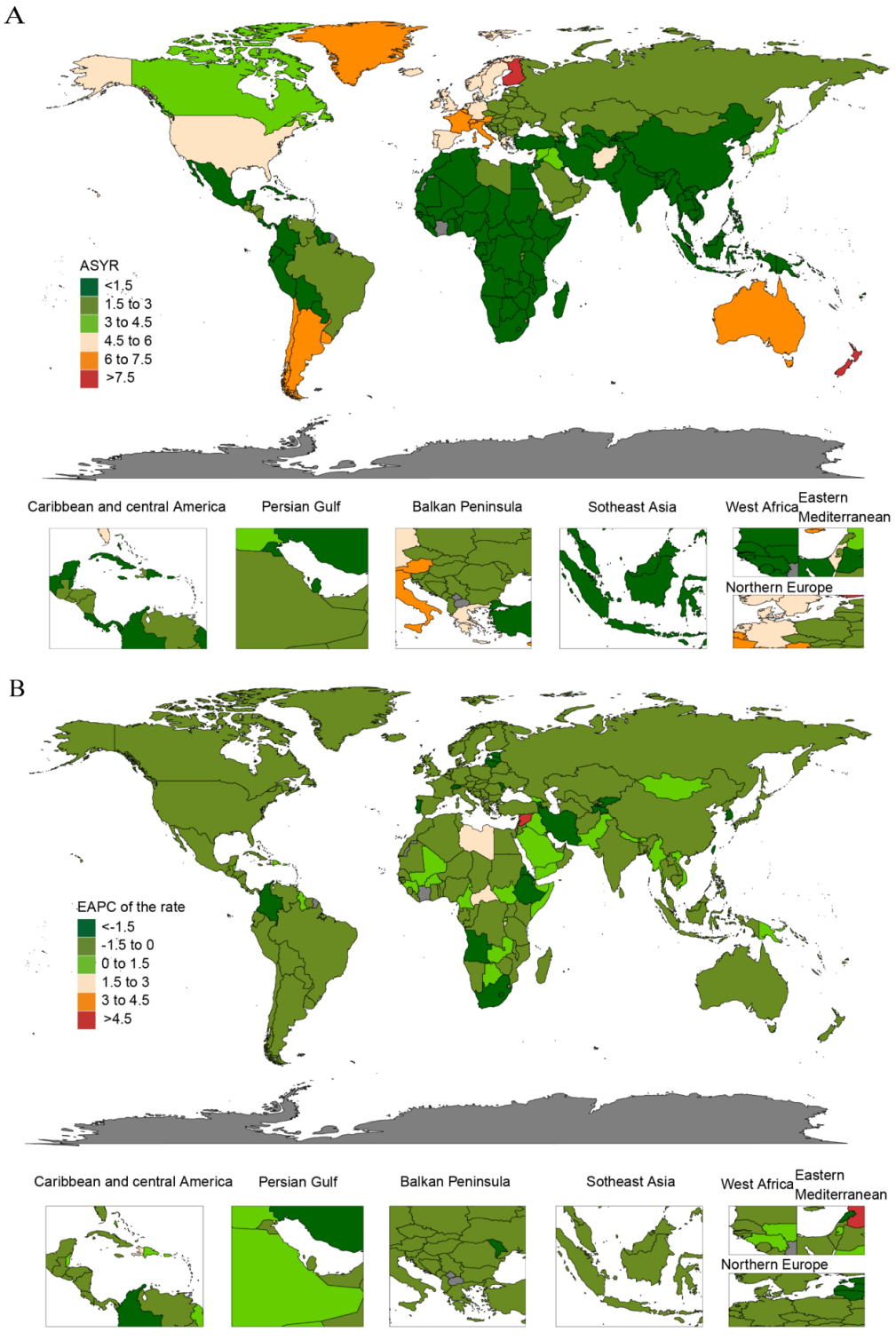

Figure 6. Temporal trend of the burden of skull fractures at the country level. (A) ASR in YLDs cases across 204 countries in 2021. (B) EAPC in YLDs rates across 204 countries from 1990 to 2021. EAPC = Estimated Annual Percentage Change

3.5. Age and sex pattern

Skull fracture incidence differed significantly between sexes and age groups. Males had the highest incidence

at 20–24 years of age, while female incidence peaked in children under five years old. Males showed higher age-standardized incidence rates (ASIR) than females across all age groups younger than 80 years, whereas females had higher ASIR in the population aged over 80 years (**Figure 7**).

Sex differences were also evident in skull fracture prevalence and YLDs. Males reached peak prevalence and YLD rates at 55–59 years, while females peaked later at 65–74 years. Males maintained higher age-standardized prevalence and YLD rates throughout adulthood until age 90, after which females exceeded males in both indicators (**Figure 7**). Male ASIR peaked in early adulthood, and female ASIR was highest in early childhood before declining steadily from 40 to 74 years. Males had higher ASIR than females across all analyzed age strata (**Figure 8**). For both sexes, the 90+ age group had the highest age-standardized prevalence (ASPR) and YLD (ASYR) rates, with males bearing a heavier fracture burden in most age groups.

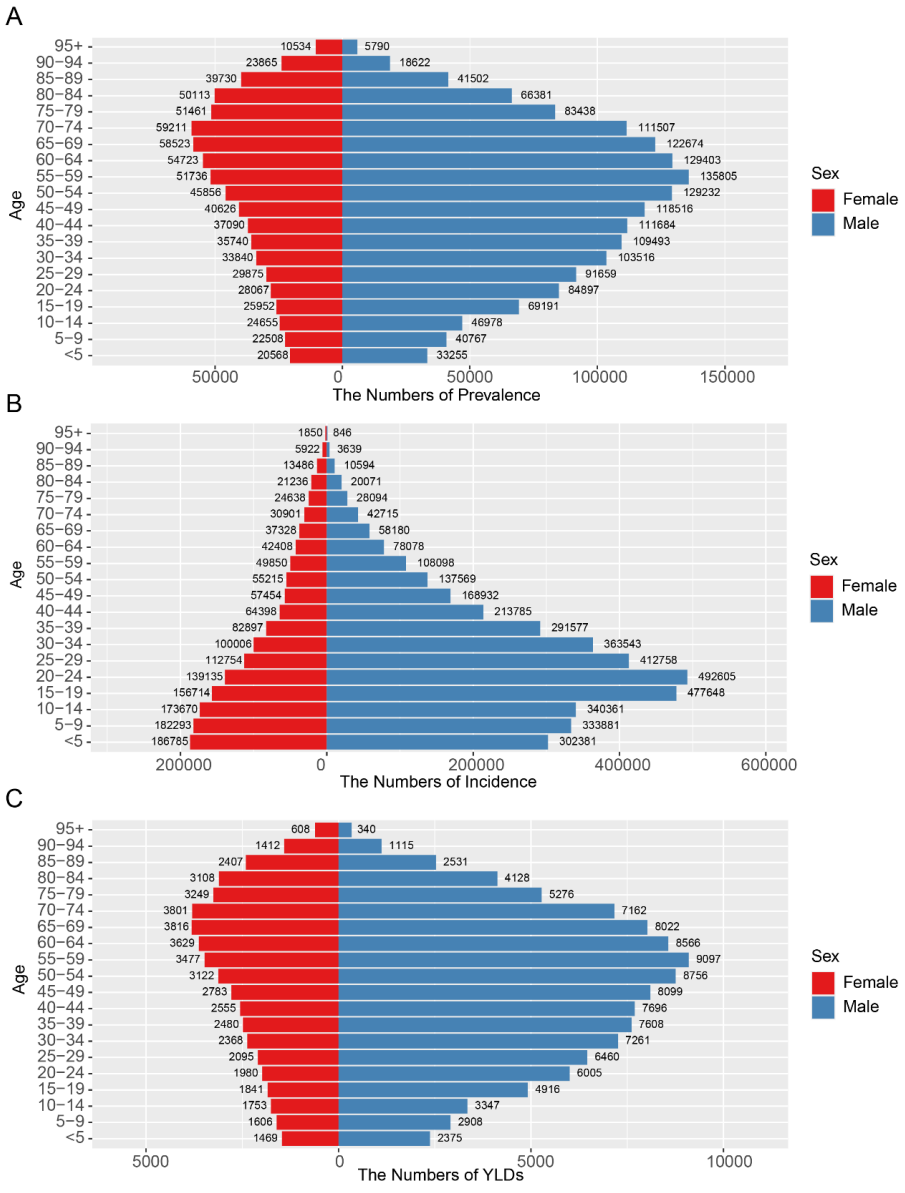

Figure 7. Prevalence, incidence, and YLDs number of skull fracture by age and sex in 2021

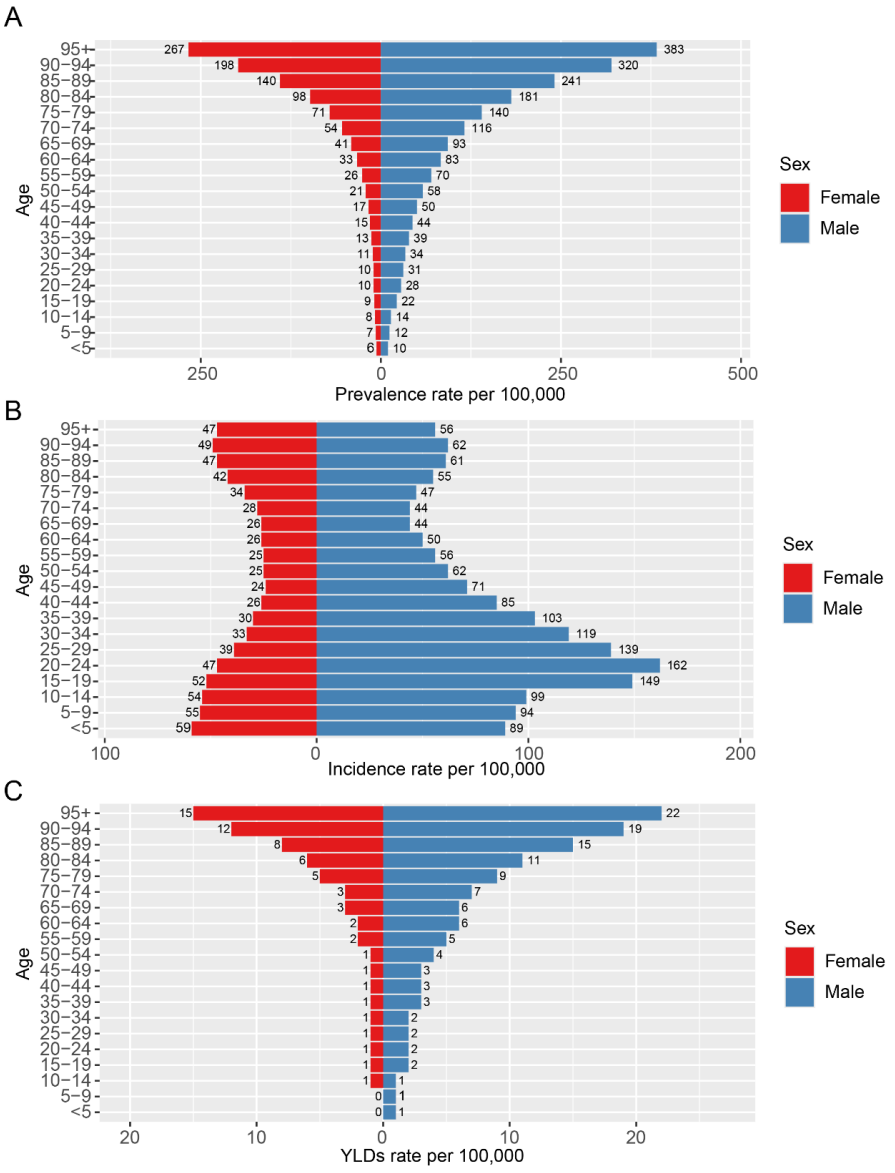

Figure 8. Prevalence, incidence, and YLDs rates of skull fracture by age and sex in 2021

3.6. The association between skull fracture burden and SDI

The study used scatter plots with fitted trend lines to analyze the correlation between skull fracture burden and socio-demographic index (SDI) across 21 GBD regions and 204 countries and territories. The results showed a positive correlation between SDI levels and skull fracture burden, with incidence, prevalence, and YLD rates increasing alongside socioeconomic improvement. Some regions and countries had a higher fracture burden than their SDI levels predicted. Australasia and Southern Latin America showed elevated burden relative to their socioeconomic status. At the national level, New Zealand, Andorra, Belgium, Finland, and Australia all presented higher-than-expected skull fracture burden (**Figures 9–12**).

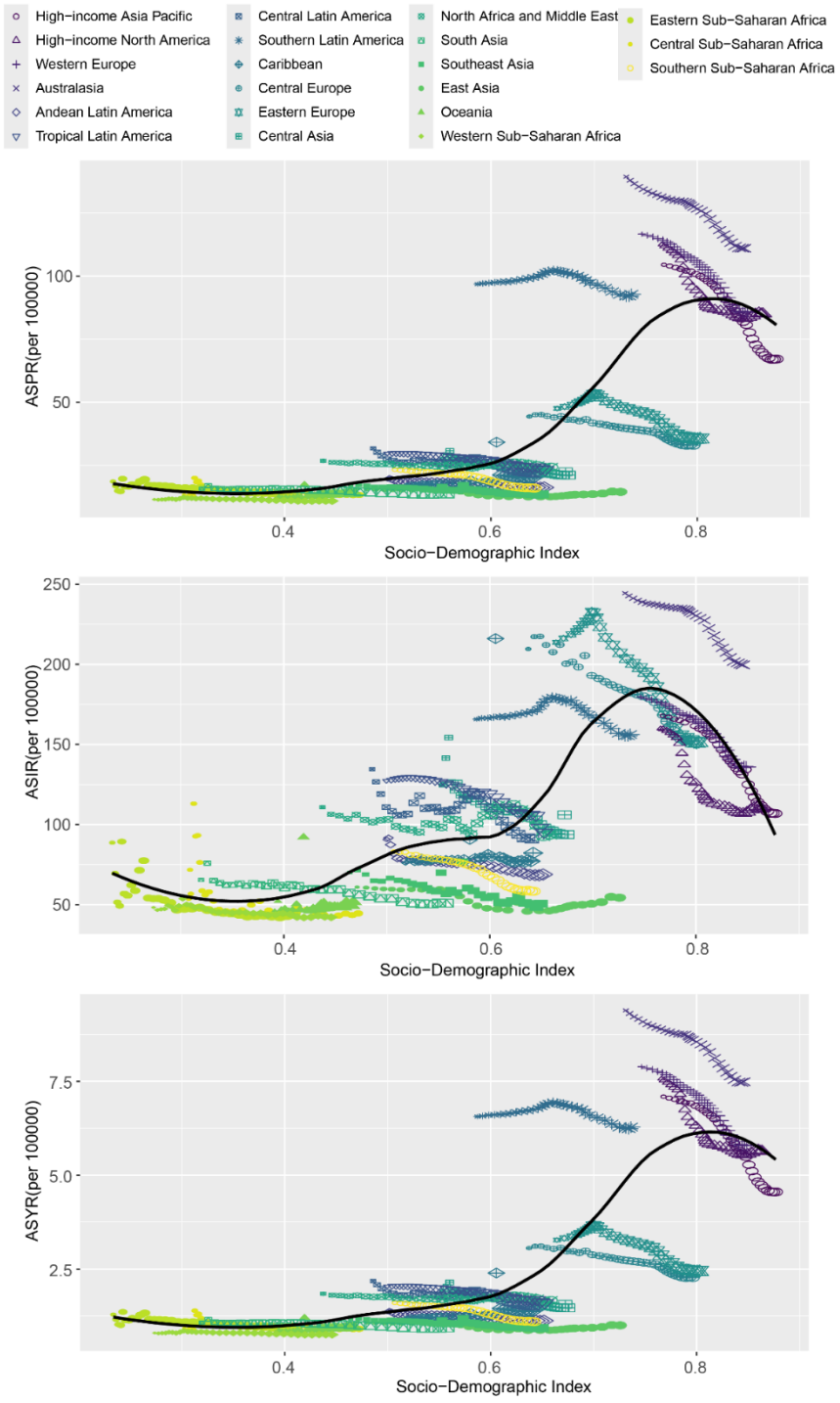

Figure 9. The associations between the SDI and ASR per 100,000 population of skull fractures across 21 GBD regions. (A) Prevalence; (B) Incidence; (C) YLDs SDI = Socio-Demographic Index, GBD = Global Burden of Disease; YLDs = Years lived with disability

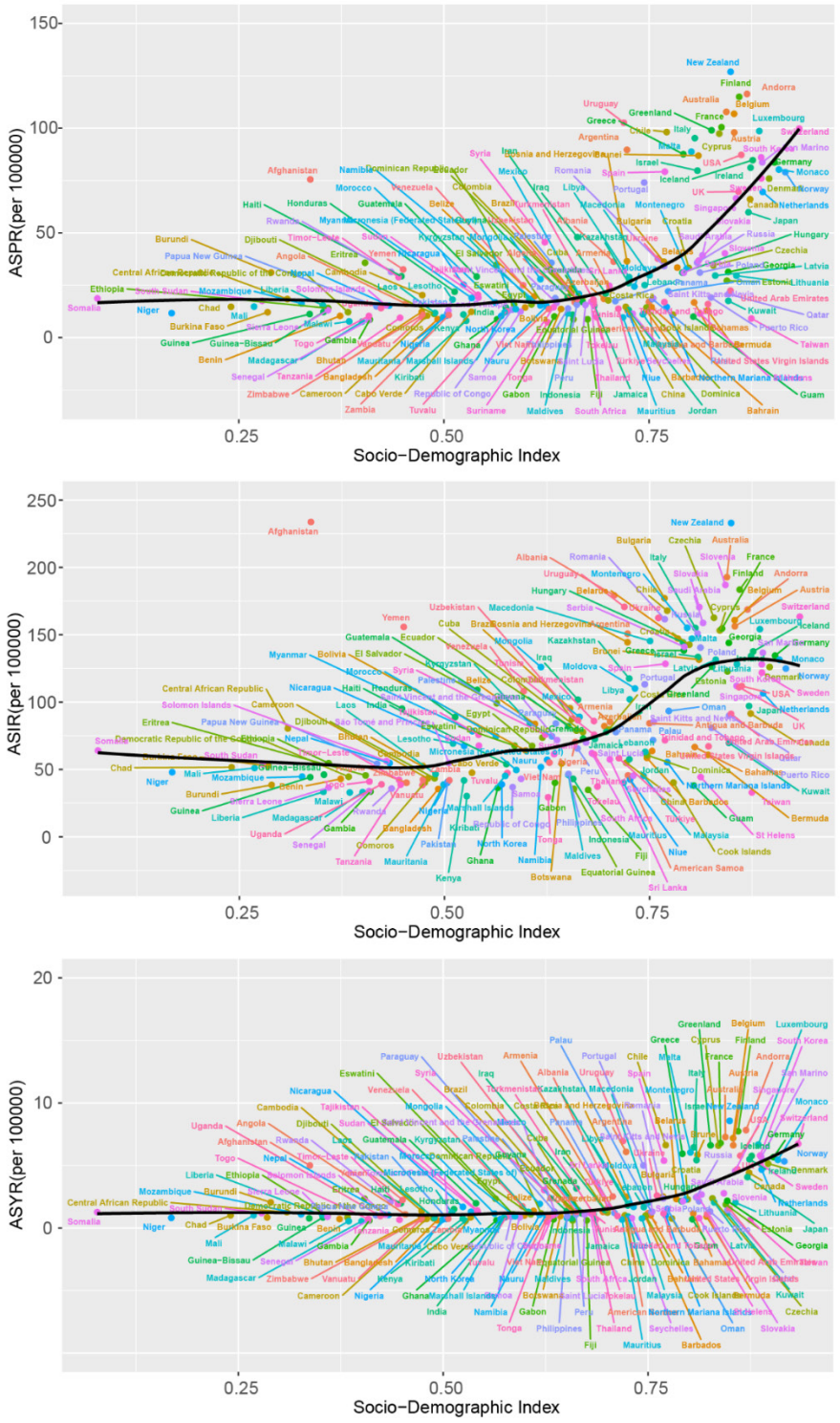

Figure 10. The associations between the SDI and ASR per 100,000 population of skull fractures across 204 GBD countries. SDI = Socio-Demographic Index, GBD = Global Burden of Disease

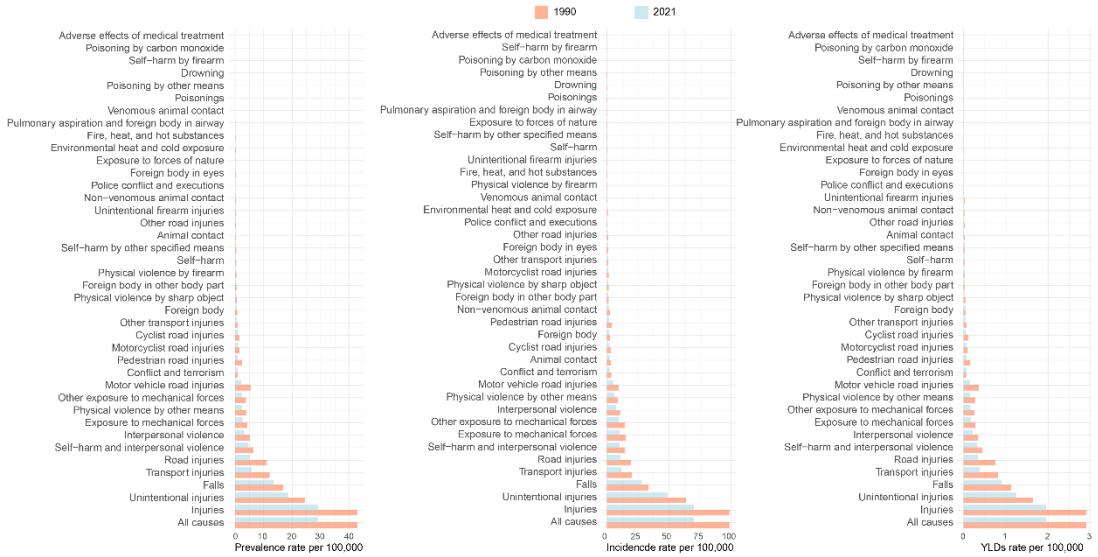

Figure 11. All causes of skull fractures. The cause composition of the number of ASPR (A), ASIR (C), and ASYR (E) of skull fractures between 1990 and 2021

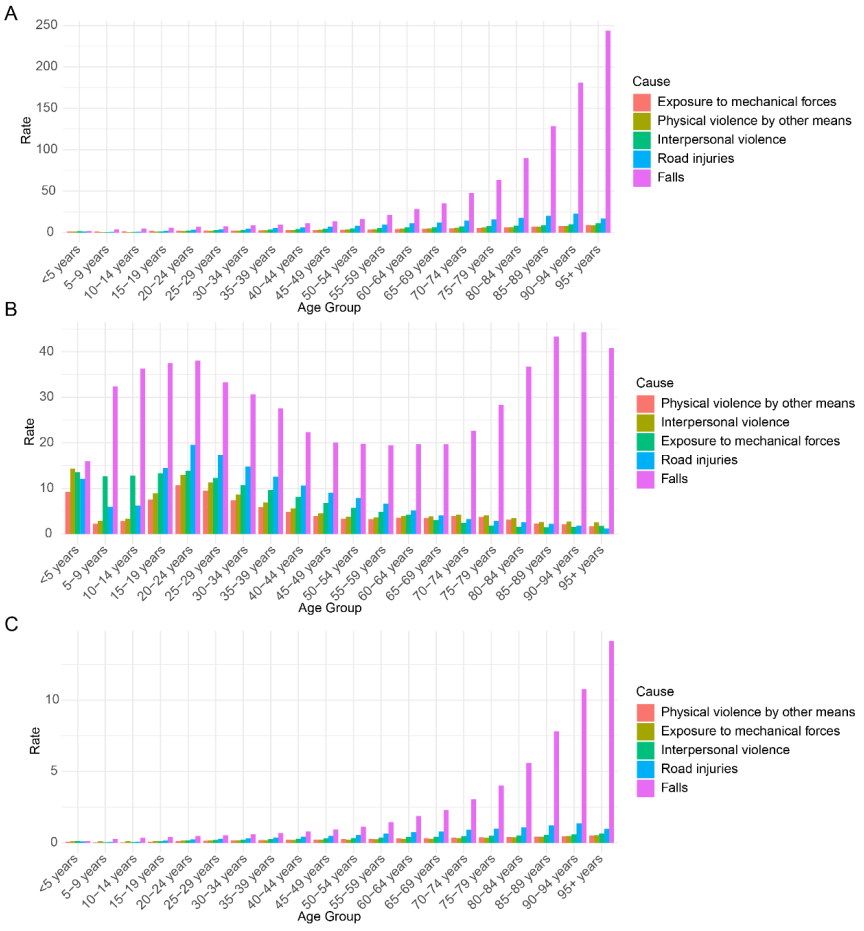

Figure 12. The top five level 3 causes for the ASR of prevalence (A), incidence(B), and YLDs (C) of facial fractures in different age groups in 2021

3.7. Disease burden from different etiologies

The GBD 2021 study identified various causes of skull fractures, detailed in Table S5. Falls were the leading cause, with an ASIR of 28.1 per 100,000 (95% UI: 15.4–49.4), ASPR of 13.6 per 100,000 (95% UI: 11.6–16.5), and ASYR of 13.6 per 100,000 (95% UI: 11.6–16.5) (**Figure 13**) While the overall ASR showed a declining trend, rates associated with conflict, terrorism, and police violence, including executions, increased. Prevalence and YLDs from falls rose significantly with age, and falls were the primary cause of fractures across all age groups. After age 40, fall incidence increased progressively, though a secondary peak was observed between ages 10 and 34 (**Figures 14–17**).

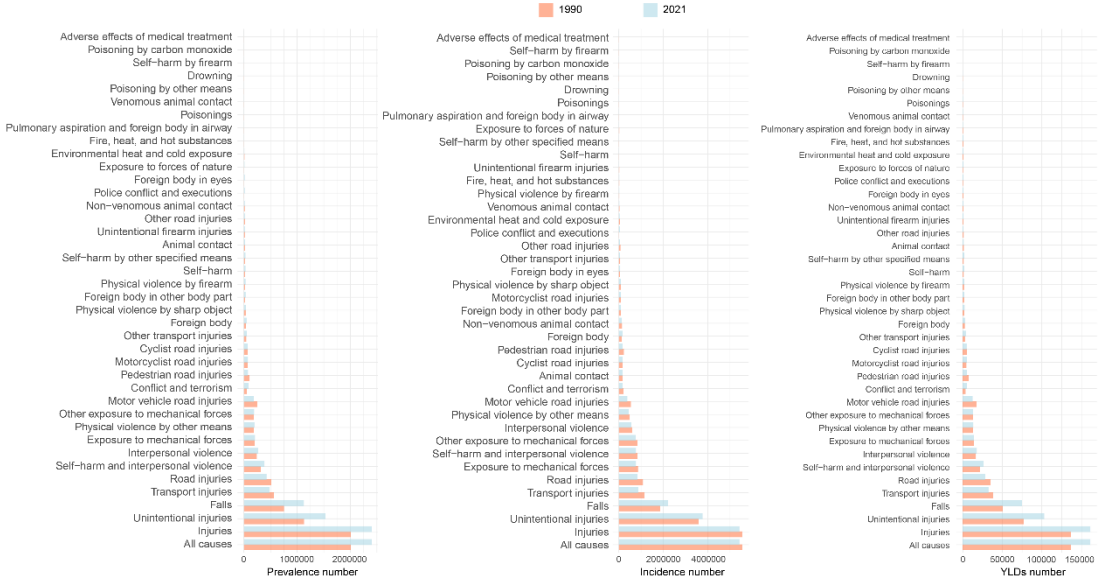

Figure 13. All causes of skull fractures. The composition of causes by prevalence. (A), Incidence (C), and YLDs (E) of skull fractures between 190 and 2021.

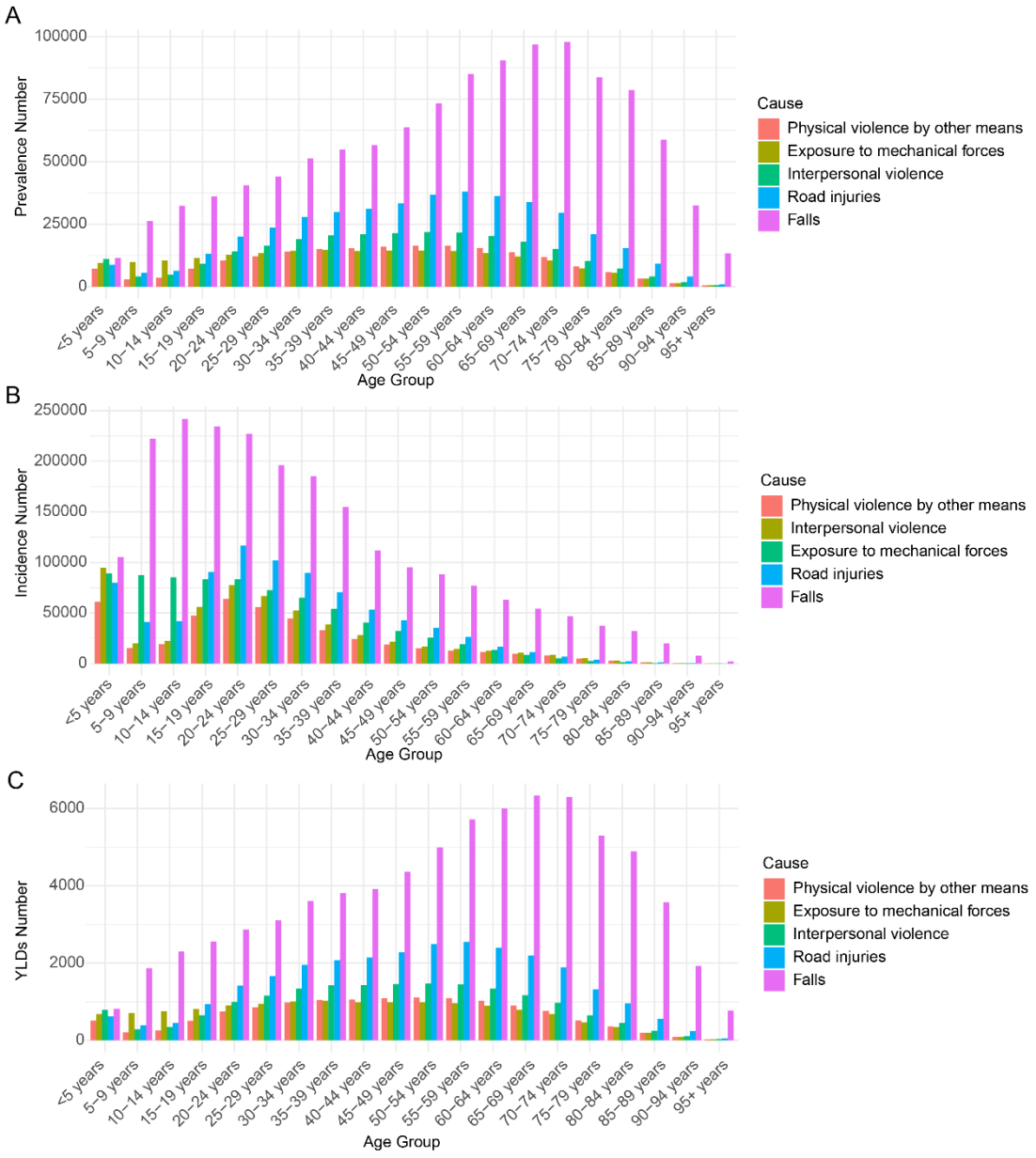

Figure 14. The top five level 3 causes by prevalence. (A), incidence (B), and YLDs (C) of facial fractures in different age groups in 2021

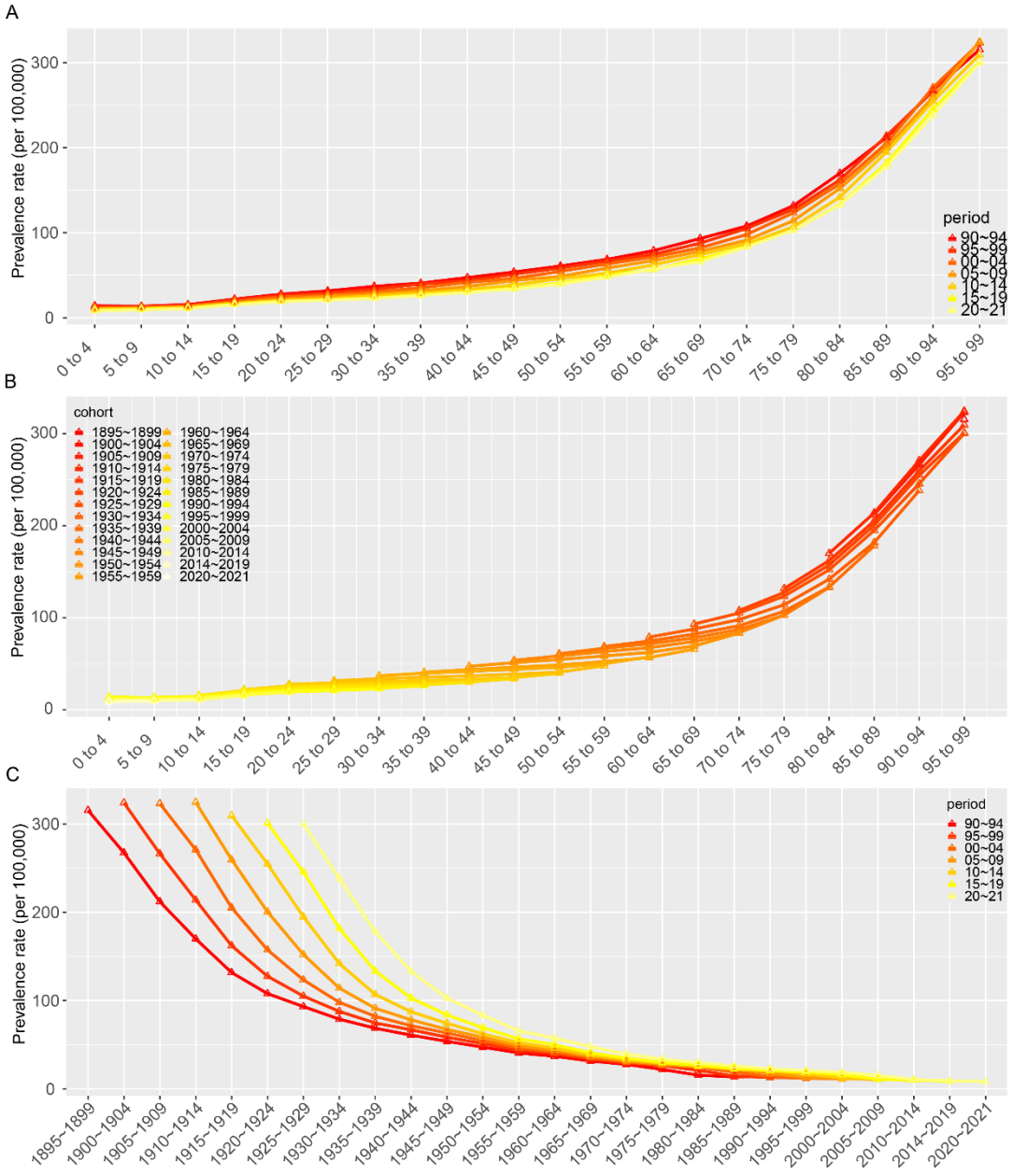

Figure 15. Age-period-cohort effects on skull fracture prevalence globally. (A) Age effects are shown by the fitted longitudinal age curves of prevalence (per 100,000 person-years) adjusted for period deviations. (B) Period effects are shown by the relative risk of prevalence (prevalence rate ratio) and computed as the ratio of age-specific rates from 1990 to 1994 (the referent period) to 2020-2021. (C) Cohort effects are shown by the relative risk of prevalence and computed as the ratio of age-specific rates from the 1895 cohort to the 2020 cohort

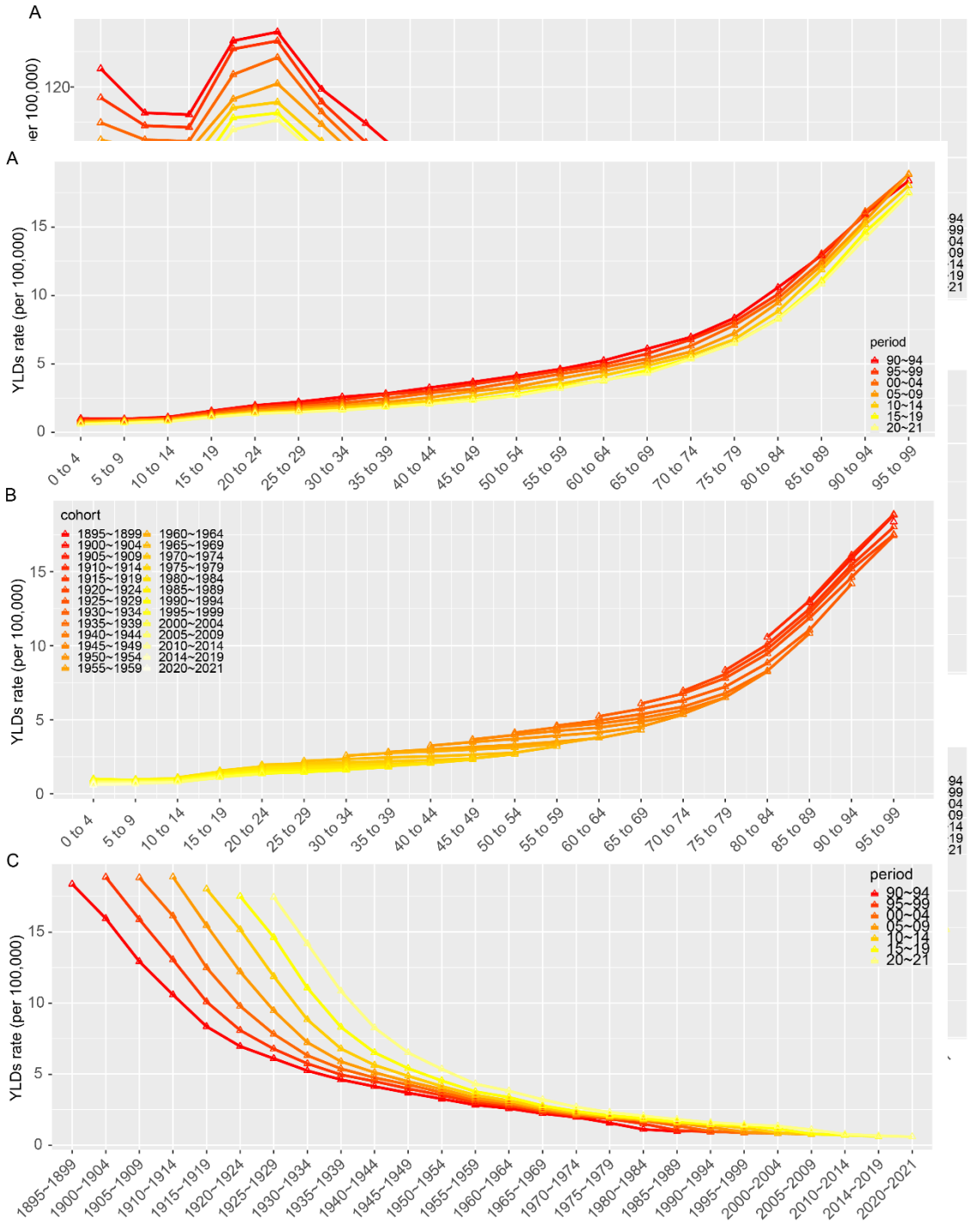

Figure 17. Age-period-cohort effects on skull fractures YLDs globally

3.8. Age-period-cohort analysis

The study also used the APC model to analyze the burden of skull fractures. Globally, the incidence of the age effect peaked at 20–24 years and nadir at 65–69 years. The incidence of skull fractures in the pediatric and teenage group is higher than in the adult and elderly group. As the years progress (period 1990–1994 to period 2020–2021), the incidence of the disease gradually decreases across all age groups except the 80+ age group.

3.9. Joinpoint regression analysis

The study employed the joinpoint regression model to detect shifts in the phase trends of the global burden of skull fractures. **Figure 18** presents the trends in prevalence, incidence, and YLDs related to skull fractures over the past three decades. Overall, the ASIR exhibited a general downward trend globally and across different SDI regions. However, the ASPR and ASYR exhibited a general downward trend globally and across different SDI regions according to the AAPC values, with the exception of Low SDI regions, from 1990 to 2021.

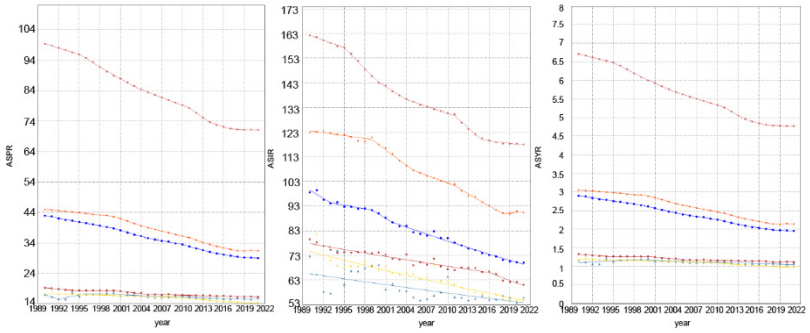

Figure 18. The trends of ASPR, ASIR, and ASYR of skull fractures in global and 5 SDI regions from 1990 to 2021

3.10. Forecasting the next 15 years' trends

The ARIMA model was applied to predict global skull fracture trends over the next 15 years. The forecasting results indicated consistent declines in age-standardized incidence, prevalence, and YLD rates worldwide, with similar downward trends observed across all SDI subgroups (**Figure 19**).

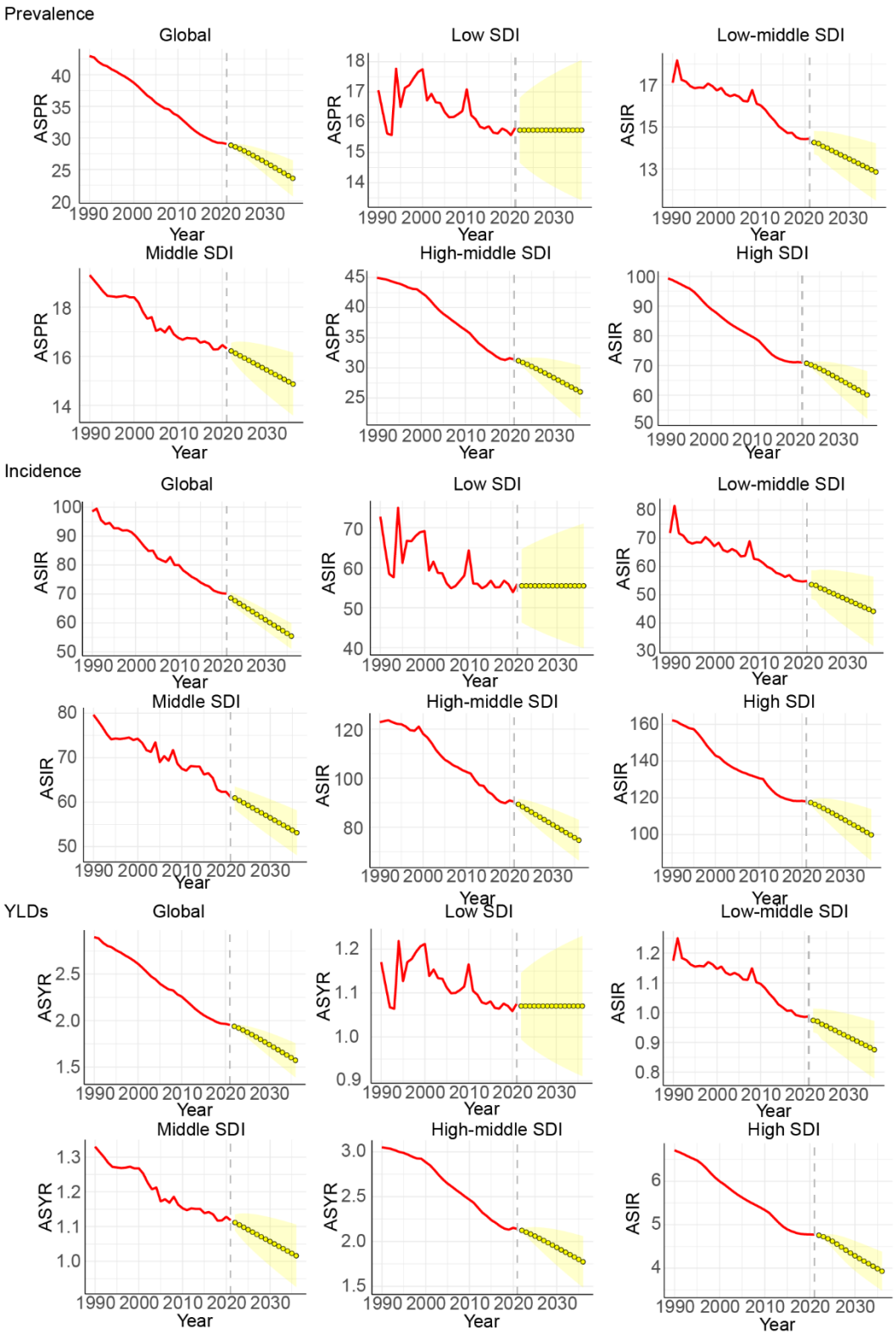

Figure 19. ASPR, ASIR, and ASYR of skull fractures in global and 5 SDI regions from 1990 to 2036

4. Discussion

Few previous studies have comprehensively assessed the global epidemiological features of skull fractures across different ages, sexes, and socioeconomic levels. This study adopted the standard GBD analytical framework to systematically evaluate global, regional, and national skull fracture burden trends from 1990 to 2021. Skull fractures are a major cause of long-term non-fatal disability, affecting populations worldwide and contributing substantially to global traumatic injury burden. Most skull fracture injuries are preventable, suggesting that targeted safety improvements and intervention measures can effectively reduce related public health losses.

Long-term trend analysis showed continuous decreases in global age-standardized incidence, prevalence, and YLD rates of skull fractures over the 31-year study period. This improvement is mainly attributed to fewer falls and traffic injuries, driven by decades of progress in public safety. Updated workplace safety rules have reduced fall-related skull injuries, while improved public traffic safety awareness and widespread head protection use have further lowered fracture risks. Notably, total prevalent cases and YLDs have continued to rise despite falling standardized rates. This opposite trend is mainly caused by global population growth and aging, which expand vulnerable populations and offset the benefits of reduced injury rates.

Correlation analysis confirmed that skull fracture burden positively correlates with regional socioeconomic development. SDI-stratified results revealed declining age-standardized fracture indicators across all five SDI tiers from 1990 to 2021. However, high-SDI regions recorded the largest number of incident cases and YLDs, indicating a heavier actual disease burden in developed regions despite their improving standardized trends.

Several factors explain the high absolute fracture burden in high-SDI regions. Developed regions have longer life expectancy and a larger elderly population. Aging is linked to higher osteoporosis risk and reduced skeletal stability, making older adults more susceptible to skull fractures. Ground-level falls are the leading cause of skull fractures in people aged 75 years and older [27], so population aging is a key driver of the high burden in high-income areas. In addition, high-SDI regions have mature healthcare systems and complete public health surveillance, ensuring full diagnosis and recording of fracture cases. This avoids underreporting, resulting in higher observed prevalence compared with low-resource regions with inadequate medical monitoring systems.

Large disparities in skull fracture burden existed across countries in 2021. Afghanistan had the highest global ASIR of skull fractures, followed by New Zealand, while Tonga had the lowest. The extremely high burden in Afghanistan stems from long-term armed conflicts and social unrest, which cause massive cranial trauma among civilians and military personnel [28–29]. Frequent explosions and violent clashes greatly increase fracture incidence. Poor road conditions, lax traffic management, and insufficient medical resources further worsen injury outcomes and delay treatment [30]. In contrast, Tonga has few traffic accidents and violent incidents, leading to low baseline head injury risk. Nevertheless, its scattered population and limited public health resources restrict systematic epidemiological monitoring, resulting in incomplete case documentation.

Sex-based differences in skull fracture burden were obvious in this study. Overall, males had higher fracture rates than females. Male incidence peaked at 20–24 years, an age group prone to high-risk behaviors including reckless driving, extreme sports, and physical conflicts, which increase cranial trauma risk. Males maintained higher age-standardized prevalence and YLD rates than females before age 90. For females, skull fracture burden was mainly concentrated in early childhood, with stable incidence in older age groups.

Children and adolescents had a higher skull fracture burden than adults and middle-aged populations, mainly due to frequent accidental trauma and risky behaviors. Blunt force trauma, traffic collisions, high falls, and stair accidents are the main causes of pediatric and adolescent skull fractures [31]. Consistent with previous studies, the results showed peak fracture burden at 20–24 years and the lowest burden at 65–69 years, with a marked increase in risk among people over 80 years old. The elevated fracture risk in the elderly is closely related to age-related osteoporosis and increased fall susceptibility [32].

The findings show that, globally, there were 5 major causes of skull fractures, including falls, road injuries, exposure to mechanical forces, interpersonal violence, and physical violence by other means. Falls represent the primary cause of hospitalized traumatic head injuries in young children, with most pediatric patients admitted for fall-related cranial trauma aged below one year. In such pediatric injury cases, simple linear parietal skull fractures constitute the most prevalent radiological abnormality, while a subset of patients also present concomitant extracranial hemorrhage [33]. Compared with standing-level falls, falls from elevated heights — including falls from caregivers' arms and stair tumbles — substantially increase the risk of sustaining skull fractures in children [34]. Beyond accidental trauma, global political turbulence, territorial disputes and external intervention have contributed to rising incidents of armed conflict, terrorism and violent confrontations. Such instabilities have driven a notable surge in traumatic head injuries and skull fractures, predominantly affecting conflict-prone regions including Ukraine, Russia, Sudan, Palestine, Israel, Yemen and the Sahel area.

This study found a gradual decline in global age-standardized skull fracture prevalence, while the total number of affected individuals continues to rise. High-risk groups included children, adolescents, males, and the oldest-old population (over 80 years old). Geographically, Australia, the Caribbean, and conflict-affected regions bore a disproportionately high burden. These findings call for targeted public health interventions to reduce skull fracture prevalence. Effective measures include safety education for young people, improved occupational safety for working-age males, and fall-prevention programs for the elderly, especially in aging high-SDI regions. Reducing regional conflicts is also critical for lowering trauma-related fractures. In addition, the 15-year prediction results suggest that the global skull fracture burden will gradually decrease in the future.

5. Limitations

This study has several limitations. First, all data were obtained from registered medical records and public health databases, which may underestimate the true global skull fracture incidence. Registry data often exclude mild, undiagnosed, and non-hospitalized cases, leading to incomplete population-level case collection. Second, severe underreporting exists in conflict areas. War-related skull injuries are rarely fully recorded during military conflicts, with the Russia–Ukraine conflict as a typical example of overlooked battlefield cases. Third, underdeveloped regions with limited healthcare funding and facilities lack standardized diagnosis and systematic surveillance. Insufficient medical recording capacity in these areas creates gaps between estimated fracture burden and actual epidemiological conditions.

6. Conclusion

In conclusion, while global age-standardized rates of skull fracture incidence, prevalence, and YLDs are

declining, the absolute number of prevalent cases and YLDs continues to rise. Reducing skull fracture incidence requires improved injury prevention strategies, greater public awareness, and robust safety measures. Stabilizing regional conflicts is also essential. Establishing a global skull fracture registry could enhance burden measurement, support research, and improve future epidemiological assessments. The burden of skull fractures is projected to decline over the next 15 years.

Disclosure statement

The authors declare no conflict of interest.

References

[1] Feigin V, Nichols E, Alam T, et al. Global, Regional, and National Burden of Neurological Disorders, 1990–2016: A Systematic Analysis for the Global Burden of Disease Study 2016. The Lancet Neurology, 2019(18): 459–480.

[2] Ye Z, Li Z, Zhong S, et al., 2024, The Recent Two Decades of Traumatic Brain Injury: A Bibliometric Analysis and Systematic Review. International Journal of Surgery (London, England), 110(6): 3745–3759.

[3] GBD 2016 Traumatic Brain Injury and Spinal Cord Injury Collaborators, 2019, Global, Regional, and National Burden of Traumatic Brain Injury and Spinal Cord Injury, 1990–2016: A Systematic Analysis for the Global Burden of Disease Study 2016. The Lancet. Neurology, 18(1): 56–87.

[4] Maas AIR, Menon DK, Adelson PD, et al., 2017, Traumatic Brain Injury: Integrated Approaches to Improve Prevention, Clinical Care, and Research. The Lancet. Neurology, 16(12): 987–1048.

[5] Maas AIR, Menon DK, Manley GT, et al., 2022, Traumatic Brain Injury: Progress and Challenges in Prevention, Clinical Care, and Research. The Lancet. Neurology, 21(11): 1004–1060.

[6] Dewan MC, Rattani A, Gupta S, et al., 2018, Estimating the Global Incidence of Traumatic Brain Injury. Journal of Neurosurgery, 130(4): 1080–1097.

[7] Bullock MR, Chesnut R, Ghajar J, et al., 2006, Surgical Management of Depressed Cranial Fractures. Neurosurgery, 58(3 Suppl): S56–60.

[8] Powell EC, Atabaki SM, Wootton-Gorges S, et al., 2015, Isolated Linear Skull Fractures in Children with Blunt Head Trauma. Pediatrics, 135(4): e851–857.

[9] Lin X, Yan Z, Kuang Z, et al., 2022, Fracture R-CNN: An Anchor-efficient Anti-interference Framework for Skull Fracture Detection in CT Images. Medical Physics, 49(11): 7179–7192.

[10] Engberg AW, Teasdale TW. A Population-based Study of Survival and Discharge Status for Survivors after Head Injury. Acta Neurologica Scandinavica, 110(5): 281–290.

[11] GBD 2021 Diseases and Injuries Collaborators, 2024, Global Incidence, Prevalence, Years Lived with Disability (YLDs), Disability-Adjusted Life-Years (DALYs), and Healthy Life Expectancy (HALE) for 371 Diseases and Injuries in 204 Countries and Territories and 811 Subnational Locations, 1990—2021: A Systematic Analysis for the Global Burden of Disease Study 2021. Lancet, 403(10440): 2133–2161.

[12] Stevens GA, Alkema L, Black RE, et al., 2016, Guidelines for Accurate and Transparent Health Estimates Reporting: the GATHER Statement. Lancet, 388(10062): e19–e23.

[13] Mathew G, Agha R, Albrecht J, et al., 2021, STROCSS 2021: Strengthening the Reporting of Cohort, Cross-sectional and Case-Control Studies in Surgery. International Journal of Surgery, 2021(96): 106165.

[14] Zura R, Xiong Z, Einhorn T, et al., 2016, Epidemiology of Fracture Nonunion in 18 Human Bones. JAMA

Surgery, 151(11): e162775.

[15] GBD 2021 Diseases and Injuries Collaborators, 2024, Global Incidence, Prevalence, Years Lived with Disability (YLDs), Disability-Adjusted Life-Years (DALYs), and Healthy Life Expectancy (HALE) for 371 Diseases and Injuries in 204 Countries and Territories and 811 Subnational Locations, 1990–2021: A Systematic Analysis for the Global Burden of Disease Study 2021. Lancet (London, England), 403(10440): 2133–2161.

[16] Liang Y, Dai X, Chen J, et al., 2025, Global Burden and Trends in Pre- and Post-Menopausal Gynecological Cancer from 1990 to 2019, with Projections to 2040: A Cross-Sectional Study. International Journal of Surgery (London, England) 111(1): 891–903.

[17] Zhang H, Huang D, Zhang Y, et al., 2023, Global Burden of Prostate Cancer Attributable to Smoking Among Males in 204 Countries and Territories, 1990–2019. BMC Cancer, 23(1): 92.

[18] Zhang ZX, Xie L, Li Z, 2024, Global, Regional, and National Burdens of Facial Fractures: A Systematic Analysis of the Global Burden of Disease 2019. BMC Oral Health, 24(1): 282.

[19] Yi Y, He X, Wu Y, et al., 2024, Global, Regional, and National Burden of Incidence, Prevalence, and Years Lived with Disability for Facial Fractures from 1990 to 2019: A Systematic Analysis for the Global Burden of Disease Study 2019. BMC Oral Health, 24(1): 435.

[20] Cen J, Wang Q, Cheng L, et al., 2024, Global, Regional, and National Burden and Trends of Migraine Among Women of Childbearing Age from 1990 to 2021: Insights from the Global Burden of Disease Study 2021. The Journal of Headache and Pain, 25(1): 96.

[21] Chen Q, Li T, Ding H, et al., 2024, Age-Period-Cohort Analysis of Epidemiological Trends in Pelvic Fracture in China from 1992 to 2021 and Forecasts for 2046. Frontiers in Public Health, 2024(12): 1428068.

[22] Rosengren BE, Björk J, Cooper C, et al., 2017, Recent Hip Fracture Trends in Sweden and Denmark with Age-Period-Cohort Effects. Osteoporosis International, 28(1): 139–149

[23] Xu B, Radojčić MR, Anderson DB, et al., 2024, Trends in Prevalence of Fractures among Adults in the United States, 1999–2020: A Population-Based Study. International Journal of Surgery (London, England), 110(2): 721–732

[24] Leslie WD, Yan L, Lix LM, et al., 2024, Time Dependency in Early Major Osteoporotic and Hip Re-Fractures in Women and Men Aged 50 Years and Older: A Population-Based Observational Study. Osteoporosis International, 33(1): 39–46.

[25] Wafa HA, Marshall I, Wolfe CDA, et al., 2024, Burden of Intracerebral Haemorrhage in Europe: Forecasting Incidence and Mortality between 2019 and 2050. The Lancet Regional Health. Europe, 2024(38): 100842.

[26] Zhang J, Zhu Y, Wang J, et al., 2024, Global Burden and Epidemiological Prediction of Polycystic Ovary Syndrome from 1990 to 2019: A Systematic Analysis from the Global Burden of Disease Study 2019. Plos One, 19(7): e0306991.

[27] Shibahashi K, Hoda H, Ishida T, et al., 2021, Older Adults with Traumatic Brain Injury in the Most Aged and Most Rapidly Aging Country: An Analysis of the Nationwide Trauma Registry of Japan. World Neurosurgery, 2021(150): e570–e576.

[28] Ashworth E, Baxter D, Gibb I, et al., 2023, Injuries in Underbody Blast Fatalities: Identification of Five Distinct Mechanisms of Head Injury. Journal of Neurotrauma. 40(1–2): 141–147.

[29] Risdall JE, Menon DK, 2011, Traumatic Brain Injury. Philosophical Transactions of the Royal Society of London. Series B, Biological Sciences, 366(1562): 241–250.

[30] Figueroa C, Linhart C, Fusimalohi L, et al., 2021, Mortality in Tonga over Three Triennia, 2010–2018. BMC

Public Health, 21(1): 36.

[31] Kirvelä A, Snäll J, Suominen A, et al., 2023, Characteristics of Associated Injuries in Children and Teenagers with Craniofacial Fractures. The Journal of Craniofacial Surgery, 34(6): 1625–1628.

[32] Watson WL, Mitchell R, 2011, Conflicting Trends in Fall-Related Injury Hospitalizations Among Older People: Variations by Injury Type. Osteoporosis International, 22(10): 2623–2631.

[33] Settle F, Lawrence D, Kummerow M, 2005, Pre-ambulatory Infants with Head Trauma: A Three-Year Retrospective Study. Journal of Paediatrics and Child Health, 41(3): 130–135.

[34] Burrows P, Trefan L, Houston R, et al., 2015, Head Injury from Falls in Children Younger than 6 Years of Age. Archives of Disease in Childhood, 100(11): 1032–1037.

Publisher's note

Bio-Byword Scientific Publishing remains neutral with regard to jurisdictional claims in published maps and institutional affiliations.

Clinical Neuroscience Research, 2026, Volume 4, Issue 3
https://bbwpublisher.com/journal/CNR
Online ISSN: 2981-8133
Print ISSN: 3083-4899

A Case Report of Schizophrenia Presenting with "Multiple Personality"-like Manifestations as the Initial Symptom

Feng Zhou, Lei Zhang, Yu Yan, Yuanping Wu, Yunfeng Yuan, Sufang Liu, Meilin Huang*

Department of Psychosomatics, Southwest Rehabilitation Hospital, Chengdu 610000, Sichuan, China

***Corresponding author:** Meilin Huang, xnyyhml@163.com

Copyright: © 2026 Author(s). This is an open-access article distributed under the terms of the Creative Commons Attribution License (CC BY 4.0), permitting distribution and reproduction in any medium, provided the original work is cited.

Abstract: *Objective:* To improve awareness of the differential diagnosis between schizophrenia and dissociative identity disorder (DID) and to reduce clinical misdiagnosis. *Methods:* The study reported the data of one adolescent patient who presented with prominent and complex "multiple personality"-like manifestations and was definitively diagnosed with schizophrenia after consultation with Professor Du Yasong at the Shanghai Mental Health Center. The clinical characteristics and key points of differential diagnosis were analyzed in conjunction with a literature review. *Results:* The patient was a 15-year-old male who initially presented with depressed mood and suicidal ideation. During the course of illness, three alternating independent "personalities" emerged ("Luomu," "Jiangyuling," and "Luofeiyu"). He had previously been diagnosed with "multiple personality disorder" and "major depressive disorder" at other hospitals. Following detailed mental status examination and expert consultation, the patient was found to have clear auditory hallucinations of a commentary and commanding nature, visual hallucinations (seeing a man following and frightening him), grandiose delusions (believing he could control other personalities within his body), affective incongruity, and severe impairment of social functioning. His "personality switching" was accompanied by partial disturbance of consciousness and memory loss, but he lacked a typical history of severe childhood trauma. The diagnosis was revised to schizophrenia. After treatment with risperidone, the psychotic symptoms improved significantly, the "personality switching" phenomenon gradually disappeared, and social functioning progressively recovered. *Conclusion:* For patients whose primary clinical presentation is "multiple personality"-like manifestations, the possibility of schizophrenia should be considered. Meticulous longitudinal history-taking, identification of core psychotic symptoms, and assessment of the state of consciousness and memory loss during "personality switching" are key to differential diagnosis.

Keywords: Schizophrenia; Dissociative identity disorder; Multiple personality

Online publication: October 19, 2026

1. Introduction

Schizophrenia is a group of severe mental disorders of unknown etiology, characterized by significant

abnormalities in multiple aspects of mental activity, including cognition, thinking, emotion, and behavior, and leading to marked impairment in occupational and social functioning. Dissociative identity disorder (DID), formerly known as multiple personality disorder (MPD), is characterized by the presence of at least two relatively enduring identities or disconnected personality states that alternately control the individual's behavior, accompanied by memory impairment for important events that cannot be explained by ordinary forgetfulness. This paper reports a case of schizophrenia in which "multiple personality"-like manifestations were the prominent clinical presentation and which had been misdiagnosed multiple times during the course of illness. Through analysis of the symptom evolution and review of key points in differential diagnosis, the authors aim to provide clinicians with insights for recognizing such atypical schizophrenia.

2. Clinical data

The patient, a 15-year-and-4-month-old male surnamed Chen, of Han ethnicity, a ninth-grade student from Guizhou, was admitted to the department on February 25, 2026, due to "depressed mood for over 2 years, accompanied by identity switching for over 9 months." He was the second of two siblings and had one older sister. His parents divorced when he was 13, and he lived with his father, who had a hot temper. The patient was introverted and had poor interpersonal relationships. He denied severe abuse, sexual assault, or long-term traumatic experiences during childhood.

Onset phase (early 2024 to March 2025): More than 2 years ago, after ending a friendship with a close friend, the patient gradually developed depressed mood, decreased interest, and social avoidance. When irritable, he used a knife to cut his arms and legs. He had planned to commit suicide by cutting his wrist, but during the attempt he suddenly became dazed and had complete amnesia for events of the previous 3 days. He also had difficulty falling asleep, poor concentration, and declining academic performance. He was sensitive and suspicious, believing that classmates were talking about him behind his back.

"Personality switching" phase (March to July 2025): Eleven months ago, auditory and visual hallucinations appeared without obvious triggers. The patient reported hearing voices out of nowhere telling him not to go to school, that life was meaningless, and to die; he also saw an adult male following him and verbally threatening him, which caused intense fear. He had visited Wenzhou Seventh People's Hospital (diagnosis and medication unknown), but treatment was ineffective. Ten months ago, after his family took him for a feudal superstitious "treatment," the "man" disappeared. About 3 days later, the patient experienced dissociative identity change for the first time, with complete amnesia for his own name and past experiences; he called himself "Luomu." This was transient, lasting 3–4 days before resolving spontaneously.

Nine months ago (from May 2025), after ending a relationship with an online friend, a second dissociated identity, "Jiangyuling," emerged. This identity was extroverted and lively, complementing the host personality. Eight months ago, after ending a friendship, a third dissociated identity, "Luofeiyu," appeared, characterized as intelligent and quick-witted, coexisting with the previous two personalities. During this phase, the host personality still intermittently appeared and remained depressed when dominant.

Pre-diagnosis phase (July 2025 to February 2026): Seven months ago, the host personality and the second personality "Jiangyuling" disappeared, and the third personality "Luofeiyu" became the long-term dominant identity. Two months ago, the third personality "Luofeiyu" again developed depressed mood and negative thoughts due to interpersonal problems, and visited Wenzhou Seventh People's Hospital, where

he was diagnosed with “multiple personality disorder” and treated with “aripiprazole and fluoxetine”; he discontinued the medication on his own due to perceived poor efficacy. One month ago, he visited Guiyang Second People’s Hospital and was diagnosed with “major depressive disorder” but did not take medication as prescribed. Half a month ago, the host personality disappeared again after being criticized by his father; thereafter, the third personality “Luofeiyu” and the second personality “Jiangyuling” alternately dominated.

Hospitalization and diagnosis phase: He was admitted to the hospital on February 25, 2026.

Post-admission auxiliary examinations: Complete blood count, liver and kidney function, thyroid panel (7 items), and sex hormones (6 items) showed no obvious abnormalities. Cardiac enzyme panel (4 items): creatine kinase 202 U/L ↑, creatine kinase-MB isoenzyme 28.2 U/L ↑. 25-hydroxyvitamin D 14.7 ng/mL ↓. Electrocardiogram: sinus arrhythmia, normal axis, J-point elevation. Cranial magnetic resonance imaging: 1. Formation of the fifth and sixth ventricles; 2. Incomplete adenoid regression; 3. Mild inflammatory changes in the paranasal sinuses. Please correlate with clinical findings.

Post-admission scale assessments: Social Disability Screening Schedule: presence of social functioning deficits. Activities of Daily Living Scale: some degree of functional decline. Self-Rating Depression Scale: 75 points, indicating severe depressive symptoms. Self-Rating Anxiety Scale: 52.5 points, indicating mild anxiety symptoms. Evoked potentials: P50 > 0.5, suggesting deficient sensory gating (anti-interference ability) of the brain, with an inability to filter out interference, indicating decreased attentional activity. MMN (mismatch negativity): moderately prolonged MMN latency, indicating reduced automatic processing of novel stimuli under conditions of no active attention, suggesting a depressive state. P300: able to accurately complete the task, normal target stimulus reaction time. P3b latency was moderately prolonged, suggesting cognitive decline during selective attention tasks. P3b amplitude showed no abnormality. Near-infrared brain function examination report: findings considered similar to characteristics of depression and anxiety tendencies. Positive and Negative Syndrome Scale: positive and negative symptoms suspicious; general psychopathology: mild. Eysenck Personality Questionnaire: psychoticism normal, introversion-extraversion typical introversion, neuroticism relatively stable, lie scale normal. Bech-Rafaelsen Mania Scale: 5 points, no obvious manic symptoms.

Diagnosis: 1. Multiple personality disorder; 2. Mental disorder, pending diagnosis. After admission, the patient was treated with risperidone 1 mg twice daily and psychotherapy. On March 5, 2026, a consultation was conducted by Professor Du Yasong from the Shanghai Mental Health Center: The patient was conscious and responded appropriately, but during communication, two other personalities emerged, with observed changes in facial expression, tone, and gaze, as well as soliloquy and affective incongruity. A history of command auditory hallucinations was elicited (hearing voices out of nowhere telling him “don’t go to school,” “life is meaningless,” “go die”), visual hallucinations (seeing an adult male following him), and self-report that he could control the other two personalities in his body, which constituted grandiose delusion; the other two personalities could converse with him and had emotional exchanges, which constituted auditory hallucinations and also contained elements of illogical thinking. He had not attended school for half a year, with severe impairment of social functioning. The final definitive diagnosis was schizophrenia, and an increase in risperidone dosage was indicated. After treatment with risperidone 2 mg twice daily, auditory and visual hallucination symptoms improved significantly, the “personality switching” phenomenon gradually disappeared, mood stabilized, and social functioning gradually recovered. At discharge, insight had recovered, and he recognized that the previous “personality” experiences were related to the illness.

3. Discussion and conclusions

This patient had been misdiagnosed with "multiple personality disorder" and "major depressive disorder" at multiple hospitals, with the misdiagnosis period lasting nearly one year. The fundamental reason lies in the fact that the patient's highly convincing "multiple personality"-like presentation masked the core symptoms of schizophrenia, leading clinicians to be misled by the surface phenomena. To reduce such misdiagnoses, meticulous differential diagnosis and analysis should be conducted from the following four key dimensions.

First: Differentiation of trauma history and triggering factors. According to the DSM-5-TR diagnostic criteria, the etiological basis of DID is almost always closely associated with prolonged, severe childhood trauma (such as repeated physical abuse, sexual abuse, or severe emotional neglect) [1]. Although this patient had a family environment involving parental divorce and a father with a volatile temper, detailed longitudinal history-taking definitively ruled out any history of severe childhood abuse or sexual assault, which fundamentally does not conform to the typical etiological characteristics of DID. Furthermore, "personality switching" in DID is usually unconsciously triggered by specific cues associated with traumatic memories (such as particular smells, scenes, or interpersonal stimuli). In contrast, the clear triggers for "personality switching" in this patient were interpersonal ruptures (ending a friendship with a close friend and breaking off contact with an online friend). This triggering pattern more likely reflects the generalization of relational delusions in schizophrenia—that is, heightened sensitivity and catastrophic interpretation of external interpersonal interactions—rather than dissociative identity dissociation.

Second: Assessment of consciousness state and memory gaps. Another core diagnostic criterion for DID is "recurrent memory gaps," whereby the individual experiences significant amnesia for events occurring during the period dominated by another personality after switching [1]. Although this patient reported brief episodes of mental clouding and memory gaps during the initial "personality switch," in the subsequent course of illness, the various "personalities" were able to know about each other, coexist, and even engage in emotional exchanges. This kind of "clear memory" and "active observation" of the process of self-identity disintegration likewise does not conform to the classic feature of "active amnesia" between personality states in DID. Instead, it is more commonly seen in ipseity disturbance in schizophrenia—that is, the disintegration of the patient's experience of themselves as a unified subject of thought, emotion, and action, from which pathological narratives of multiple selves emerge.

Third: The deceptive nature of symptom presentation and essential differences. The three "personalities" presented by the patient ("Luomu," "Jiangyuling," and "Luofeiyu") each possessed independent names, personality traits, and behavioral patterns, and could alternately dominate consciousness. This surface phenomenon is highly likely to be confused with DID. However, the core feature of DID lies in the "passive intrusion" and "loss of control" of personality states—that is, the individual experiences involuntary takeover by personality states [1]. This patient was exactly the opposite, claiming that he "could control the other personalities within his body." This awareness and active sense of control over multiple identities is not a feature of DID but is more consistent with grandiose delusions or thought-logic disorder in schizophrenia—that is, the patient attempts to explain his abnormal self-experience using a delusional framework.

Fourth: Identification of core psychotic symptoms. This is the most critical and direct evidence in differential diagnosis. Although patients with DID may also experience auditory hallucinations, their hallucinations are mostly internal dialogues, flashbacks of traumatic memories, or internal communication between different personalities, and usually do not have the typical characteristics of auditory hallucinations

in schizophrenia. In contrast, this patient had already experienced clear auditory hallucinations of a commentary and commanding nature before the emergence of "personality switching," such as hearing voices out of nowhere saying "don't go to school," "there is no meaning in living," and "go die," accompanied by visual hallucinations (seeing an adult male following and frightening him). These persistent hallucinatory experiences, which are external, commanding, and threatening in nature, are characteristic symptoms of schizophrenia [2]. If clinicians are distracted by the "personality switching" phenomenon during consultation and neglect in-depth inquiry and assessment of these core psychotic symptoms, misdiagnosis can easily occur.

In summary, when encountering patients whose chief complaint is "multiple personality," clinicians should not be satisfied with phenomenological descriptions but must conduct a thorough and systematic psychiatric examination. The focus should be on: 1. Detailed tracing of childhood trauma history; 2. Careful assessment of the state of consciousness, degree of memory loss, and the patient's subjective sense of control during "personality switching"; 3. Particularly high vigilance and careful screening for the presence of core psychotic symptoms such as auditory hallucinations of a commentary and commanding nature and delusions. Only through comprehensive and dynamic assessment across multiple dimensions—including history, triggering factors, nature of hallucinations, and state of consciousness—can schizophrenia and dissociative identity disorder be accurately distinguished, misdiagnosis avoided, and precise treatment plans formulated for patients. In this case, after adequate treatment with risperidone, the psychotic symptoms and the "personality switching" phenomenon disappeared simultaneously, which conversely confirmed the correctness of the schizophrenia diagnosis.

Funding

Project of Chengdu Municipal Health Commission (No. 2025541); Joint Innovation Fund of Chengdu Municipal Health Commission and Chengdu Medical College (WXLHCXJJ25-13).

Disclosure statement

The authors declare no conflict of interest.

References

[1] American Psychiatric Association, 2022, Diagnostic and Statistical Manual of Mental Disorders (5th ed., text rev.). American Psychiatric Publishing, Washington, DC.

[2] Foote B, Park J, 2008, Dissociative Identity Disorder and Schizophrenia: Differential Diagnosis and Theoretical Issues. Current Psychiatry Reports, 10(3): 217–222.

Publisher's note

Bio-Byword Scientific Publishing remains neutral with regard to jurisdictional claims in published maps and institutional affiliations.

Clinical Neuroscience Research, 2026, Volume 4, Issue 3
https://bbwpublisher.com/journal/CNR
Online ISSN: 2981-8133
Print ISSN: 3083-4899

Analysis of the Clinical Efficacy and Safety of CT-Guided Precision Nerve Block for the Treatment of Lumbar Disc Herniation

Pengfei Yao, Lu Cai*

Jiangyin Hospital of Traditional Chinese Medicine, Jiangyin 214400, Jiangsu, China

***Corresponding author:** Lu Cai, 396513625@qq.com

Copyright: © 2026 Author(s). This is an open-access article distributed under the terms of the Creative Commons Attribution License (CC BY 4.0), permitting distribution and reproduction in any medium, provided the original work is cited.

Abstract: *Objective*: To investigate the clinical efficacy and safety of CT-guided nerve block therapy in patients with lumbar disc herniation. *Methods*: The study population consisted of inpatients at our hospital diagnosed with lumbar disc herniation in the L4–L5 or L5–S1 segments. Patients were enrolled from December 2024 to June 2026, with a total sample size of 60 cases. Groups were assigned using a random number table, resulting in two groups, each with 30 cases. The control group received conventional epidural block therapy, while the observation group underwent CT-guided precise anterolateral epidural space block therapy. Clinical efficacy was assessed by comparing patients' Visual Analog Scale (VAS) pain scores and Oswestry Disability Index scores at preoperative, 3-day postoperative, 7-day postoperative, and 30-day postoperative follow-up visits. The safety parameters of CT-guided precise anterolateral epidural space block therapy were also analyzed. *Results*: Pain levels and the degree of lumbar functional impairment were assessed in both groups prior to intervention; there were no statistically significant differences in the assessment indicators between the groups ($P > 0.05$). In the observation group, the Visual Analog Scale (VAS) pain scores and Oswestry Disability Index scores at 3 days, 7 days, and 30 days postoperatively were all lower than those in the control group ($P < 0.05$). The overall response rate in the observation group was higher than that in the control group ($P < 0.05$). No cases of precise block failure were observed in the observation group; the distance between the medial margin of the articular process and the lateral margin of the dural sac ranged from a minimum of 3.0 mm to a maximum of 5.8 mm. *Conclusion*: CT-guided precise nerve block therapy for lumbar disc herniation is highly effective, providing significant pain relief and alleviating lumbar dysfunction. The minimum safe distance observed in this cohort between the medial margin of the articular process and the lateral margin of the dural sac was 3.0 mm.

Keywords: CT-guided precise nerve block; Lumbar disc herniation; Clinical efficacy; Safety

Online publication: October 19, 2026

1. Introduction

Lumbar disc herniation is a common degenerative condition in clinical practice. When intervertebral disc tissue herniates and compresses the nerve roots, it causes symptoms such as lower back and leg pain, sensory abnormalities in the lower extremities, and motor dysfunction, severely impacting patients' quality of life [1]. While many patients experience significant symptom relief following conservative treatment and physical therapy, some patients still have poor treatment outcomes and require nerve block therapy to alleviate their discomfort [2–3]. Conventional epidural blocks involve blind puncture guided by superficial anatomical landmarks. Although this procedure is simple, the puncture process is significantly influenced by individual anatomical variations, resulting in poor puncture accuracy and insufficient targeted drug distribution, which in turn affects treatment efficacy. With the continuous advancement of interventional imaging techniques, CT-guided nerve blocks enable visualization of the puncture path, allowing for precise localization of the anterolateral epidural space and improving both the safety of the puncture and the targeted distribution of the medication [4]. CT-guided precise nerve block therapy has been applied in the field of neuropathic pain treatment with good analgesic outcomes; however, research on its use in the treatment of lumbar disc herniation is scarce. Based on this, this study will analyze the clinical efficacy of CT-guided precise nerve block therapy for lumbar disc herniation and determine the minimum safe distance for puncture, thereby providing a basis for the further clinical promotion and application of this therapeutic approach.

2. Materials and methods

2.1. General materials

The study sample consisted of patients hospitalized at our hospital with a confirmed diagnosis of lumbar disc herniation at the L4–L5 or L5–S1 segments. Cases were enrolled from December 2024 to June 2026, with a total sample size of 60 patients. Grouping was performed using a random number table, resulting in two groups, each with 30 patients. Control Group: 17 males and 13 females; age range 33–68 years, mean (50.45 ± 8.69) years; affected segments: 18 cases in the L4–L5 segment and 12 cases in the L5–S1 segment. Observation Group: 16 males and 14 females; ages ranging from 32 to 67 years, with a mean age of (49.08 ± 8.41) years; affected segments: 17 cases at the L4–L5 segment and 13 cases at the L5–S1 segment. The general demographic characteristics of the two groups were comparable ($P > 0.05$), meeting the criteria for intergroup comparison.

2.1.1. Inclusion criteria

(1) Meets the diagnostic criteria for lumbar disc herniation, with disc herniation at the L4-L5 or L5-S1 levels [5];

(2) First episode of related clinical symptoms, with a disease duration of < 2 weeks; (3) History of recurrence, currently in the acute phase;

(4) Chronic lumbar disc herniation with an established clinical diagnosis, for which standard conservative treatment has been administered for at least 3 months with poor results;

(5) Age 20~70 years.

2.1.2. Exclusion criteria

(1) Severe organic lesions of the spinal canal or tuberculosis;

(2) Concomitant organ lesions, malignant tumors, hematological disorders, etc.;
(3) Conditions associated with mental disorders;
(4) Severe localized skin infections or open wounds;
(5) A history of hyperthyroidism or a pathological condition predisposing the body to bleeding.

2.2. Methods

The control group received conventional epidural block therapy: The patient was positioned in the lateral decubitus position. The interspinous space at the lesion site was identified, disinfected according to standard procedures, and anesthetized locally. A No.12, 10 cm lumbar epidural needle was then slowly advanced, sequentially penetrating the supraspinous and interspinous ligaments. A distinct sense of giving way was felt upon penetrating the yellow ligament; there was no resistance when air was injected, and no blood or cerebrospinal fluid was observed upon aspiration. The analgesic mixture was then slowly injected (containing 3 mL of inflammatory immune extract from rabbits vaccinated with bovinepox vaccine, 100 mg of vitamin B6, 1 mg of vitamin B12, 50 mg of 2% lidocaine, and 2.5 mL of normal saline) at a total volume of 10 mL. After treatment, the patient is observed in a supine position for 30 minutes.

The observation group underwent CT-guided precise anterolateral epidural space block: Using a multi-slice spiral CT scanner (Siemens SOMATOM go.Up), the patient was positioned prone with a thin pillow placed under the abdomen. A plain CT scan was performed to identify the puncture site. The medial margin of the affected facet joint was designated as the primary target, and the superficial projection points of the puncture path were marked with a positioning pen. After disinfecting the lumbosacral region, a sterile drape was applied. Following local anesthesia of the puncture site with 1% lidocaine, a 1.0 mm diameter, 10 cm long puncture needle was inserted at the marked point, entering the spinal canal vertically along the medial margin of the facet joint. A distinct sensation of breakthrough was felt as the needle tip passed through the ligamentum flavum. The needle core was then withdrawn, and an empty syringe was attached. After confirming that no blood or cerebrospinal fluid is aspirated, proceed under real-time CT guidance along the puncture path to position the needle tip in the anterolateral epidural space at the level of the target intervertebral space. Inject a small amount of contrast agent locally; once the contrast agent is observed to diffuse into the epidural space and around the nerve roots, and after confirming that it has not entered the subarachnoid space, slowly inject the analgesic mixture (containing 3 mL of inflammatory immune extract from rabbits vaccinated with vaccinia virus, 100 mg of vitamin B6, 1 mg of vitamin B12, 50 mg of 2% lidocaine, and 2.5 mL of normal saline) for a total of 10 mL. Withdraw the needle, apply pressure to the puncture site for 5 minutes, and cover with a sterile dressing.

2.3. Monitoring indicators

2.3.1. Pain intensity

Assessed using the Visual Analog Scale at preoperative, 3 days postoperative, 7 days postoperative, and 30 days postoperative follow-up visits. Scores range from 0 to 10, with higher scores indicating more severe pain.

2.3.2. Oswestry disability index

Assessed at preoperative, 3 days postoperative, 7 days postoperative, and 30 days postoperative follow-up visits. It consists of 10 items, with a total score ranging from 0 to 50; a higher score indicates a more severe

degree of lumbar dysfunction.

2.3.3. Efficacy assessment

Efficacy was determined based on the Oswestry Disability Index score. The efficacy index is defined as the percentage of the difference between the baseline and follow-up scores relative to the baseline score; a value of 90% or higher is classified as "cured," 70% or higher but less than 90% as "marked improvement," 30% or higher but less than 70% as "improvement," and less than 30% as "no improvement." Overall Response Rate = (Number of cases classified as "Complete Remission" + "Marked Improvement" + "Improvement") / Total Number of Cases × 100%.

2.3.4. Determination of the safe range

The observation group underwent real-time CT monitoring during the puncture procedure to measure the distance between the medial margin of the articular process and the lateral margin of the dural sac. If the patient experienced intolerable pain, or if the contrast agent diffused into the subarachnoid space after the puncture—indicating failure of precise nerve block—this distance is not suitable for precise nerve block therapy and carries a high risk.

2.4. Statistical methods

Statistical analysis of all data in this study was performed using SPSS 26.0 statistical software. Quantitative data followed a normal distribution and are presented as ($\overline{x} \pm s$); independent samples *t*-tests were used for comparisons between groups. Count data are presented as [n(%)], and a x^2 test is performed. Statistical significance was set at $P < 0.05$.

3. Results

3.1. Comparison of pain intensity

As shown in **Table 1**, there was no statistically significant difference in preoperative visual analog scale pain scores between the two groups ($P > 0.05$). However, when comparing the postoperative assessment results at different time points (3 days, 7 days, and 30 days) between the two groups, the scores in the observation group were lower than those in the control group ($P < 0.05$).

Table 1. Comparison of pain intensity ($\overline{x} \pm s$, scores)

Category	Preoperative	3 days postoperative	7 days postoperative	30 days postoperative
Control group (*n*=30)	7.19±1.07	5.12±0.91	4.06±0.84	2.75±0.72
Observation Group (*n*=30)	7.25±1.11	3.73±0.76	2.38±0.68	1.31±0.42
t value	0.213	6.421	8.514	9.462
P value	0.832	<0.001	<0.001	<0.001

3.2. Comparison of the Oswestry Disability Index

As shown in **Table 2**, the Oswestry Disability Index scores were comparable between the two groups at baseline, with no statistically significant difference ($P >0.05$); however, when comparing the postoperative assessment results at different time points (3 days, 7 days, and 30 days) between the two groups, the scores in

the observation group were lower than those in the control group ($P < 0.05$).

Table 2. Comparison of the Oswestry Disability Index ($\overline{x} \pm s$, scores)

Category	Preoperative	3 days postoperative	7 days postoperative	30 days postoperative
Control group (n=30)	61.68±7.38	51.16±6.79	41.07±6.32	30.62±5.68
Observation Group (n=30)	62.52±7.22	40.37±6.18	28.84±5.46	16.31±4.41
t value	0.446	6.437	8.021	10.900
P value	0.658	<0.001	<0.001	<0.001

3.3. Comparison of clinical efficacy

As shown in **Table 3**, the clinical efficacy evaluation revealed that the overall response rate in the observation group was higher than that in the control group ($P < 0.05$).

Table 3. Comparison of clinical efficacy [n (%)]

Category	Recovery	Taking effect	Valid	Invalid	Overall Efficiency
Control group (n=30)	12 (40.00)	7 (23.33)	4 (13.33)	7 (23.33)	23 (76.67)
Observation Group (n=30)	21 (70.00)	6 (20.00)	2 (6.67)	1 (3.33)	29 (96.67)
x^2 value	—	—	—	—	5.192
P value	—	—	—	—	0.023

3.4. Safety parameters for CT-guided precision nerve block therapy

None of the patients in the observation group experienced failure of precise blockage; the minimum distance between the medial margin of the articular process and the lateral margin of the dural sac was 3.0 mm, and the maximum was 5.8 mm.

4. Discussion

Lumbar disc herniation can cause pain in the lower back and legs. The primary pathological mechanism of this condition is the irritation of nerve roots by the herniated disc, leading to localized aseptic inflammation and tissue edema [6]. The mechanism of action for interventional nerve block therapy involves injecting anti-inflammatory and analgesic medications into the target area surrounding the nerve roots to alleviate local inflammation and clinical symptoms [7]. Conventional blind epidural block needle placement is subject to inaccuracies due to factors such as patient obesity and anatomical variations, which can easily cause the medication to diffuse into non-target spaces and compromise clinical efficacy. CT-guided precise nerve block therapy enables the visualization of the puncture path, target space, and surrounding critical anatomical structures, thereby overcoming the limitations of conventional puncture; however, its clinical efficacy and safety in patients with lumbar disc herniation require further clinical studies for validation.

In this study, there was no statistically significant difference in preoperative visual analog scale pain scores between the two groups ($P > 0.05$). However, when comparing the postoperative assessment results at different time points (3 days, 7 days, and 30 days), the scores in the observation group were lower than those in the control group ($P < 0.05$). This suggests that, compared with conventional epidural block therapy, CT-guided precise nerve block therapy can further alleviate pain. Analysis of the reasons: Conventional

epidural blocks involve blind puncture; in some patients, it is difficult to precisely position the needle tip in the lateral epidural space during the procedure, preventing the medication from fully acting on the target area of the affected nerve root, resulting in limited pain relief. CT guidance allows for the visualization of anatomical structures and the puncture path, enabling precise placement of the needle tip in the anterolateral epidural space of the affected segment [8]. This allows the medication to act concentrically on the compressed nerve root and the area of aseptic inflammation in the intervertebral disc, more effectively eliminating local inflammatory edema, blocking pain signal transmission, and significantly reducing pain intensity [9]. At baseline, the Oswestry Disability Index scores were comparable between the two groups, with no statistically significant difference ($P > 0.05$); however, when comparing the assessment results at different postoperative time points (3 days, 7 days, and 30 days), the scores in the observation group were lower than those in the control group ($P < 0.05$); the overall response rate in the clinical efficacy assessment was higher in the observation group than in the control group ($P < 0.05$). These findings suggest that, compared with conventional epidural block therapy, CT-guided precise nerve block therapy can further alleviate lumbar dysfunction and yield better clinical outcomes. Analysis of Causes: Lumbar dysfunction is caused by a combination of factors, including persistent lower back and leg pain, restricted lumbar mobility due to nerve root irritation, and protective muscle spasms. Since CT-guided precise nerve block can more thoroughly and sustainably alleviate inflammatory compression of the nerve roots, it provides greater relief from pain stimuli, thereby significantly reducing lumbar muscle spasm, eliminating factors that restrict lumbar spine mobility, and achieving more pronounced improvement in lumbar spine dysfunction, which in turn leads to better clinical treatment outcomes [10]. None of the patients in the observation group experienced failure of the precise block; the minimum distance between the medial margin of the articular process and the lateral margin of the dural sac was 3.0 mm, and the maximum was 5.8 mm. However, the minimum distance of 3.0 mm observed in this study represents only the lower limit of the measured values for this group of cases and cannot be regarded as a universal absolute safety threshold. In clinical practice, conditions such as lumbar osteophytes, thickening of the ligamentum flavum, and hypertrophy of the facet joints can all lead to a further narrowing of this space. Even with CT guidance, patients with such narrow spaces remain at a higher risk of dural injury. Clinically, the feasibility of puncture should be thoroughly assessed for these patients, and the approach or treatment plan should be modified as necessary.

5. Conclusion

In summary, CT-guided precise nerve block therapy for lumbar disc herniation is highly effective, providing significant pain relief and alleviating lumbar dysfunction. The minimum safe distance observed in this case series between the medial margin of the articular process and the lateral margin of the dural sac is 3.0 mm.

Funding

Jiangyin Science and Technology Innovation Special Fund (Social Development Science and Technology Demonstration Project), Project No. JY0603A011014240009PB.

Disclosure statement

The authors declare no conflict of interest.

References

[1] Xu B, Huang ZL, Zhang L, et al., 2023, Meta-analysis of the Prevalence of Lumbar Disc Herniation in the Chinese Population. Traditional Chinese Orthopedics, 2023, 35(9): 17–23.

[2] Xu SS, Wang Q, Wei C, 2026, A Study on the Efficacy of Early Acupuncture-Knife Therapy Following Neuroblockade Combined with Ozone Ablation in Patients with Lumbar Disc Herniation. Chinese Journal of Integrated Traditional and Western Surgery, 32(1): 19–23.

[3] Wang XW, Yang KX, Sun K, et al., 2023, Network Meta-Analysis of Nerve Block Combined with Traditional Chinese Medicine for the Treatment of Lumbar Disc Herniation. Journal of Hainan Medical University, 29(7): 530–539.

[4] Xu YM, Liu TT, Zhang ZL, et al., 2023, The Effect of CT-Guided Pulsed Radiofrequency Modulation Combined with Thoracic Paravertebral Nerve Block on Pain Severity and Quality of Life in Patients with Postherpetic Neuralgia. Stroke and Neurological Diseases, 30(1): 49–54.

[5] Basic Research and Translational Medicine Working Group, Spine and Spinal Cord Professional Committee, Chinese Society of Rehabilitation Medicine, 2022, Guidelines for the Diagnosis, Treatment, and Rehabilitation Management of Lumbar Disc Herniation. Chinese Journal of Surgery, 60(5): 401–408.

[6] Qiu ZJ, Zhou HC, 2023, Advances in the Puncture Technique for Lumbar Sympathetic Nerve Block. Chinese Journal of Pain Medicine, 29(1): 44–49.

[7] Xu YS, Zhang JH, Ma SS, et al., 2023, Observation on the Efficacy of Nerve Root Block Combined with Intervertebral Foramen Endoscopy for the Treatment of Lumbar Disc Herniation. Chinese Journal of Biomedical Engineering, 29(1): 72–76.

[8] Gao Q, Li BF, Liu B, et al., 2024, A Clinical Study on the Efficacy of CT-Guided Pulsed Radiofrequency Combined with Continuous Nerve Block for the Treatment of Intractable Postherpetic Neuralgia. Journal of Interventional Radiology, 33(3): 264–268.

[9] Tang B, Zhang L, Zhang Q, et al., 2022, A Discussion on the Clinical Value of CT- and Ultrasound-Guided Celiac Ganglion Block. Chinese Journal of CT and MRI, 20(5): 151–153.

[10] Zhao W, 2023, Efficacy and Safety of CT-Guided Percutaneous Trigeminal Ganglion Balloon Compression for Trigeminal Neuralgia in Awake Patients. Chinese Medical Journal, 103(7): 493.

Publisher's note

Bio-Byword Scientific Publishing remains neutral with regard to jurisdictional claims in published maps and institutional affiliations.

Clinical Neuroscience Research, 2026, Volume 4, Issue 3
https://bbwpublisher.com/journal/CNR
Online ISSN: 2981-8133
Print ISSN: 3083-4899

Diagnosis and Treatment Report of Parkinson's Disease Complicated by Cerebrovascular Disease, Mood Disorder, and Gastrointestinal Dysfunction

Haowen Zhang*

Laixi People's Hospital, Qingdao 266600, Shandong, China

Author to whom correspondence should be addressed.

Copyright: © 2026 Author(s). This is an open-access article distributed under the terms of the Creative Commons Attribution License (CC BY 4.0), permitting distribution and reproduction in any medium, provided the original work is cited.

Abstract: Parkinson's disease is a degenerative disease of the central nervous system with a high incidence in middle-aged and elderly people. In addition to typical motor impairment, non-motor symptoms can occur throughout the entire disease course, and mood disorders and gastrointestinal autonomic dysfunction are the most common comorbid manifestations. Clinically, Parkinson's motor symptoms, anxiety and depression, and gastrointestinal somatic symptoms interact with each other, forming a vicious cycle and increasing the difficulty of diagnosis and treatment. This article reports a 63-year-old male patient, Guo Zunbo, who successively underwent cataract intraocular lens implantation in the ophthalmology department of the hospital, visited the gastroenterology outpatient clinic multiple times for gastroesophageal reflux, and was diagnosed in the neurology department with primary Parkinson's disease, ischemic cerebrovascular disease, and comorbid anxiety and depression. After adding Madopar combined with pramipexole, the overall condition improved. This case suggests that when clinically encountering patients with Parkinson's disease, attention should not be limited to motor manifestations such as tremor and rigidity; clinicians should also actively identify mood and gastrointestinal autonomic impairment, while taking into account comorbidities in geriatric ophthalmology, break the interaction chain among multisystem symptoms, and improve the overall diagnosis and treatment effect in elderly patients with multiple coexisting diseases.

Keywords: Parkinson's disease; Autonomic dysfunction; Anxiety and depression; Gastroesophageal reflux; Intraocular lens implantation

Online publication: October 19, 2026

1. Disease overview

Parkinson's disease (PD) is a common chronic progressive degenerative disease of the central nervous system in neurology, mostly seen in middle-aged and elderly people. Traditional understanding focuses on the four

core motor symptoms: bradykinesia, resting tremor, rigidity, and postural instability. Recent clinical studies have confirmed that Parkinson's disease extensively involves the limbic system and autonomic nerve centers of the brain, and non-motor symptoms may appear earlier than motor symptoms and persist throughout the entire disease course [1]. Among various non-motor symptoms, mood disorders and gastrointestinal dysfunction have the highest comorbidity rate. Elderly patients often have multiple systemic diseases such as cataracts and cardiovascular and cerebrovascular diseases, and multimorbidity further increases the difficulty of clinical assessment and medication management [2].

2. Case summary

The patient, Guo Zunbo, is a 63-year-old male farmer currently residing in Laixi City. Chief complaints: dizziness, slow response, and bradykinesia for 11 months, with recurrent intermittent pharyngeal foreign body sensation. The disease began 11 months ago without clear inducement, with dizziness accompanied by slow response and limb bradykinesia, aggravated after activity, without limb hemiplegia, and with a chronic progressive course. He had an anxious tendency, and emotional fluctuations could induce pharyngeal foreign body sensation. He had been diagnosed with gastroesophageal reflux and treated symptomatically. Parkinson's disease was diagnosed in the neurology department, and symptoms improved significantly after treatment with Madopar combined with pramipexole; occasional palpitations and arrhythmia improved after drug intervention. In April 2026, he underwent bilateral intraocular lens implantation for senile cataract, and postoperative visual acuity recovered to 1.0. He had a history of anxiety and had taken flupentixol, melitracen, and flunarizine. He had a long history of alcohol consumption, now abstinent, and his daily hobby is table tennis. Previous examinations showed emphysema, right pulmonary bullae, small bilateral pulmonary nodules, and aortic and coronary artery calcification; atrophic gastritis with pyloric ostium inflammation and bile reflux. No history of drug allergy. Physical examination: clear consciousness, poor mental state, masked facies, normal muscle strength in the limbs, and increased muscle tone. No abnormalities in the heart, lungs, or abdomen. Bilateral intraocular lenses in place, visual acuity 1.0, and normal intraocular pressure. Auxiliary examinations: electrocardiogram showed sinus arrhythmia and ST-T changes; chest CT and gastroscopy findings were the same as before; upper abdominal CT showed no obvious abnormalities.

3. Diagnosis and differential diagnosis

3.1. Clinical diagnosis

(1) Parkinson's disease
(2) Ischemic cerebrovascular disease
(3) Anxiety and depression (Parkinson's disease-related mood disorder with gastrointestinal somatization symptoms)
(4) Chronic atrophic gastritis with bile reflux and gastroesophageal reflux
(5) Postoperative intraocular lens implantation (both eyes)
(6) Emphysema, right pulmonary bullae; small bilateral pulmonary nodules
(7) Aortic and coronary artery calcification

3.2. Diagnostic evidence

3.2.1. Core motor impairment of Parkinson's disease

The patient had an 11-month chronic progressive course, with dizziness, slow response, and bradykinesia; physical examination showed masked facies and increased muscle tone in the limbs. After adding Madopar combined with pramipexole for anti-Parkinsonian treatment in the neurology department, motor symptoms improved significantly, consistent with the clinical features of primary Parkinson's disease.

3.2.2. Evidence of multisystem non-motor symptoms

(1) Mood disorder: Parkinson's disease causes disturbances in brain dopamine and 5-hydroxytryptamine neurotransmitters, directly inducing anxiety and depression; emotional agitation can induce pharyngeal foreign body sensation, suggesting that emotion participates in the regulation of somatic symptoms.

(2) Gastrointestinal autonomic nerve injury: Damage to the autonomic nerve centers in Parkinson's disease slows gastrointestinal peristalsis and decreases coordination of the esophageal sphincter, inducing gastroesophageal reflux and atrophic gastritis, and causing pharyngeal foreign body sensation. Gastrointestinal discomfort, as a somatization stimulus, further aggravates anxiety; increased anxiety then amplifies Parkinson's motor symptoms, and the three types of symptoms interact with each other.

3.2.3. Ophthalmic comorbidity

The patient had senile cataract and underwent bilateral intraocular lens implantation successively. Postoperative ophthalmology re-examinations showed normal intraocular lens position and good recovery of visual acuity in both eyes.

3.2.4. Exclusionary evidence

The patient had no acute limb paralysis, imaging showed no lesion consistent with acute stroke, and motor symptoms improved after drug adjustment, so secondary Parkinson's syndrome was not supported at present.

3.3. Differential diagnosis

3.3.1. Vascular parkinsonism

This patient had comorbid ischemic cerebrovascular disease, so differentiation is needed. Most patients with vascular parkinsonism have a history of recurrent stroke, and the clinical manifestations are mainly gait disturbance of both lower limbs, with poor response to levodopa drugs [3]. This case had bradykinesia and rigidity as the core manifestations, combined with multisystem involvement of mood, autonomic nerves, and the gastrointestinal tract, and responded well to Madopar and pramipexole, which is more consistent with the multisystem damage characteristics of primary Parkinson's disease. Head MRI should be further performed to evaluate lacunar infarction in the basal ganglia region for further differentiation.

3.3.2. Drug-induced parkinsonism

The patient had previously taken flunarizine for a long time. This drug is a calcium channel blocker, and long-term use carries the risk of inducing reversible parkinsonian extrapyramidal symptoms [4]. Flunarizine has been discontinued clinically, and symptoms should be dynamically followed up. Flupentixol and melitracen were used to improve anxiety and relieve somatic discomfort induced by the gastrointestinal tract. During diagnosis and treatment, adverse drug reactions should be continuously distinguished from symptoms

caused by the disease itself.

3.3.3. Functional globus pharyngeus (pharyngeal paresthesia)

The patient had a sensation of a foreign body in swallowing, and gastroscopy found no esophageal space-occupying lesion, only suggesting atrophic gastritis with bile reflux. Simple globus is mostly caused by anxiety somatization, whereas in this patient, pharyngeal foreign body sensation was superimposed on esophageal motility abnormality caused by Parkinson's autonomic dysfunction, so it cannot be simply classified as a purely functional disease.

3.3.4. Essential tremor

The core manifestations of this disease are postural and action tremor, without bradykinesia or rigidity, which is inconsistent with the clinical features of this patient and can be excluded.

4. Treatment plan and medication analysis

Following the comprehensive treatment idea of "starting with a low dose, individualized administration, simultaneously addressing motor symptoms, mood disorders, and autonomic gastrointestinal symptoms, and taking into account the postoperative ophthalmic condition," this approach is consistent with the stepwise management concept of domestic guidelines for the diagnosis and treatment of Parkinson's disease.

4.1. Treatment of core motor symptoms of Parkinson's disease

Madopar (Levodopa and Benserazide Hydrochloride Tablets): individualized oral dosage. As a levodopa preparation, it directly supplements the dopamine precursor in the brain and improves bradykinesia, masked facies, and increased limb muscle tone. Pramipexole Hydrochloride Tablets (Qishuning) 0.25 mg × 30: 0.125 mg each time, three times daily, orally. This product is a non-ergot dopamine receptor agonist, and combined with Madopar, it synergistically improves bradykinesia and increased limb muscle tone. Treatment should be gradually titrated from a small dose, with close monitoring for adverse reactions such as dizziness, nausea, and lower limb edema. In addition to improving motor function, this class of drugs has a mild improving effect on depression associated with Parkinson's disease, simultaneously addressing both motor and emotional problems [5]. Treatment effect: After adding the Madopar combined with pramipexole regimen, symptoms such as bradykinesia and slow response improved significantly.

4.2. Symptomatic treatment of ischemic cerebrovascular disease and dizziness

Ginkgo and Armillaria Oral Solution: 10 mL each time, three times daily, orally. It improves cerebral microcirculation and is used for dizziness and discomfort caused by ischemic cerebrovascular disease.

4.3. Combined intervention for mood disorder and gastrointestinal somatic symptoms

Flupentixol and Melitracen Tablets (self-provided). Shugan Jieyu Capsules: 2 capsules each time, twice daily, orally. Esomeprazole Magnesium Enteric-coated Dry Suspension 40 mg: 40 mg each time, once daily, orally. Simethicone Emulsion: 10 mL each time, temporarily taken orally before and after gastroscopy to ensure smooth completion of endoscopic examination. Treatment rationale: Control gastrointestinal inflammation and gastroesophageal reflux, reduce sources of somatic discomfort stimulation, and lower

triggers of anxiety attacks; after emotional improvement, reduce the patient's sensory hypersensitivity to the pharynx and gastrointestinal tract, while also reducing fluctuations in Parkinson's motor symptoms; as the central neurotransmitter disturbance in Parkinson's disease improves, autonomic nerve function subsequently improves, and the probability of gastrointestinal symptom recurrence decreases, thereby interrupting the vicious cycle among the three [6]. The patient's condition was stable after bilateral intraocular lens implantation, and intraocular pressure should be monitored during medication to avoid drug effects on the ocular state.

4.4. Rehabilitation and nursing plan

4.4.1. Rehabilitation training

Carry out gait correction, balance function training, and facial expression training to improve masked facies and bradykinesia. Continue to adhere to table tennis. The patient enjoys table tennis; rhythmic physical exercise not only improves Parkinson's motor function but also regulates brain neurotransmitters, relieves anxiety, and promotes gastrointestinal peristalsis, achieving multi-target benefits for nerves, emotion, and the gastrointestinal tract [7].

4.4.2. Safety protection

The patient has bradykinesia and increased muscle tone, with a relatively high risk of falls. Family members and table tennis friends should strengthen daily companionship, and the home environment should be made anti-slip. After bilateral intraocular lens implantation, the patient should pay attention to eye rest, avoid strong light stimulation, and have regular ophthalmology follow-up visits.

4.4.3. Diet and lifestyle management

A low-salt, low-fat, high-fiber diet, ensuring adequate water intake, and maintaining smooth bowel movements. Strictly abstain from alcohol and avoid spicy and irritating foods. The timing of anti-Parkinsonian drug administration should be separated from high-protein diets, choosing to take them 1 hour before meals or 2 hours after meals; self-discontinuation of drugs is strictly prohibited, as abrupt withdrawal of Madopar and pramipexole carries the risk of inducing malignant withdrawal syndrome (**Table 1**).

Table 1. Brief table of the comprehensive intervention plan for this patient

Intervention dimension	Specific measures	Key points
Motor symptom drugs	Levodopa and Benserazide Hydrochloride Tablets (Madopar) + Pramipexole Hydrochloride Tablets 0.125 mg tid orally	Small-dose titration, monitor dizziness, edema, nausea; do not stop abruptly
Cerebrovascular symptomatic treatment	Ginkgo and Armillaria Oral Solution 10 mL tid orally	Improve cerebral circulation
Emotional regulation	Shugan Jieyu Capsules 2 capsules bid orally; flupentixol and melitracen self-provided	Reduce anxiety somatization and reduce episodes of pharyngeal foreign body sensation
Gastrointestinal treatment	Esomeprazole Magnesium Enteric-coated Dry Suspension 40 mg qd; simethicone as needed	Acid suppression, control bile reflux, relieve globus sensation
Ophthalmology follow-up	Regular ophthalmology re-examination after intraocular lens implantation	Monitor visual acuity and intraocular pressure; use eyes reasonably

Intervention dimension	Specific measures	Key points
Rehabilitation exercise	Gait, balance, and facial training + table tennis	Persist long-term; improve motor function and mood; promote gastrointestinal peristalsis
Lifestyle management	Low-salt, low-fat, high-fiber diet; avoid high-protein diet when taking medication; abstain from alcohol; prohibit abrupt drug withdrawal	Family collaborative supervision, home anti-slip, regular ophthalmology follow-up

5. Prognosis and follow-up recommendations

There is currently no cure for Parkinson's disease, and the course is chronic and progressive. This patient's condition is complex: Parkinson's motor impairment, anxiety, and gastroesophageal reflux interact with each other, and poor control of any one link will aggravate the other two groups of symptoms; the patient also has comorbid ischemic cerebrovascular disease, postoperative cataract intraocular lens implantation, pulmonary nodules, coronary calcification, and other geriatric comorbidities. Through standardized drug treatment, after adding the Madopar combined with pramipexole regimen, the patient's motor symptoms improved. Combined with long-term rehabilitation training and simultaneous management of neurological, emotional, gastrointestinal, and ophthalmic symptoms, the vicious cycle can be effectively interrupted, clinical symptoms relieved, disease progression delayed, and a relatively good quality of life maintained [8].

Follow-up recommendations:

(1) Monthly regular follow-up in the neurology outpatient clinic to dynamically assess UPDRS motor scores and mood scales; simultaneously follow up in gastroenterology for gastritis and gastroesophageal reflux, and evaluate changes in pharyngeal foreign body sensation.

(2) Regularly recheck liver and kidney function, blood routine, and electrocardiogram, and monitor aortic and coronary calcification; regularly follow up chest CT for pulmonary nodules and bullae.

(3) Ophthalmology outpatient re-examination every 3 months to monitor bilateral intraocular lenses, visual acuity, and intraocular pressure.

(4) Immediate medical attention is required if there is sudden worsening of symptoms, severe adverse drug reactions, frequent falls or hallucinations and agitation, or persistently aggravated swallowing foreign body sensation, hematemesis, or melena.

(5) In the later stage, if drug efficacy declines and motor complications occur, the indication for DBS surgery can be evaluated.

Disclosure statement

The author declares no conflict of interest.

References

[1] Chinese Society of Parkinson's Disease and Movement Disorders, Chinese Medical Association, 2020, Chinese Guidelines for the Treatment of Parkinson's Disease (4th edition). Chinese Journal of Neurology, 53(12): 973–986.

[2] Chen B, Li SH, 2021, Recognition and Management of Non-motor Symptoms in Parkinson's Disease. Chinese Journal of Neurology, 54(6): 622–627.

[3] Wang XD, 2017, Diagnosis and Differential Diagnosis of Vascular Parkinsonism. Chinese Journal of Geriatric Heart Brain and Vessel Diseases, 19(5): 449–451.

[4] Zhang Y, Wu ZG, 2022, Clinical Research Progress of Drug-Induced Parkinsonism. Chinese Journal of Pharmacovigilance, 24(3): 289–294.

[5] Liu ZG, Gan J, 2019, Rational Use of Dopamine Receptor agonists in Parkinson's Disease. Chinese Journal of Nervous and Mental Diseases, 45(8): 497–500.

[6] Yang MH, Li SD, 2023, Expert Consensus on Integrated Traditional Chinese and Western Medicine Intervention for Parkinson's Disease Complicated with Depression and Anxiety. Chinese Journal of Integrated Traditional and Western Medicine, 43(2): 145–152.

[7] Parkinson's Disease Rehabilitation Professional Committee of Chinese Association of Rehabilitation Medicine, 2018, Chinese Expert Consensus on Rehabilitation of Parkinson's Disease. Chinese Journal of Rehabilitation Theory and Practice, 24(7): 745–752.

[8] Chinese Society of Gastroenterology, Chinese Medical Association, 2022, Chinese Guidelines for the Diagnosis and Treatment of Gastroesophageal Reflux Disease (2022, Xi'an). Chinese Journal of Digestion, 42(10): 649–665.

Publisher's note

Bio-Byword Scientific Publishing remains neutral with regard to jurisdictional claims in published maps and institutional affiliations.

Clinical Neuroscience Research, 2026, Volume 4, Issue 3
https://bbwpublisher.com/journal/CNR
Online ISSN: 2981-8133
Print ISSN: 3083-4899

A Resting-state Functional Magnetic Resonance Imaging Study on Macroscale Topological Properties of Whole-brain Functional Networks in Patients with Post-traumatic Stress Disorder

Yumei Zhang[1]†, Qi Chen[1]†, Jun Lu[1], Yuanyuan Hu[2], Chengwei Wang[1]*

[1]Medical Imaging Center, the First Affiliated Hospital of Shihezi University, Shihezi 832008, Xinjiang Uygur Autonomous Region, China
[2]Department of Clinical Psychology, the First Affiliated Hospital of Shihezi University, Shihezi 832008, Xinjiang Uygur Autonomous Region, China
†These authors contributed equally to this work and share the first authorship.

Author to whom correspondence should be addressed.

Copyright: © 2026 Author(s). This is an open-access article distributed under the terms of the Creative Commons Attribution License (CC BY 4.0), permitting distribution and reproduction in any medium, provided the original work is cited.

Abstract: *Objective*: To investigate alterations in resting-state functional connectivity in patients with post-traumatic stress disorder (PTSD). *Methods*: This was a retrospective case-control study. Forty-five patients with PTSD and 45 healthy control group (HCG) subjects were included. Resting-state functional magnetic resonance imaging (rs-fMRI) scans were performed, and between-group differences in functional connectivity were compared. *Results*: This study did not find significant differences in macroscopic brain network functional connectivity between patients with PTSD and healthy individuals. *Conclusion*: There were no significant between-group differences in global efficiency, mean local efficiency, mean clustering coefficient, or number of rich-club connections of the whole-brain functional network between patients with PTSD and HCG, suggesting that brain network abnormalities in PTSD may not be changes in whole-brain macroscopic topological organization.

Keywords: Post-traumatic stress disorder; Resting-state functional magnetic resonance imaging; Functional connectivity imaging; Graph theory analysis

Online publication: October 19, 2026

1. Introduction

Post-traumatic stress disorder (PTSD) is a delayed-onset psychiatric disorder induced after exposure to severe traumatic events. It is often accompanied by altered brain functional connectivity and represents a chronic mental impairment that persists after trauma exposure [1]. Resting-state functional magnetic resonance

imaging combined with graph theory analysis can quantitatively describe global information integration, local information segregation, and rich-club core network features of the brain functional network, providing a research approach for elucidating the neural mechanisms of PTSD [2]. Previous graph theory studies on brain networks in PTSD have yielded controversial results: some studies suggest that PTSD is accompanied by topological reorganization of the whole-brain functional network, whereas other studies have not detected between-group differences, indicating that whole-brain network topological changes in PTSD are not stable [3–4]. At present, there is still insufficient evidence to clarify whether the whole-brain macroscopic network architecture in patients with PTSD differs from that in healthy individuals.

This study used resting-state functional magnetic resonance imaging to construct a whole-brain functional network. Global efficiency, mean local efficiency, mean clustering coefficient, and number of rich-club connections were selected to compare whole-brain network topological properties between patients with PTSD and a healthy control group (HCG), and to explore whether PTSD involves abnormal functional network organization at the whole-brain level.

2. Materials and methods

2.1. Participants

This was a retrospective case-control study. The PTSD group included 45 patients diagnosed with PTSD in the Department of Psychology of the First Affiliated Hospital of Shihezi University from March 2023 to October 2024. The interval from trauma exposure to enrollment in this imaging examination was 3–24 months for all subjects. The HCG consisted of 45 healthy individuals recruited from the hospital during the same period who were accompanying patients or undergoing routine physical examinations. This study was approved by the Ethics Committee of the First Affiliated Hospital of Shihezi University, approval No. KJ2025-609-01. Subjects signed broad informed consent for magnetic resonance imaging (MRI) examination. All data in this study were de-identified, with no risk of subject privacy disclosure. The study procedures complied with the ethical principles of the Declaration of Helsinki.

Inclusion criteria for the PTSD group: (1) met the diagnostic criteria for PTSD in the Diagnostic and Statistical Manual of Mental Disorders, Fifth Edition (DSM-5) of the American Psychiatric Association, with a total score of no less than 22 on the PTSD Checklist for Diagnostic and Statistical Manual of Mental Disorders-5 (PCL-5), confirmed by two psychiatrists; (2) aged 18–60 years, right-handed, with an education level of primary school or above; (3) newly diagnosed PTSD, without having received any trauma-related medication or psychological intervention.

Inclusion criteria for HCG: (1) no history of psychological trauma; (2) aged 18–60 years, right-handed, with an education level of primary school or above.

Exclusion criteria: (1) history of psychoactive substance or drug abuse; (2) mental retardation, intellectual disability, or comorbid other psychiatric disorders (such as schizophrenia, bipolar disorder, etc.); (3) long-term use of medications that may affect cognitive function, including nootropics, benzodiazepines (continuous use for more than 90 days), cholinergic receptor antagonists, etc.; (4) moderate-to-high risk on passive suicide risk assessment; (5) organic parenchymal brain lesions after trauma such as cerebral contusion and laceration, intracranial hemorrhage, and encephalomalacia; (6) pregnant or lactating women.

2.2. Examination and diagnostic methods

2.2.1. General information questionnaire

This study used a self-designed general information questionnaire covering demographic information, handedness, smoking and drinking history, and PTSD diagnosis and treatment history. All surveys were conducted and recorded by trained psychiatrists.

2.2.2. PTSD checklist-5 (PCL-5)

The scale was developed based on the DSM-5 diagnostic criteria for PTSD. It contains 20 items covering four core symptom clusters: symptom cluster B (items 1–5), symptom cluster C (items 6–7), symptom cluster D (items 8–14), and symptom cluster E (items 15–20). The questionnaire uses a 5-point scale: 0 = not at all; 1 = mild; 2 = moderate; 3 = severe; 4 = extreme. Diagnosis of PTSD requires at least: 1 B item (items 1–5), 1 C item (items 6–7), 2 D items (items 8–14), and 2 E items (items 15–20). Each item score ranges from 0 to 4, and the total score ranges from 0 to 80. Higher PCL-5 scores indicate more severe symptoms. For unintentional injury trauma type, the optimal cutoff score is above 22. The scale has good reliability, with an internal consistency Cronbach's α of 0.96 and a test-retest reliability r of 0.84 [5–6].

2.2.3. Scanning methods

Scanning was performed using a GE MR750 3.0 T superconducting MRI scanner with a standard orthogonal head coil. Before scanning, subjects lay in the supine position, wore earplugs to reduce noise interference, and were asked to keep their head as still as possible, remain awake with eyes closed, and breathe naturally and calmly. The scanning environment, noise protection, and head fixation were identical for all subjects, eliminating scanning operation bias. The MRI protocol consisted of routine cranial MRI and functional MRI. First, routine cranial MRI was performed in all subjects, including axial T1-weighted imaging (T1WI), T2-weighted imaging (T2WI), T2-weighted fluid-attenuated inversion recovery (T2-FLAIR), and sagittal T2WI, to exclude organic lesions such as cerebral infarction and space-occupying lesions.

The rs-fMRI (BOLD-fMRI) sequence parameters were: TR = 2000 ms, TE = 30 ms, FOV = 240 mm × 240 mm, matrix = 64 × 64, flip angle = 90°, slice thickness = 4 mm, number of slices = 32, slice gap = 0 mm, scan time = 8 min 20 s, including 245 time points.

2.2.4. Data postprocessing

Image postprocessing was performed using the uAI Research Portal (uRP). Raw Digital Imaging and Communications in Medicine (DICOM) data were imported into the platform, converted to Neuroimaging Informatics Technology Initiative (NIfTI) format, and anonymized. Preprocessing included removal of the first 10 time points, slice timing correction, motion correction, co-registration of anatomical images, normalization to standard space, spatial smoothing, temporal filtering (0.01–0.08 Hz), and regression of nuisance signals including motion, white matter, and cerebrospinal fluid. Then, the brain was parcellated into 116 regions based on the Automated Anatomical Labeling (AAL) atlas, and the mean signal time series of each region was calculated. A 116 × 116 functional connectivity matrix was constructed by calculating Pearson correlation coefficients between each pair of regions. Finally, graph-theoretic metrics were calculated, including global efficiency, mean local efficiency, mean clustering coefficient, and number of rich-club connections.

Blinded manual visual quality control was performed simultaneously. Two researchers with more than

15 years of neuroimaging analysis experience checked the segmentation rendering results case by case on the platform's 3D visualization interface. Samples with contour shift, boundary mismatch, or under/over-segmentation were excluded. The entire analysis was a fully automated pipeline, with no manual tracing or manual parameter adjustment. Image processing personnel were blinded to subject grouping to avoid subjective bias. Thirty samples were selected for a test-retest experiment. According to the Shrout-Fleiss criteria, the intraclass correlation coefficient ICC(3,1) was used to evaluate test-retest reliability of the pipeline. The ICCs for all metrics were 0.961–0.987, and the corresponding 95% confidence intervals overall ranged from 0.922 to 0.992.

2.3. Sample size estimation

G*Power software was used to estimate sample size based on a two-sample independent *t*-test. A two-sided significance level of $\alpha = 0.05$ and power of $1-\beta = 0.80$ were set. Referring to similar neuroimaging studies, an effect size of Cohen's $d = 0.5$ was selected [7]. Under these conditions, the theoretical minimum sample size was calculated to be 64 per group. Given the strict inclusion and exclusion criteria for PTSD cases in this study, requiring subjects to be newly diagnosed and to have not received any trauma-related medication or psychological intervention, and requiring MRI images to pass strict quality control, recruitment of clinical samples meeting all conditions was difficult. Considering the actual case resources available at the center, 58 PTSD subjects and 56 HCG subjects were initially enrolled. After excluding cases with poor image quality or missing clinical data, 45 subjects were finally included in each of the PTSD and HCG groups. Post hoc power analysis indicated that this sample size had insufficient power to detect a medium effect of $d = 0.5$ and only had good ability to detect medium-to-large effects. Although some observed indicators were subsequently analyzed using two independent samples rank-sum tests, existing literature indicates that sample sizes estimated based on *t*-tests can meet the power requirements of nonparametric tests [8].

2.4. Statistical methods

Statistical analysis was performed using Statistical Package for the Social Sciences (SPSS) 27.0 software (https://www.ibm.com/spss). Continuous data were described according to normality test results: normally distributed data are expressed as mean ± standard deviation, and non-normally distributed data as median (interquartile range); categorical data are described as frequency (percentage). Continuous variables were first tested for normality. When normally distributed, an independent samples *t*-test or Welch's corrected *t*-test was selected according to the variance homogeneity result; when not normally distributed, Mann-Whitney U test (two groups) or Kruskal-Wallis H test (multiple groups) was used.

3. Results

3.1. General clinical data and scales

There were no statistically significant differences in age, sex, or education level between the PTSD group and HCG ($P > 0.05$) (**Table 1**). The differences in smoking and drinking history between the two groups were statistically significant ($P < 0.01$).

Table 1. Comparison of demographic and clinical characteristics between the PTSD group and the HCG

Variable	PTSD group (*n*=45)	HCG (*n*=45)	z/x^2	*P* value
Age	44 (22.0)	36 (23.0)	−1.203	0.229
Sex (male/female)	12/33	18/27	1.800	0.180
Education level	1/12/10/22	1/6/8/30	−1.760	0.078
Smoking history (yes/no)	13/32	31/14	14.407	<0.001
Drinking history (yes/no)	16/29	32/13	11.429	0.001
PCL-5 score	59 (17.0)	13 (10.5)	−8.127	<0.001

Note: Education level was grouped as primary school/junior high school/senior high school or technical secondary school/junior college and above; age and PCL-5 scores were analyzed using the Mann-Whitney U rank-sum test; education level was analyzed using the Kruskal-Wallis H test; sex, smoking history, and drinking history were analyzed using the x^2 test; PTSD, post-traumatic stress disorder; HCG, healthy control group; PCL-5, PTSD Checklist for DSM-5.

3.2. Resting-state brain network functional connectivity analysis

Between-group comparisons were performed for six global graph-theoretic metrics of the whole brain and local network topological parameters of 116 brain regions. The results showed that after FDR correction for multiple comparisons, there were no statistically significant differences in whole-brain global metrics (**Table 2**) or local graph-theoretic metrics of all 116 brain regions between the PTSD group and HCG (all *P*FDR > 0.05).

Table 2. Comparison of graph-theoretic metrics of brain networks between the PTSD group and HCG

Indicator	HCG (*n*=45)	PTSD group (*n*=45)	*t*	*P*	*P* value (FDR-corrected)
Global efficiency	0.035 ± 0.010	0.033 ± 0.009	0.848	0.399	0.479
Mean local efficiency	0.018 ± 0.005	0.017 ± 0.004	1.036	0.303	0.479
Mean clustering coefficient	0.013 ± 0.004	0.012 ± 0.003	1.049	0.297	0.479
Number of rich-club connections	3.810 ± 1.541	3.540 ± 1.436	0.859	0.392	0.479
Bridging connections	16.048 ± 5.109	14.977 ± 4.219	1.085	0.281	0.479
Local connections	24.564 ± 6.582	23.676 ± 5.591	0.689	0.492	0.492

Note: Data are expressed as mean ± standard deviation; between-group comparisons used an independent-samples *t*-test; the six metrics were corrected for multiple comparisons using the Benjamini-Hochberg False Discovery Rate (FDR) method. Global efficiency, mean local efficiency, and mean clustering coefficient are dimensionless metrics; the number of rich-club connections, bridging connections, and local connections are expressed as counts (connection edge counts). PTSD, post-traumatic stress disorder; HCG, healthy control group.

4. Discussion

4.1. Analysis of demographic data

Clinical observations have found that patients with PTSD often have higher rates of smoking and drinking, which is consistent with the results of this study [9]. The high prevalence of smoking and drinking behaviors among patients with PTSD may reflect the self-medication effect of nicotine on PTSD symptoms [10–11].

4.2. Discussion of negative resting-state functional connectivity results

This study constructed a brain functional network based on resting-state functional magnetic resonance imaging and selected graph-theoretic topological metrics including global efficiency, mean local efficiency,

mean clustering coefficient, and number of rich-club connections to compare brain network organization patterns between patients with PTSD and HCG. The results showed no significant statistical differences in the above network topological parameters between the two groups. Some previous functional brain network studies suggested that PTSD involves an imbalance between brain network integration and segregation, manifested as decreased global efficiency, altered local clustering, or impairment of the rich-club core network, which is considered to be involved in the neural mechanisms of abnormal fear regulation in PTSD. However, this study did not reproduce the above between-group differences, suggesting that topological changes in brain functional networks in PTSD are not stably detectable under all research conditions. The potential reasons for the negative results may include the following:

4.2.1. Clinical heterogeneity of PTSD

PTSD is highly heterogeneous in trauma type, disease course, symptom burden, comorbidity, and medication status. Previous studies reporting abnormal brain network topology mostly included severe, chronic PTSD populations with relatively homogeneous trauma types [2, 4]. The sample in this study had a wide range of disease durations, scattered symptom severity distribution, and mixed trauma exposure backgrounds, which may dilute between-group differences in brain network topology. Brain network topological parameters may not be a stable dichotomous feature at the PTSD group level, but may be continuously associated with individual symptom severity.

4.2.2. Brain network construction and threshold selection

Functional brain network topological metrics are highly sensitive to network construction strategies, including atlas selection, edge definition, and thresholding strategy. Under different thresholds, the effect sizes of global efficiency, clustering coefficient, and rich-club structure may change markedly. The threshold settings and network sparsity selections in previous positive studies differ from those in this study, which may lead to inconsistent results [12]. At the same time, the number of rich-club connections describes the network connection backbone of core brain regions, and its changes may have a relatively small effect size, making it difficult to detect under the sample conditions of this study.

4.2.3. Sample size and statistical power

Between-group effect sizes of brain network topology are usually small. This study simultaneously tested multiple topological metrics and used multiple comparison correction to control type I error, which reduces test sensitivity and raises the possibility of type II error. The between-group difference in brain network topology between PTSD and HCG is itself weak, and the statistical power of the current sample size is insufficient to identify this between-group difference.

4.2.4. Biological meaning of the metrics

Global efficiency, clustering coefficient, and number of rich-club connections are macroscopic topological metrics of the whole-brain network, reflecting the brain’s overall capacity for information integration and segregation. Even if PTSD involves altered functional connectivity in local brain regions, such local connectivity disturbance may not necessarily translate into significant changes in whole-brain macroscopic network topological parameters. In other words, functional connectivity abnormalities in PTSD may be confined to local subnetworks, while the overall network architecture at the whole-brain level remains

relatively stable. This explains the absence of differences in macroscopic topological metrics between the two groups in this study.

4.2.5. fMRI scanning confounders

Resting-state functional magnetic resonance imaging signals are susceptible to head motion interference. Although head motion quality control was performed in this study, residual motion artifacts may still affect the functional connectivity matrix and subsequently interfere with the estimation of brain network topological parameters, potentially masking true between-group differences.

Although no between-group differences were detected, this study still has certain reference value. Current graph theory studies on brain networks in PTSD are dominated by published positive results, with obvious publication bias. The negative evidence provided by this study helps to objectively evaluate the stability of whole-brain macroscopic topological metrics in PTSD research. The results suggest that it is difficult to distinguish patients with PTSD from healthy individuals using only whole-brain macroscopic network topological metrics such as global efficiency, mean local efficiency, mean clustering coefficient, and number of rich-club connections. PTSD-related functional network changes may be more reflected at the local subnetwork level rather than in the overall whole-brain network architecture. Future PTSD brain network research may shift toward local subnetwork topological analysis rather than being limited to whole-brain macroscopic graph-theoretic metrics.

4.3. Limitations

This MRI study still has several limitations. First, a cross-sectional study cannot clarify the causal temporal relationship between brain structural abnormalities and PTSD symptoms or cognitive impairment. Second, the sample size was limited. The sample size in this study was 45 per group, which has limited power to detect a medium effect at the level of Cohen's d = 0.5. The positive brain region changes detected in this study mostly involved medium-to-large effects, but some moderate brain structure-cognition associations may still have been missed. Third, brain network topological results depend on the brain atlas and thresholding scheme, and different construction strategies may yield different conclusions. This study did not perform local subnetwork topological analysis, so changes in local networks could not be evaluated. In addition, resting-state fMRI is susceptible to confounders such as subject state during scanning and head motion. Fourth, the sample had a wide range of trauma types and disease durations, and subgroup analyses stratified by trauma subtype or disease course were not performed, making it difficult to resolve disease heterogeneity. Future studies need to expand the sample and conduct longitudinal multimodal imaging stratified research.

5. Conclusion

This study did not find significant between-group differences between patients with PTSD and HCG in whole-brain functional network global efficiency, mean local efficiency, mean clustering coefficient, or number of rich-club connections. This suggests that brain functional network changes in PTSD may not be manifested at the whole-brain macroscopic network architecture level, and it is difficult to distinguish patients with PTSD from healthy individuals using only the above macroscopic graph-theoretic metrics. This study supplements negative evidence on brain networks in PTSD. Future studies may further explore local subnetwork topological features.

Funding

Clinical and Basic Research Project of the First Affiliated Hospital of Shihezi University (No. LC2023008).

Disclosure statement

The authors declare no conflict of interest.

References

[1] Yu SJ, Xu JW, 2026, Neuroimaging and Genetic Mechanisms of Post-Traumatic Stress Disorder. Chinese Journal of Behavioral Medicine and Brain Science, 35(2): 181–186.

[2] Harrington DL, Shen Q, Angeles QA, et al., 2025, Linking Intrinsic Brain Dysfunction to Behavioral Outcomes in Combat-Exposed Males with PTSD Symptoms. Front Psychiatry, 2025(16): 1591938.

[3] Huang C, Hagan T, Kritikos M, et al., 2024, Graph Theory-Based Analysis Reveals Neural Anatomical Network Alterations in Chronic Post-Traumatic Stress Disorder. Imaging Neuroscience, 2024(2): imag_a_00141.

[4] Tomas CW, Fitzgerald JM, Baird CL, et al., 2025, Data-Driven Approach to Dynamic Resting State Functional Connectivity in Post-Traumatic Stress Disorder: An ENIGMA-PGC PTSD Study. Human Brain Mapping, 46(11): e70116.

[5] Bovin MJ, Marx BP, Weathers FW, et al., 2016, Psychometric Properties of the PTSD Checklist for Diagnostic and Statistical Manual of Mental Disorders-Fifth Edition (PCL-5) in Veterans. Psychological Assessment, 28(11): 1379–1391.

[6] Jiang C, Xue G, Yao S, et al., 2023, Psychometric Properties of the Post-traumatic Stress Disorder Checklist for DSM-5 (PCL-5) in Chinese Stroke Patients. BMC Psychiatry, 2023(23): 16.

[7] Cohen J, 1988, Statistical Power Analysis for the Behavioral Sciences. 2nd ed. Lawrence Erlbaum Associates, Hillsdale.

[8] Skovlund E, Fenstad GU, 2001, Should We Always Choose a Nonparametric Test when Comparing Two Apparently Nonnormal Distributions? Journal of Clinical Epidemiology, 54(1): 86–92.

[9] Quinones MM, Gallegos AM, Lin FV, et al., 2020, Dysregulation of Inflammation, Neurobiology, and Cognitive Function in PTSD: An Integrative Review. Cognitive, Affective, & Behavioral Neuroscience, 20(3): 455–480.

[10] Hua JPY, Cano M, Batki SL, et al., 2023, Impact of Alcohol Use, Traumatic Stress, and Cigarette Smoking on Cognitive Functioning in Veterans With Co-occurring Alcohol Use Disorder and Posttraumatic Stress Disorder. Military Medicine, 188(7–8): e2208–e2216.

[11] Girotti M, Bulin SE, Carreno FR, 2024, Effects of Chronic Stress on Cognitive Function — From Neurobiology to Intervention. Neurobiology of Stress, 2024(33): 100670.

[12] Luppi AI, Gellersen HM, Liu ZQ, et al., 2024, Systematic Evaluation of fMRI Data-Processing Pipelines for Consistent Functional Connectomics. Nature Communications, 15(1): 4745.

Publisher's note

Bio-Byword Scientific Publishing remains neutral with regard to jurisdictional claims in published maps and institutional affiliations.

Clinical Neuroscience Research, 2026, Volume 4, Issue 3
https://bbwpublisher.com/journal/CNR
Online ISSN: 2981-8133
Print ISSN: 3083-4899

Effect of Sequential Therapy with Edaravone Dexborneol on Prognosis in Patients with Progressive Cerebral Infarction

Yong Yang, Bing Wang, Fei Wu, Hao Wen, Mei Jin

Heilongjiang Provincial Hospital, Harbin 150036, Heilongjiang, China

Copyright: © 2026 Author(s). This is an open-access article distributed under the terms of the Creative Commons Attribution License (CC BY 4.0), permitting distribution and reproduction in any medium, provided the original work is cited.

Abstract: *Objective*: To analyze the effects of sequential therapy with edaravone dexborneol on neurological function, inflammatory factors, and prognosis in patients with progressive cerebral infarction. *Methods*: Sixty patients with acute progressive cerebral infarction treated in our hospital from June 2025 to December 2025 were enrolled and divided into two groups by the random number table method, with 30 subjects in each group. The control group received conventional antiplatelet therapy, while the observation group received sequential therapy with edaravone dexborneol in addition to the control treatment. The intervention outcomes were compared between the two groups. *Results*: The total clinical effective rate and improvements in neurological function and inflammatory indicators in the observation group were better than those in the control group, and Hcy, NSE, and the incidence of adverse reactions were lower ($P < 0.05$). *Conclusion*: Sequential therapy with edaravone dexborneol can improve neurological function, reduce inflammation and neurological injury, and has good safety in patients with progressive cerebral infarction, warranting clinical promotion.

Keywords: Edaravone dexborneol; Sequential therapy; Progressive cerebral infarction; Neurological function; Inflammatory factors

Online publication: October 19, 2026

1. Introduction

Progressive cerebral infarction is a type of ischemic stroke. Within 6 hours to 7 days after onset, neurological function may still deteriorate despite active treatment, accounting for approximately 25%–40% of cerebral infarctions [1]. Its onset is insidious, and progression is rapid; the infarct focus expands, neurological injury worsens, and disability and mortality rates are high. Inflammatory responses damage the ischemic penumbra. After ischemia, proinflammatory mediators are released, inflammatory cells infiltrate, the blood-brain barrier is disrupted, and neuronal injury is aggravated [2]. Timely clearance of inflammatory factors and inhibition of oxidative stress can promote angiogenesis and ameliorate neurological injury. Currently, reperfusion therapy is limited by the time window, and many patients miss the optimal opportunity [3]. Neuroprotective therapy

can serve as a supplement. Edaravone dexborneol is composed at a 4:1 ratio and can scavenge free radicals and exert anti-inflammatory effects. Since the launch of sublingual tablets, post-discharge sequential therapy has become possible. This study aimed to investigate its effects on neurological function, inflammatory factors, and prognosis in such patients. The details are as follows:

2. Materials and methods

2.1. General data

Sixty patients with acute progressive cerebral infarction treated in our hospital from June 2025 to December 2025 were enrolled and divided into two groups by the random number table method, with 30 subjects in each group. In the observation group, there were 16 males and 14 females; age ranged from 56 to 78 years, with a mean age of (63.28 ± 2.01) years; 18 had hypertension, 12 had diabetes, and 15 had hyperlipidemia. In the control group, there were 16 males and 14 females; age ranged from 57 to 76 years, with a mean age of (64.01 ± 1.90) years; 17 had hypertension, 11 had diabetes, and 14 had hyperlipidemia. There was no significant difference between the groups ($P > 0.05$). This study was approved by the hospital ethics committee.

2.1.1. Inclusion criteria

(1) all met the clinical diagnostic criteria for acute progressive cerebral infarction;
(2) all were definitively diagnosed by CT or MRI;
(3) neurological deficit signs showed continuous deterioration from 6 h to 7 d after onset;
(4) patients and their relatives were willing to cooperate with this study.

2.1.2. Exclusion criteria

(1) concurrent major diseases of the liver, kidney, cardiovascular system, etc.;
(2) concurrent malignant tumors;
(3) incomplete follow-up data;
(4) allergy to the study drugs.

2.2. Methods

The control group received conventional antiplatelet therapy with oral aspirin enteric-coated tablets (manufactured by Bayer HealthCare Co., Ltd.; National Drug Approval No. J20171021; 100 mg per tablet), once daily, 100 mg each time, for 30 consecutive days. Meanwhile, basic regulatory treatment for blood pressure, blood glucose, and blood lipid levels and symptomatic adjunctive therapy were administered.

The observation group received sequential therapy with edaravone dexborneol on the basis of the control treatment. In the initial phase, edaravone dexborneol injection (produced by Simcere Pharmaceutical Co., Ltd.; National Drug Approval No. H20200007; 5 mL per vial) was administered twice daily, 15 mL per dose, by intravenous infusion for 7 consecutive days. From the 7th day onward, edaravone dexborneol sublingual tablets were used for subsequent treatment, twice daily, one tablet sublingually each time, for 4 consecutive weeks. After 14 days from discontinuation of edaravone dexborneol sublingual tablets, a second cycle of sequential therapy was initiated, lasting 14 days.

2.3. Outcome measures

(1) Clinical efficacy: marked improvement was defined as a reduction in neurological deficit score ≥90%; effective as a reduction of 50%–89%; ineffective as failure to meet the above criteria or deterioration. Total effective rate = (marked improvement + effective)/total cases × 100%.
(2) Neurological deficit score: the criteria of the Academic Conference on Cerebrovascular Diseases were used; the higher the score, the more severe the deficit.
(3) Inflammatory factors: hs-CRP and IL-6 were measured before and after treatment.
(4) Hcy and NSE were measured.
(5) Adverse reactions such as dizziness, fatigue, and somnolence were recorded.

2.4. Statistical analysis

SPSS 26.0 was used. Continuous variables were expressed as mean ± standard deviation and compared between groups using the *t*-test; categorical data were expressed as n (%) and tested by the chi-square test. $P < 0.05$ was considered a significant difference.

3. Results

3.1. Comparison of clinical efficacy between the two groups

The total effective rate was higher in the observation group ($P < 0.05$), as shown in **Table 1**.

Table 1. Comparison of clinical efficacy between the two groups [n (%)]

Group	*n*	Marked improvement	Effective	Ineffective	Total effective rate
Observation group	30	18 (60.00)	10 (33.33)	2 (6.67)	28 (93.33)
Control group	30	12 (40.00)	10 (33.33)	8 (26.67)	22 (73.33)
x^2					4.320
P					0.038

3.2. Comparison of neurological deficit scores between the two groups

After treatment, the neurological function score in the observation group was lower than that in the control group ($P < 0.05$), as shown in **Table 2**.

Table 2. Comparison of neurological deficit scores between the two groups ($\overline{x} \pm s$, points)

Group	*n*	Before treatment	After treatment	*t*	*P*
Observation group	30	22.45 ± 3.67	8.32 ± 2.15	18.196	0.000
Control group	30	22.78 ± 3.82	13.56 ± 2.87	10.569	0.000
t		0.341	8.004		
P		0.734	0.000		

3.3. Comparison of inflammatory factor levels between the two groups before and after treatment

After treatment, hs-CRP and IL-6 in the observation group were lower than those in the control group ($P < 0.05$), as shown in **Table 3**.

Table 3. Comparison of inflammatory factor levels between the two groups ($\overline{x} \pm s$)

Group	*n*	hs-CRP (mg/L)	hs-CRP (mg/L)	IL-6 (pg/mL)	IL-6 (pg/mL)
		Before treatment	After treatment	Before treatment	After treatment
Observation group	30	12.56 ± 3.21	4.23 ± 1.15	28.67 ± 5.34	12.45 ± 3.21
Control group	30	12.89 ± 3.45	7.56 ± 1.87	29.12 ± 5.67	18.76 ± 4.12
t		0.384	8.308	0.316	6.617
P		0.703	0.000	0.753	0.000

3.4. Comparison of Hcy and NSE levels between the two groups

After treatment, Hcy and NSE in the observation group were lower than those in the control group ($P < 0.05$), as shown in **Table 4**.

Table 4. Comparison of Hcy and NSE levels between the two groups ($\overline{x} \pm s$)

Group	*n*	Hcy (μmol/L)	Hcy (μmol/L)	NSE (μg/L)	NSE (μg/L)
		Before treatment	After treatment	Before treatment	After treatment
Observation group	30	18.67 ± 4.23	10.34 ± 2.56	16.78 ± 3.45	8.12 ± 2.01
Control group	30	18.92 ± 4.45	14.67 ± 3.12	17.01 ± 3.67	11.89 ± 2.67
t		0.223	5.876	0.250	6.179
P		0.824	0.000	0.803	0.000

3.5. Comparison of the incidence of adverse reactions between the two groups

The incidence of adverse reactions in the observation group was lower than that in the control group ($P < 0.05$), as shown in **Table 5.**

Table 5. Comparison of the incidence of adverse reactions between the two groups [n (%)]

Group	*n*	Dizziness	Fatigue	Somnolence	Incidence
Observation group	30	1 (3.33)	1 (3.33)	0 (0.00)	2 (6.67)
Control group	30	3 (10.00)	3 (10.00)	2 (6.67)	8 (26.67)
x^2					4.320
P					0.038

4. Discussion

Progressive cerebral infarction is a common type of ischemic stroke. Its main feature is continuous deterioration of neurological function. Compared with ordinary cerebral infarction, the disease progresses more rapidly. Patients may have only mild symptoms on admission, but within hours to days they may continue to worsen, even to complete paralysis or coma [4]. Pathologically, this is related to the continuous loss of the ischemic penumbra. The penumbra is an area around the infarct core that is supplied by collateral circulation, structurally intact but functionally impaired. If blood flow is restored in time, it can survive; if ischemia continues, it becomes part of the infarct. Disease deterioration involves several links: decreased perfusion pressure, thrombus enlargement or embolization, and aggravated inflammatory response. Advanced age, diabetes, blood pressure fluctuation, and fever can also promote progression. Therefore, in addition to

reperfusion therapy, a regimen of continuous neuroprotection is clinically needed.

This study showed that the total effective rate was higher in the observation group. This indicates that sequential therapy with edaravone dexborneol can improve outcomes in patients with progressive cerebral infarction. Efficacy was determined by the degree of reduction in neurological deficit score. The drug can increase the effective rate because it continuously interferes with key links of ischemic injury. In the past, only injection was used, and treatment was interrupted after discharge; residual neurons in the penumbra lost protection and might die due to inflammation or oxidative stress. Sequential therapy ensures continuity of protection from the acute phase to the recovery phase. Intravenous administration acts quickly, scavenging free radicals and inhibiting early inflammation; sublingual tablets maintain stable drug levels, continuously inhibiting delayed inflammation and creating a good environment for neurological recovery. This "acute-phase attack + recovery-phase maintenance" strategy is more consistent with the developmental pattern of the disease. A higher total effective rate means that more patients change from ineffective to effective or markedly improved, which can reduce disability and may also reduce rehabilitation and nursing costs.

After treatment, the neurological deficit score in the observation group was lower. This again demonstrates the neuroprotective effect of this sequential therapy. The greater reduction in scores in this study indicates that the drug can prevent disease progression and promote functional recovery. Edaravone scavenges free radicals, reduces oxidative damage, and protects penumbral neurons. Dexborneol exerts anti-inflammatory effects, inhibits inflammatory damage to the neurovascular unit, and reduces secondary injury. After penumbral neurons are protected, electrophysiological and synaptic functions gradually recover, and scores decrease accordingly [5]. Neurological recovery is a dynamic process. The advantage of sequential therapy over conventional therapy lies mainly in the longer administration time, covering the critical period of neural repair. Recovery is most active within weeks after cerebral infarction; without protection, recovery may be hindered. Continuous use of sublingual tablets provides support for post-discharge repair, which may explain why the difference in scores between the two groups widened over time.

The results showed that both inflammatory indicators were significantly lower in the observation group after treatment. hs-CRP and IL-6 not only reflect the degree of inflammation but are also associated with neurological deterioration. The reduction of inflammatory factors in the observation group indicates that the anti-inflammatory effect of dexborneol is clinically effective. Post-ischemic inflammation is dual in nature: moderate inflammation can clear necrotic tissue, while excessive inflammation aggravates injury. Patients with progressive cerebral infarction often experience uncontrolled inflammation, with massive release of proinflammatory factors, forming a positive feedback loop, recruiting peripheral immune cells, and aggravating blood-brain barrier disruption and neuronal death. Dexborneol inhibits the expression of TNF-α, IL-1β, COX-2, etc., weakening the initiation of inflammation at the source, thereby reducing hs-CRP and IL-6. This effect improves indicators, protects the blood-brain barrier, and reduces cerebral edema [6]. After inflammation is controlled, vascular endothelial injury is reduced, microcirculation is maintained, and penumbral blood supply is improved, laying the foundation for neurological recovery. Better inflammation control in the observation group also explains its efficacy.

In this study, Hcy and NSE were lower in the observation group after treatment. Hcy is an intermediate product of methionine metabolism. Its elevation can damage vascular endothelium and promote atherosclerosis and thrombosis. Hyperhomocysteinemia can damage endothelium through oxidative stress, endoplasmic reticulum stress, and inflammation, promoting thrombus extension and worsening perfusion.

The reduction of Hcy by sequential therapy with edaravone dexborneol may be related to its antioxidant and anti-inflammatory effects. After oxidative and inflammatory responses are inhibited, endothelial function improves, Hcy toxicity is reduced, and the liver's ability to metabolize Hcy may also recover. NSE marks neuronal injury, and its level is positively correlated with infarct volume and degree of deficit. The reduction of NSE in the observation group indicates that this treatment reduced irreversible neuronal injury. Edaravone scavenges free radicals, protects neuronal membranes, and reduces NSE release. Dexborneol inhibits glutamate excitotoxicity and reduces neuronal necrosis. Simultaneous improvement in Hcy and NSE indicates that this treatment protects both blood vessels and neurons.

The incidence of adverse reactions in the observation group was lower, suggesting that sequential therapy with edaravone dexborneol has good safety. In this study, adverse reactions in the observation group were mainly dizziness, fatigue, and somnolence; symptoms were mild, tolerable, and no serious adverse events occurred. Edaravone has clear targets and little interference with normal physiology; dexborneol is derived from natural components and has high safety. Sublingual tablets avoid local irritation and infection risk associated with injections, improving safety. Fewer adverse reactions can improve compliance, reduce discontinuation due to adverse reactions, and ensure completion of sequential therapy. Good safety is a key prerequisite for the widespread use of drugs in patients with progressive cerebral infarction, and this treatment has clear advantages.

5. Conclusion

In summary, sequential therapy with edaravone dexborneol has a clear effect in patients with progressive cerebral infarction. It can improve neurological function, reduce inflammation and neurological injury, and lower Hcy and NSE. The therapy has few adverse reactions and good safety. Sublingual tablets allow patients to continue sequential therapy after discharge, compensating for the previous shortcoming that sequential therapy was difficult with injection alone. After sublingual tablets are launched and promoted, more patients may benefit. However, this study had a small sample size and short follow-up. Future studies should expand the sample and prolong follow-up to verify long-term efficacy and safety.

Disclosure statement

The authors declare no conflict of interest.

References

[1] Wang F, Kang J, Chen XF, et al., 2025, Efficacy of Edaravone Dexborneol Combined with Compound Troxerutin in Patients with Acute Progressive Cerebral Infarction. Chinese Journal of Drug Application and Monitoring, 22(3): 416–420.

[2] Li YC, Han GS, Dou ST, et al., 2023, Clinical Study of Edaravone Dexborneol Combined with Butylphthalide Injection in the Treatment of Patients with Acute Progressive Cerebral Infarction. The Chinese Journal of Clinical Pharmacology, 39(6): 763–767.

[3] Wang K, Rong MM, Yang JM, et al., 2025, Clinical Observation of Compound Brain Peptide Ganglioside Combined with Edaravone Dexborneol in the Treatment of Progressive Cerebral Infarction. Chinese Journal of

Practical Nervous Diseases, 28(2): 202–206.

[4] Lei M, Geng JC, Zhu J, et al., 2024, Effect of Honglonggen Decoction Combined with Edaravone Dexborneol on the Risk of Progressive Cerebral Infarction in Patients with Cerebral Infarction after Thrombolysis. Acta Chinese Medicine, 39(12): 2678–2684.

[5] Xia XS, Chen K, Yu W, et al., 2025, Effect of Butylphthalide Combined with Edaravone Dexborneol on Patients with Acute Progressive Cerebral Infarction. Sichuan Journal of Physiological Sciences, 47(5): 1054–1056.

[6] Wan YD, 2023, Clinical Effect of Edaravone Dexborneol in the Treatment of Acute Progressive Large-Artery Atherosclerotic Cerebral Infarction. Chinese and Foreign Medical Research, 21(35): 26–29.

Publisher's note

Bio-Byword Scientific Publishing remains neutral with regard to jurisdictional claims in published maps and institutional affiliations.

Clinical Neuroscience Research, 2026, Volume 4, Issue 3
https://bbwpublisher.com/journal/CNR
Online ISSN: 2981-8133
Print ISSN: 3083-4899

With a View to Fear Extinction and to Brain Functional Change: A Neurotheoretical Hypothesis About Traditional Health-Preserving Exercises as Treatments for Post-Aortic Dissection Kinesiophobia

Xiangyang Hu, Jia Liu, Jieyu Cao, Zhengwen Lei*

Department of Cardiothoracic and Vascular Surgery, The First Affiliated Hospital of Hengyang Medical School, University of South China, Hengyang 421001, Hunan, China

***Corresponding author:** Zhengwen Lei, leizhengwen0803@163.com

Copyright: © 2026 Author(s). This is an open-access article distributed under the terms of the Creative Commons Attribution License (CC BY 4.0), permitting distribution and reproduction in any medium, provided the original work is cited.

Abstract: Post-aortic dissection kinesiophobia is one of the most frequent clinical problems—greatly impairing rehabilitation adherence-yet its neural underpinnings remain largely unexplained. Taking recent progress in studies of fear-related neural circuits (learning and extinction) as a basis, the present paper suggests that post-aortic dissection kinesiophobia corresponds to a conditioned fear phenomenon essentially of the type described with insufficient vmPFC inhibition and with an overactive amygdala, the present discussion proposes the "fear extinction-brain functional remodeling" neurotheoretical hypothesis: traditional health-preserving exercises-by virtue of their three-dimensional synergy (of body regulation, breath control, and mental calm)—help to regulate top-down vmPFC-amygdala activity, to optimize DMN functional connectivity and internetwork dynamics, to acquire and solidify fear extinction learning, and so to relieve kinesiophobia and to improve long-term prognosis. It now gives a systematic account of indirect evidence for this hypothesis and outlines multimodal fMRI studies as well as a mediation analysis research agenda.

Keywords: Aortic dissection; Kinesiophobia; Extinction of fear; Standard health-maintaining exercises; Remodeling of brain function

Online publication: October 19, 2026

1. Introduction

1.1. Kinesiophobia: The invisible barrier to post-aortic dissection rehabilitation

Aortic dissection (AD) is a cardiovascular emergency with a sudden onset and very high mortality. With modern surgical methods and better perioperative care, survival following post-AD events has improved

greatly, yet rehabilitation—after surgery—is hampered by an often-neglected problem called kinesiophobia [1]. The previous surgery-related studies gave an estimate of 46.2% for the incidence of kinesiophobia [2]. A later 2026 study added further evidence of the heterogeneity of post-AD kinesiophobia: of the 309 examined cases, 73.14% (*n*=226) had kinesiophobia. They could be assigned to three subtypes—Type A (25.2%), Type B (17.7%), or Type C (57.1%). Age above 65 years, Stanford Type A dissection, lack of a spouse, low education level, and highly invasive surgery seem to be connected with higher fear levels [3]. Kinesiophobia has direct negative effects on participation in rehabilitation exercises and may itself feed back in an unending cycle into poor postoperative functioning, bad mental health, or reduced quality of life. Current research on post-AD kinesiophobia tends mainly to treat it as a psychobehavioral phenomenon [4]. But, in terms of neuroscience, the clinical manifestations of kinesiophobia—specific hypervigilance toward exercise-related cues, long-standing avoidance acts, and fear that is hard to remove even with medical reassurance—seem to closely match the behavioral traits of conditioned fear responses. Such observations encourage the authors to consider the neural basis of fear learning and of extinction as central to an explanation of post-AD kinesiophobia.

1.2. Advances in research on the neural circuits of fear extinction

Within the past two decades, work on the neural basis of fear learning and of its extinction has achieved major advances [5–6]. According to the classical model, the amygdala, hippocampus, and medial prefrontal cortex are central to fear processing, with many mutual connections—both forward and backward-among them [7–8]. With regard to conditioning of fear, the basolateral amygdala (BLA) is the primary location for formation and for manifestation of such memories; the hippocampus helps to supply contextual details which regulate fear responses; and the ventromedial prefrontal cortex (vmPFC) is centrally involved in fear extinction [9–10]. The essential neural basis of extinction learning is top-down suppression of the amygdala by the vmPFC [11]. Functional magnetic resonance imaging (fMRI) data repeatedly confirm that retrieval of an extinction memory—when it succeeds—is associated with enhanced functional connectivity between the vmPFC and amygdala [12]. An important study has shown that those people whose vmPFC-amygdala functional connectivity was stronger following a fear memory recall had more effective fear suppression in the extinction trials that followed [13]. Further mechanistic work has now clarified the role of theta oscillations—of information flow between the vmPFC and amygdala—as an electrophysiological basis for extinction learning—theta transmission from the vmPFC to the amygdala helps to acquire a sense of safety, whereas retention of threat data in the amygdala is slowly lost during extinction [14].

1.3. Traditional health—Some preserved exercises as mind-body interventions that may affect the nervous system

Among traditional forms of health-preserving exercise (such as Tai Chi, Baduanjin, Qigong, etc.), there is a three-dimensional synergy called “body regulation, breath regulation, and mind regulation.” Over the past few years, some neuroimaging investigations have begun to clarify their special brain regulatory effects [15]. For people who regularly do Tai Chi, there are definite changes—of low-frequency type—in the default mode network (DMN) and frontoparietal network [16]. Both Tai Chi and Baduanjin are capable of influencing functional connectivity in the cognitive control network, and Tai Chi practitioners display marked changes—relative to controls—in resting-state functional coupling between the dorsolateral prefrontal cortex and

anterior cingulate cortex [17–18]. As far as emotion regulation is concerned, systematic reviews give evidence that Tai Chi reduces amygdala activation, helps to normalize prefrontal-limbic relations, and improves autonomic tone [17, 19]. Such observations seem to confirm that traditional forms of health-promoting exercise may affect several nodes of the fear extinction system by means of multi-target neuromodulation, thereby offering a non-drug-based, widely applicable approach to treatment of post-AD kinesiophobia.

1.4. Purpose of this paper

The present paper proposes an integration of findings about the neural circuits of fear extinction, of clinical cases involving post-AD kinesiophobia, and of prior neuroimaging studies of ordinary health-promoting exercises-all of which seem relevant-to formulate the "fear extinction–brain functional remodeling" neurotheoretical hypothesis, and to lay out both theory and program for later systematic testing.

2. Neural mechanisms of fear learning and extinction

2.1. Fear conditioning: Synergy of the amygdala, hippocampus, and prefrontal cortex

Fear conditioning is an associative learning phenomenon that is conserved across species [7]. With regard to the classical fear conditioning model, if a neutral stimulus (conditioned stimulus, CS) is paired many times with something unpleasant (unconditioned stimulus, US), then the CS alone may lead to a fear reaction (conditioned response, CR). Such a behavioral outcome depends upon synaptic plasticity of the basolateral amygdala; long-term potentiation (LTP) and NMDA receptor-related protein synthesis are involved. The hippocampus is responsible for contextual modulation of fear conditioning. With regard to contextual fear conditioning, the hippocampus must encode environmental cues, and its projections to the vmPFC help to regulate fear expression through such context-dependent information. The prefrontal cortex-specifically the vmPFC-defines a cap on fear intensity during the conditioning period by limiting amygdala activation, so as not to exaggerate threat-related responses. Dynamic interaction of these three areas is central to the neural basis of fear learning.

2.2. Fear extinction: Top-down inhibition of the amygdala by the vmPFC

Fear extinction should not be regarded as forgetting fear memory but as building a new, competitive safety memory. The central neural mechanism of such a process involves top-down inhibition of the amygdala by the vmPFC. With regard to its glutamatergic pathway leading to amygdala intercalated cells (ITCs), the vmPFC triggers activity in ITCs and blocks fear-related neurons in the BLA, thus suppressing fear responses. On the network level, extinction learning may be understood as involving dynamic reorganization of large-scale brain networks. An fMRI investigation has shown that for extinction learning, functional connectivity in the DMN, in the frontoparietal area, or in the ventral attention system rises appreciably between early and late stages [20–21]. This observation is of major theoretical value: it denies that extinction learning is just a matter of local circuit plasticity but shows global network-level reorganization.

2.3. Fear memory reinstatement and extinction retention: The role of the DMN

The fragility of extinction memory presents a basic difficulty for exposure therapy—it tends to be disrupted by fear reinstatement or by spontaneous recovery, renewal [22–23]. Now some recent studies are beginning to consider the role of the DMN in retention and in retrieval of extinction memory [24]. Prefrontal glucocorticoid

receptors help to regulate the relationship of the salience network with DMN during fear memory formation. A number of studies have shown that in the transition of fear memory—from recent (hippocampus-dependent) to remote (cortex-dependent)—there is a reorganization of the retrieval network going from a "salience network-like" configuration to a "DMN-like" configuration [25–26]. This seems to indicate that the DMN is central—perhaps essential—to remote fear memory storage and recall. Among the core nodes of the DMN-posterior cingulate/precuneus, medial prefrontal cortex, and hippocampus—each has strong structural or functional links with the vmPFC–amygdala circuit; dysfunction of the DMN may cause both recurrence of fear memory and failure of extinction consolidation.

2.4. The role of the autonomic nervous system and endocrine system in fear responses

Peripheral expression of fear responses is jointly controlled by the autonomic nervous system and the neuroendocrine system [27]. Activation of the sympathetic nervous system brings about higher heart rate, increased blood pressure, and greater skin conductance; hypothalamic-pituitary-adrenal (HPA) axis activation is associated with cortisol release. With regard to extinction learning, a high vagal tone seems closely bound to the consolidation of extinction memory [28]. Vagus nerve stimulation (VNS) may help to achieve extinction learning in the BLA through an increase in locus coeruleus noradrenergic activity, with rapid consolidation of extinction memory. Transcutaneous auricular vagus nerve stimulation (tVNS) is now known to facilitate long-term recall of extinction memory in human subjects. Such evidence is helpful in figuring out the neuromodulatory role of the breath-related part of traditional health-preserving exercises.

3. Neuropathological hypothesis of post—Aortic dissection kinesiophobia

3.1. Traumatic events as well as surgery: Robust consolidation of fear memory

The beginning of AD is marked by highly traumatic features. Sudden intense chest pain, an intrusive episode of emergency surgery, and persistent stress following the postoperative ICU phase all fit a "multiple US" fear conditioning context. Within such contexts, it is possible for exercise-linked interoceptive signals (elevated heart rate or more profound breathing) to act as conditioned stimuli and to establish solid connections with fear responses with regard to interoceptive conditioning mechanisms. From a neurobiological standpoint, the huge surge of stress hormones (norepinephrine, cortisol) at AD onset seems to offer neurochemical help for the over-consolidation of fear memory. Animal evidence suggests that stress hormones may facilitate synaptic plasticity in the amygdala, thus helping fear memory to be more tenacious [29–30]. Post-AD individuals suffer from a fear memory that has already been "super-consolidated," which is one reason why giving them medical reassurance alone rarely eliminates kinesiophobia.

3.2. Misinterpretation of "avoid exercise" medical advice: Reinforcement of fear conditioning

Post-AD patients are generally told to observe strict limits on exercise, namely no excessive physical effort, no hard training, and no Valsalva maneuvers. Such instructions are medically justified, yet if one lacks both communication and a slow introduction to exercise, the patient may end up thinking that "exercise=danger." Behaviorally speaking, this cognitive generalization produces an avoidance pattern that applies broadly to various forms of exercise, and such avoidance sustains or worsens fear thanks to negative reinforcement—each instance of avoidance relieves anxiety briefly but denies the possibility of extinction learning. More

importantly, the early postoperative recurrence of avoidance behavior may help to solidify the initial fear memory by means of the "reconsolidation" process. Every time a patient resorts to avoidance in thinking about exercise, the old fear memory comes back and is modified, which complicates its eventual extinction.

3.3. Hypothesis of insufficient vmPFC inhibition and amygdala hyperactivation

With regard to studies of the fear extinction neural circuit, it is now possible to suggest that the basic neuropathological element of post-AD kinesiophobia may be a failure of top-down inhibition of the amygdala by the vmPFC, combined with amygdala hyperactivity and reactivity. Several indirect pieces of evidence back up this hypothesis. Indeed, diminished vmPFC–amygdala coupling (in terms of function) and increased amygdala reactivity seem to be commonly noted phenomena in patients with anxiety disorders. High anxiety together with kinesiophobia in post-AD cases seems to reflect similar neural circuit anomalies. Second, post-AD patients suffer from disturbances of cerebral blood flow perfusion. A study using arterial spin labeling reports reduced cerebral blood flow in a number of areas of post-AD brains—namely, key network sites for thought, attention, or emotional control [31–32]. Should the vmPFC's perfusion fail to reach normal levels, its top-down inhibition may not operate fully, and fear extinction could become less likely.

3.4. DMN dysfunction and repeated retrieval of fear memory

Among the prominent clinical features of post-AD kinesiophobia is the "stubbornness" of fear-even though rational arguments confirm the safety of physical exercise, fear responses persist. Such persistence may be linked to a frequent return of fear memory and to trouble with extinction memory brought about by DMN dysfunction. The DMN is centrally involved in self-directed thinking and in retrieval of past events. With abnormal DMN function, self-referential memories of fear about exercise seem to come up too often, generating intrusive ideas such as "I am unsafe" or "exercise will cause dissection recurrence." At the same time, context-safety associations newly built by extinction learning run a real risk of not being well integrated with self-referential memory via the DMN. Furthermore, post-AD patients may show an impaired dynamic balance between the DMN and frontoparietal system, which complicates their ability to let go of fear thoughts (self-related) and to begin safe, task-oriented exercise experiences.

3.5. Autonomic imbalance and enhanced cardiovascular stress responses

Post-AD patients commonly show signs of autonomic nervous system dysfunction. Heart rate variability data make it clear that low-frequency power, high-frequency power, and LF/HF ratio are very poorly developed in post-AD people-a sign of cardiac sympathetic and parasympathetic denervation [33–34]. The present autonomic imbalance is harmful to cardiovascular health and may encourage fear by means of interoceptive interaction. With regard to interoceptive predictive coding, the cardiovascular system of post-AD patients—after surgery and with denervation—generates abnormal "interoceptive noise." The brain may misread such interoceptive irregularities as "danger signals," and then begin to feel fear in consequence. On the other hand, heart rate increases, or blood pressure rises brought about by exercise (normal phenomena for healthy people) may now be wrongly associated with "harbingers of dissection recurrence" in post-AD subjects, thus strengthening the link between exercise and fear. Such a vicious cycle—of autonomic disturbance and heightened fear—constitutes a significant peripheral factor in the maintenance of post-AD kinesiophobia.

4. Traditional health-preserving exercises and their neuromodulatory parts

4.1. Body regulation: Use of a safe exercise experience to reverse fear conditioning

Among traditional health-preserving exercises, one finds low-intensity, slow, fluid movements, with an unmistakable "safe exercise experience" for post-AD patients [35]. With regard to fear extinction, body regulation is basically an instance of interoceptive exposure [36]. For those who do Tai Chi or Baduanjin, the physical effects of the exercise they experience (mild acceleration of the heart, more vigorous breathing) occur in a safe, controlled situation with no aversive outcome. Such a process matches well the basic logic of extinction learning: with the CS (interoceptive signals from exercise) still active, the US (recurrence of dissection/danger) is absent, hence creating a new CS-safety link [37]. More importantly, the movement design of traditional health-preserving exercises makes it possible to avoid Valsalva maneuvers and abrupt changes in blood pressure, thus helping the patient to keep hemodynamics more or less stable during exercise. Such safety is not merely medical but also neurobehaviorally helpful: extinction training—i.e., the key to extinction learning—is facilitated by the certainty of US absence during CS exposure, and traditional health-preserving exercises yield exactly this "certainty of safe experience."

4.2. Breath regulation: Vagal activation and autonomic balance

Breath regulation is a central element of traditional health-preserving exercises, and it calls for slow, deep breathing from the abdomen. Such breathing is known to lead to substantial improvement of vagal tone as well as to an increased high-frequency part of heart rate variability. With regard to fear extinction, the regulation of respiration—probably via the vagus—may help to establish or consolidate extinction memory in a direct fashion. Stimulation of the vagus nerve seems to help consolidate fear extinction—by means of increased locus coeruleus noradrenergic transmission and LTP in the BLA-a fact now well established in animal studies [38–39]. As far as humans are concerned, transcutaneous auricular vagus nerve stimulation is known to facilitate both immediate suppression of fear and long-term recall of extinction memory. Among the components of traditional health-preserving exercises, breath regulation may foster a neuromodulatory climate favorable to extinction learning—through similar vagal activation mechanisms—with the cooperative release of norepinephrine and acetylcholine helping to improve synaptic flexibility in the vmPFC and amygdala, and thus to encode or consolidate extinction memory [40]. In addition, the autonomic regulatory effects of slow breathing seem to be capable of correcting post-AD autonomic imbalance [41]. With higher parasympathetic tone and less sympathetic overactivity, the breath regulation component is likely to ease cardiovascular strain during exercise and to prevent fear responses caused by interoceptive noise.

4.3. Mind regulation: Promotion of fear extinction learning through mindful attention

The mind regulation part is concerned with keeping attention directed toward immediate bodily feelings and toward one's own breathing, without prejudice or evasion. Such mindful attention seems to help in many ways with the process of fear extinction learning. First of all, it fosters an improved awareness of actual sensory facts, which may lead to clearer identification of both "threat-relatedsignals" and safety signals. Extinction learning is basically a form of discriminative learning—learners must come to distinguish between CS+ (threat cues joined with US) and CS− (safety cues). Training in mindfulness—which increases interoceptive accuracy—seems helpful in achieving such discrimination. Second, mindful attention brings about less dependence upon cognitive avoidance or emotion control with regard to fear memory. fMRI work has indicated that mindfulness training facilitates extinction memory retrieval, by means of direct modulation

of subcortical threat-processing areas (like the amygdala) instead of depending on top-down cognitive control [42]. This "direct modulation" mode coincides very closely with the mind-regulation traits of known health-promoting exercises—mindful attention is not obliged to push patients toward an active "suppress" of fear but helps extinction through modification of the relationship with fear experiences. Third, mindfulness training seems able to improve hippocampus-mediated contextual retrieval and thus allow flexible extinction memory across contexts [43]. Such flexibility is especially significant for post-AD kinesiophobia since people with this disorder tend to have generalized fears of exercise, which call for an extinction memory not limited to one context.

4.4. Three-dimensional synergy: Advantages of multi-target neuromodulation

Among the advantages of traditional health-preserving exercises is the three-dimensional synergy of body regulation, breath regulation, and mind regulation. Compared with either single-exposure treatment or with mindfulness alone, such synergy offers a more favorable setup for extinction learning. Body regulation furnishes a secure environment for interoceptive exposure; breath regulation gives rise to a neuromodulatory environment that encourages extinction consolidation and benefits the mind in its regulation—both of states and of contexts—during extinction learning. The two factors taken together seem to yield a more potent effect than either alone. From the standpoint of network neuroscience, three-dimensional synergy implies joint control of many brain systems: body regulation is largely connected with the sensor. The motor and interoceptive networks; regulation of breath is essentially handled by autonomic regulatory pathways (i.e., by the brainstem and insula); mind regulation is essentially linked to the DMN and to the executive network. Modulation of several networks together seems likely to help with consolidation of extinction memory for long-term recall of extinction memory; one needs widespread synaptic plasticity across many networks.

5. Proposal of the neurotheoretical hypothesis

5.1. Hypothesis 1: Conventional health—Saving exercises may help to improve vmPFC-amygdala connectivity

Consistent practice of traditional health-preserving exercises seems to help in post-AD cases with regard to resting-state or task-state functional connectivity of the vmPFC and amygdala. Such an improvement is likely to result from two interwoven mechanisms. First, the interoceptive exposure of the body regulation part offers many repeated "practice" occasions for vmPFC inhibition of the amygdala; the strengthening of the vmPFC–amygdala pathway is similar to what occurs with extinction training. Second, the combination of breath regulation and mind regulation brings about favorable neuromodulatory and hemodynamic states-specifically higher vagal tone and prefrontal activity-for the vmPFC. From a clinical standpoint, the authors expect that an 8-to 12-week course of traditional health-promoting exercise may lead to substantial improvement in vmPFC–amygdala connectivity for post-AD patients, with such improvement linked closely to falling kinesiophobia scores.

5.2. Hypothesis 2: Conventional health-preserving exercises may help to optimize DMN internal and internetwork connectivity

Standard health-preserving exercises are likely to bring about an improvement in functional connectivity of the DMN and to promote a better dynamic balance—between the DMN and the frontoparietal network

and the salience network. More specifically, the authors anticipate that functional connectivity of the DMN (notably the vmPFC–posterior cingulate or precuneus circuit) is going to increase, with extinction memory being more efficiently integrated, now being considered in connection with self-referential knowledge structures. At the same time, the anticorrelation between the DMN and frontoparietal network seems possibly stronger now, which would help explain both a reduction of self-bound fear and an increase in task-oriented safety (exercise) feelings. With regard to low-frequency amplitude of the DMN and frontoparietal network, Tai Chi users show marked changes-an indirect initial support for this hypothesis.

5.3. Hypothesis 3: Brain functional remodeling mediates the decline in kinesiophobia

Increased vmPFC–amygdala functional connectivity as well as optimized DMN function seem to mediate the relation between conventional health-preserving exercise interventions and reduced kinesiophobia. More specifically, the intervention lowers fear responses by means of top-down suppression of the amygdala—by the vmPFC—and by less frequent recall of fear memories (due to better DMN function), both of which help explain the behavioral relief from kinesiophobia. Such an idea is amenable to mediation analysis: the mediating factor is change in brain connectivity, the independent factor is traditional health-preserving exercise, and TSK-SV Heart score changes are the dependent variables-all to be used in testing the indirect effect's significance.

5.4. Hypothesis 4: Brain functional remodeling further mediates long-term prognosis improvement

Functional remodeling of the brain is not merely responsible for an initial reduction of kinesiophobia but may also help to improve long-term prognosis. It seems likely that the amount of improvement—whether in vmPFC–amygdala connectivity or in DMN function—after traditional health-preserving exercise treatment will predict how well one adheres to exercise rehabilitation, how much physical function is restored, and what quality of life results at 6-12 months post-intervention. Such prediction needs validation, preferably by means of a longitudinal study showing time-ordered causality between brain changes and long-term medical results.

5.5. Overall framework of the hypothesis

Among the four hypotheses mentioned, there is a causal chain—from neural mechanisms up to clinical results: three-dimensional synergistic use of traditional health-preserving exercises seems to improve vmPFC–amygdala interaction and DMN optimization; it helps with extinction of fear; it reduces kinesiophobia; it promotes long-term recovery. Each of the links in this causal chain is amenable to individual testing, yet the general hypothesis offers a well-ordered plan for scientific investigation.

6. Indirect evidence as well as theoretical justification for the hypothesis

6.1. On the question of Tai Chi's ability to improve prefrontal connectivity

Among traditional health-preserving practices, Tai Chi is a clear example having considerable imaging evidence concerning the regulatory effects it may have on prefrontal connectivity. A randomized brain imaging study reports that a remote Tai Chi treatment brings about significant increases in dorsolateral prefrontal functional connectivity for those with knee osteoarthritis [44]. With regard to fibromyalgia patients,

12 weeks of Tai Chi practice—without concurrent drug therapy—produces substantial improvement in resting-state functional connectivity of the cognitive control network (relative to) the anterior cingulate/medial prefrontal cortex [45]. Even if the cited studies were not done in post-AD groups, their findings on the prefrontal–limbic regulation by Tai Chi still help confirm Hypothesis 1.

6.2. Promoting effects of mindfulness meditation on fear extinction

Mindfulness meditation is the basic technique used in the mind-regulation part of traditional health-preserving exercises. A randomized controlled trial—using 7T fMRI—has shown that mindfulness training helps with extinction-related memory retrieval and with the suppression of both behavioral and neural threat responses following extinction [42]. It is important to note that the effect of mindfulness training was not obtained by increased activation of the cognitive control areas; rather, it is manifested as a direct decrease—rather than an increase—in subcortical threat-related activation (especially in the amygdala). The "direct modulation" mode implies that mindfulness may encourage extinction by means of neural effects not found in ordinary exposure therapy, which seems to match the special way in which mental regulation operates within traditional health-preserving exercises.

6.3. Enhancing effects of regular exercise on fear extinction learning

Exercise of the regular type is itself helpful for fear extinction learning. Studies with animals reveal that wheel running—given once—after extinction training may help retrieve extinction memories, and such an effect relies on the central mTOR signaling pathway [46]. With regard to humans, moderate-intensity aerobic exercise carried out either during or following extinction learning seems to aid consolidation of extinction memory. Traditional health-preserving exercises (which are low-to-moderate-intensity mind-body activities) seem to foster extinction memory consolidation by means of similar mTOR-related processes [47]. At the same time, these traditional forms of exercise add—beyond aerobic activity—control of breathing and control of mental state, which may yield extinction-enhancing results not achieved otherwise [48].

6.4. Clinical observations of post-aortic dissection kinesiophobia

Clinical features of post-AD kinesiophobia give an indirect behavioral basis for this hypothesis. The high frequency, marked diversity, and inverse relationship between post-AD kinesiophobia and exercise self-efficacy all seem to agree with the behavioral pattern of conditioned fear responses [49]. Even more important is the finding that moderate-intensity home-based exercise is not harmful to cardiovascular patients and may "help patients rebuild trust" [50]. The present finding accords well with the behavioral logic of fear extinction—safe forms of exercise seem to perform the role of extinction learning. Yet the trial under discussion says nothing about neural processes or about systematic use of extinction learning-oriented treatment protocols. Standard health-promoting exercises—three-dimensionally—seem to encourage extinction learning by virtue of that fact.

7. Validation strategy and research agenda

7.1. Multimodal fMRI validation pathway

Testing this hypothesis calls for the use of multimodal neuroimaging techniques. Resting-state fMRI (rs-fMRI) is well suited for studying shifts—before and after treatment—of vmPFC–amygdala functional connectivity

and DMN internal as well as internetwork connectivity. Task-state fMRI lends itself to paradigms involving fear conditioning or to exercise-related interoceptive exposure in order to analyze activation patterns and dynamics of functional connectivity of the vmPFC and amygdala with respect to extinction learning. Diffusion tensor imaging (DTI) offers a means of determining the anatomical quality of the vmPFC–amygdala white matter pathway, and of evaluating—on an individual basis—possible links between microstructural change and functional connectivity. A longitudinal plan is advised: baseline study, 8–12 weeks of standard health-promoting exercise intervention, post-treatment evaluation, and a 6-month follow-up, to trace the time course of such brain effects and of extinction retention phenomena.

7.2. Correlation analysis between TSK-SV heart and brain functional connectivity

Assessment of kinesiophobia should use the Chinese version of the TSK-SV Heart scale, which has already been tested for reliability and validity with regard to Chinese cardiac patients, and which gives a Cronbach's α value of 0.790, having four dimensions—danger perception, kinesiophobia, exercise avoidance, and functional impairment. For correlation analysis, it is recommended to apply seed-based whole-brain functional connectivity and network-based statistics to check the relations between TSK-SV Heart total scores (or dimension scores) and vmPFC–amygdala connectivity, DMN internal connectivity, and DMN–frontoparietal network connectivity. The main hypothesis is: the improvement post-intervention of vmPFC–amygdala functional connectivity correlates positively with the drop in kinesiophobia magnitude.

7.3. Theoretical design of mediation analysis and structural equation modeling

To test the hypotheses labeled "brain functional remodeling mediates the decline in kinesiophobia" and "brain functional remodeling further mediates long-term prognosis improvement," one uses mediation analysis. The theoretical model to be considered has this form: the independent variable is the treatment group (traditional health-preserving exercises or standard rehabilitation); the mediating variable is brain functional connectivity changes (vmPFC–amygdala and DMN-associated indicators) considered here; dependent variables include kinesiophobia changes (TSK-SV Heart) and long-term prognosis factors (exercise adherence, physical condition, quality of life). Structural equation modeling (SEM) is well suited to check several mediation models at once and to assess the global fit of the model. Bootstrap analysis is advocated for testing the statistical relevance of indirect effects, with age, sex, operation type, and initial fear controlled as covariates.

7.4. Key scientific questions for future research

Systematic validation of this hypothesis brings with it a need to answer the following major scientific questions:

(1) Is there a dose-response relationship—between traditional health-preserving exercises and the enhancement of vmPFC–amygdala connectivity? What is the smallest effective dose of such an intervention?

(2) How do the three elements of body regulation, breath regulation, and mind regulation contribute separately?

(3) How does the brain's functional state change over time? Is there an earlier (pre-behavioral) stage of functional connectivity that predicts improvement?

(4) Are the various kinesiophobia subtypes (namely "low risk perception-high kinesiophobia" versus "severe

kinesiophobia") differently affected by traditional health-promoting exercise intervention?

(5) Does extinction memory stay retained indefinitely, or is it dependent upon continuous or limited practice?

8. Conclusion

Post-aortic dissection kinesiophobia is a very common clinical problem whose neural basis is not fully known. The present paper argues that the "fear extinction–brain functional remodeling" neurotheoretical hypothesis offers a unified theoretical approach to this particular phenomenon. According to the hypothesis, post-AD kinesiophobia is basically a conditioned fear reaction, and its basic neuropathology lies in inadequate top-down inhibition of the amygdala by the vmPFC and DMN dysfunction. Traditional health-preserving exercises—whether they regulate body states (with safe interoceptive exposure) or breathing (with better vagal tone and extinction consolidation) or the mind (with attentional focus or contextual adaptability)—act three-dimensionally to improve vmPFC–amygdala functional connectivity and to optimize DMN functional connectivity; extinction of kinesiophobia and improvement of long-term prognosis are thereby achieved. The hypothesis is indirectly substantiated by work on neural circuits of fear extinction, by neuroimaging of well-known health-preserving exercises, and by observations of post-AD patients, and lends itself to systematic validation with multimodal fMRI, mediation techniques, or longitudinal investigations. Should it prove correct, traditional health-preserving exercises seem to offer a secure, feasible, and neuroscience-based treatment of post-AD kinesiophobia.

Funding

Hunan Provincial Degree and Postgraduate Teaching Reform Research and Postgraduate Scientific Research Innovation Project (Project No.: 2025JGYB286).

Disclosure statement

The authors declare no conflict of interest.

References

[1] Tsao CW, Aday AW, Almarzoog ZI, et al., 2023, Heart Disease and Stroke Statistics–2023 Update: A Report from the American Heart Association. Circulation, 2023(147): e93–e621.

[2] Chen Y, Peng Y, Huang X, et al., 2024, Postoperative Kinesiophobia in Patients with Acute Type A Aortic Dissection: A Cross-Sectional Study. Reviews in Cardiovascular Medicine, 25(8): 304.

[3] Yang X, Luo Y, Wang D, 2026, Heterogeneity in Kinesiophobia among Postoperative Aortic Dissection Survivors: Associations with Exercise Self-Efficacy, Family Support, and Coping Styles. Frontiers in Psychology, 2026(17): 1800841.

[4] Caseras X, Mataix-Cols D, Trasovares MV, et al., 2010, Dynamics of Brain Responses to Phobic-Related Stimulation in Specific Phobia Subtypes. European Journal of Neuroscience, 32(8): 1414–1422.

[5] Huang MQ, Liang XL, Lin XT, et al., 2025, Amygdala-dependent Signaling Pathways and Regulating Circuits in Fear Memory. Synapse, 79(5): e70026.

[6] Bouton ME, Maren S, McNally GP, 2021, Behavioral and Neurobiological Mechanisms of Pavlovian and Instrumental Extinction Learning. Physiological Reviews, 101(2): 611–681.

[7] Johansen JP, Cain CK, Ostroff LE, et al., 2011, Molecular Mechanisms of Fear Learning and Memory. Cell, 147(3): 509–524.

[8] Xu R, Shi D, Wang K, et al., 2025, Progress in Spatiotemporal Regulation of Fear Memory: Neural Circuit Mechanisms and Implications for PTSD. General Psychiatry, 2025, 38(4): e102224.

[9] Rich M T, Sacko T J, Rohilla H K, et al. Fear conditioning enhances subsequent cocaine self-administration and amygdala neuronal activity only in male rats. Neuropharmacology, 2026, 298: 111079.

[10] Zhang X, Lan Z, Huang Y, et al., 2026, Identification of Somatostatin Inhibitory Engrams for Extinction in the Basolateral Amygdala. Proceedings of the National Academy of Sciences of the United States of America, 123(12): e2511528123.

[11] Lange I, Goossens L, Michielse S, et al., 2020, Neural Responses during Extinction Learning Predict Exposure Therapy Outcome in Phobia: Results from A Randomized-Controlled Trial. Neuropsychopharmacology, 45(3): 534–541.

[12] Lyons A L, Jiang X, Rawliuk T, et al., 2026, Ventromedial Prefrontal Cortex Activity during Extinction Recall Suggests Successful Extinction Learning via Mental Imagery. Social Cognitive and Affective Neuroscience, 21(1): nsag031.

[13] Andrys NRR, Johnson EA, Rowe EB, et al., 2026, Daily Rhythms in Fear Extinction Memory Reflect Structural and Functional Changes in a Prefrontal-Amygdala Circuit. Brain Structure & Function, 231(8): 136.

[14] Lu P, Chen D, Xia W, et al., 2025, Theta Oscillations between the Ventromedial Prefrontal Cortex and Amygdala Support Dynamic Representations of Threat and Safety. NeuroImage, 2025(310): 121164.

[15] Jin X, Chen J, Zhang X, 2026, Tai Chi Exercise and Neuroplasticity: A Narrative Review According to Neural Mechanisms and Clinical Utilizations in Brain Health. Frontiers in Neuroscience, 2026(20): 1769779.

[16] Zhang Y, Song Q, Li X, et al., 2026, Long-term Tai Chi Practice Modulates Cortical-Muscular Interactions during Walking in Older Adults: A Cross-Sectional Study. Clinical Interventions in Aging, 2026(21): 615470.

[17] Zhong X, Dai Z, Chu L, et al., 2026, Tai Chi Modulating Multimodal Connectivity Patterns and Cognitive Function in Cerebral Small Vessel Disease. Geroscience, 48(6): 7961–7976.

[18] Wang X, Si K, Gu W, et al., 2023, Mitigating Effects and Mechanisms of Tai Chi on Mild Cognitive Impairment in the Elderly. Frontiers in Aging Neuroscience, 2023(14): 1028822.

[19] Wang R, Chen J, Zhu D, 2026, Tai Chi Modulates Resting Alpha and Theta EEG Rhythms in Female Individuals with Amphetamine-Type Stimulant Dependence during Compulsory Detoxification. Frontiers in Psychiatry, 2026(17): 1904447.

[20] de Vos J H, Baldi S, Lange I, et al., 2026, Intrinsic Connectivity Networks during Fear and Safety Learning in Youth. British Journal of Psychiatry, advance online publication, 1–8.

[21] Das S, Meyyappan S, Bekker EM, et al., 2026, The Ventral Attention Network Mediates Attentional Reorienting to Cross-Modal Expectancy Violations: Evidence from EEG and fMRI. The Journal of Neuroscience, 46(7): e0720252026.

[22] Pacheco-Estefan D, Bouyeure A, Jacob G, et al., 2026, Representational Dynamics during Extinction of Fear Memories in the Human Brain. Nature Human Behaviour, 10(1): 29–48.

[23] Kida S, 2023, Interaction between Reconsolidation and Extinction of Fear Memory. Brain Research Bulletin, 2023(195): 141–144.

[24] Axmacher N, Pacheco-Estefan D, Bouyeure A, et al., 2026, Extinction Memories: Putting Learning into Context. Trends in Cognitive Sciences, 30(2): 107–109.

[25] Park H, Kaang BK, 2026, Role of the Hippocampus in Systems Consolidation of Remote Fear Memory. Experimental & Molecular Medicine, 58(4): 1010–1016.

[26] Kupke J, Loizou S, Bengtson CP, et al., 2025, Hippocampal DNA Methylation Promotes Contextual Fear Memory Persistence by Facilitating Systems Consolidation and Cortical Engram Stabilization. Biological Psychiatry, 98(5): 394–403.

[27] Wickramasuriya DS, Faghih RT, 2020, A Mixed Filter Algorithm for Sympathetic Arousal Tracking from Skin Conductance and Heart Rate Measurements in Pavlovian Fear Conditioning. PLoS One, 15(4): e0231659.

[28] Noble LJ, Chuah A, Callahan KK, et al., 2019, Peripheral Effects of Vagus Nerve Stimulation on Anxiety and Extinction of Conditioned Fear in Rats. Learning & Memory, 26(7): 245–251.

[29] Mary A, Nematollahi H, Torres D, et al., 2026, Transcutaneous Vagus Nerve Stimulation Enhances Episodic Memory Across Valences and Memory Stages. Brain Stimulation, 19(2): 103051.

[30] Phillips I, Johns MA, Pandža NB, et al., 2025, Three Hundred Hertz Transcutaneous Auricular Vagus Nerve Stimulation (taVNS) Impacts Pupil Size Non-Linearly as a Function of Intensity. Psychophysiology, 62(2): e70011.

[31] Bernetti C, D'Andrea V, Buoso A, et al., 2025, Arterial Spin Labeling MRI in Alzheimer's Disease: A Systematic Review of Cerebral Perfusion Biomarkers. Journal of Neuroimaging, 35(2): e70035.

[32] Xue P, Yu H, Zhu Y, et al., 2026, Quantitative Perfusion Assessment with Arterial Spin Labeling Magnetic Resonance Imaging for Predicting Cognitive Decline in Alzheimer's Disease: A Systematic Review and Meta-Analysis. Journal of Clinical Neuroscience, 2026(143): 111711.

[33] Fang Y, Zhang Y, Wang G, et al., 2025, Autonomic Function Effects on Postoperative Sleep Disorder: A Prospective Cohort Study. International Journal of Surgery, 111(10): 7010–7020.

[34] Akiya A, Takahashi K, Iwahara K, et al., 2026, Impact of Nonlinear Heart Rate Variability in Postoperative Complex Congenital Heart Disease: Insights from Repaired Tetralogy of Fallot and Fontan Palliation. Pediatric Cardiology, 47(5): 2241–2249.

[35] Zhao X, Zou R, Miao H, et al., 2026, The Efficacy of Traditional Chinese Exercises in Patients with Chronic Heart Failure: An Umbrella Review and Meta-Analysis. Reviews in Cardiovascular Medicine, 27(3): 46055.

[36] Wan Y, Fu Y, Bian Z, et al., 2026, Effects of Traditional Chinese Exercises for Upper-limb Dysfunction Following Breast Cancer Surgery: Protocol for a Systematic Review and Meta-analysis. BMJ Open, 16(5): e112564.

[37] Tanaka Y, Ito Y, Shibata M, et al., 2025, Heartbeat Evoked Potentials Reflect Interoceptive Awareness during an Emotional Situation. Scientific Reports, 15(1): 8072.

[38] Qi R, Wang J, Pei H, et al., 2026, Vagus Nerve Stimulation Enhances Memory and Long-term Potentiation via the Hippocampal NE/β-AR Signaling Pathway in Pilocarpine Rats. Brain Research Bulletin, 2026(237): 111789.

[39] Hyakumura T, Payne SC, Matarazzo JV, et al., 2025, Abdominal Vagus Nerve Stimulation Increases Firing in the Rat Locus Coeruleus. Neuromodulation, 28(8): 1239–1247.

[40] Driskill C, Vu L, Jalilvand S, et al., 2026, Pairing Extinction Training with Vagus Nerve Stimulation Reduces Drug-Seeking by Altering Activity in Afferents to the Medial Prefrontal Cortex. Frontiers in Neuroscience, 2026(20): 1756644.

[41] Noble DJ, Hochman S, 2019, Hypothesis: Pulmonary Afferent Activity Patterns during Slow, Deep Breathing Contribute to the Neural Induction of Physiological Relaxation. Frontiers in Physiology, 2019(10): 1176.

[42] Björkstrand J, Olsson E, Clancy OH, et al., 2026, Effect of App-Based Mindfulness on Extinction Recall—A 7T-fMRI Study. Scientific Reports, 16(1): 9957.

[43] Blades RB, Boyle CC, Eisenberger NI, et al., 2026, Neural Mechanisms of Mindfulness: Reduced Neural Reactivity to Social-Evaluative Threat Accounts for Mindfulness Intervention Effects on Inflammatory Gene Expression. Brain, Behavior, and Immunity, 2026(133): 106284.

[44] Liu X, Tang T, Liang S, et al., 2026, Effects of Tai Chi Combined with Transcranial Direct Current Stimulation on Pain in Knee Osteoarthritis: A Randomized Controlled Neuroimaging Trial. BMC Medicine, 24(1): 265.

[45] Kong J, Wolcott E, Wang Z, et al., 2019, Altered Resting State Functional Connectivity of the Cognitive Control Network in Fibromyalgia and the Modulation Effect of Mind-Body Intervention. Brain Imaging and Behavior, 13(2): 482–492.

[46] Ko YJ, Ko IG, 2020, Voluntary Wheel Running Improves Spatial Learning Memory by Suppressing Inflammation and Apoptosis via Inactivation of Nuclear Factor Kappa B in Brain Inflammation Rats. International Journal of Neurobiology, 24(Suppl 2): 96–103.

[47] Zhan Z, Pan L, Zhu Y, et al., 2023, Moderate-intensity Treadmill Exercise Promotes mTOR-dependent Motor Cortical Neurotrophic Factor Expression and Functional Recovery in a Murine Model of Crush Spinal Cord Injury (SCI). Molecular Neurobiology, 60(2): 960–978.

[48] Kolb H, Martin S, Kempf K, 2025, Traditional Health Practices May Promote Nrf2 Activation Similar to Exercise. International Journal of Molecular Sciences, 26(23): 11546.

[49] Wang J, Chen Y, 2025, Pain Catastrophizing, Kinesiophobia, and Exercise Adherence in Postoperative Cardiovascular Surgery Patients: The Mediating Role of Exercise Self-Efficacy. Journal of Rehabilitation Medicine, 2025(57): jrm43853.

[50] Kraal JJ, Peek N, Van den Akker-Van Marle ME, et al., 2014, Effects of Home-based Training with Telemonitoring Guidance in Low to Moderate Risk Patients Entering Cardiac Rehabilitation: Short-Term Results of the FIT@ Home Study. European Journal of Preventive Cardiology, 21(2 Suppl): 26–31.

Publisher's note

Bio-Byword Scientific Publishing remains neutral with regard to jurisdictional claims in published maps and institutional affiliations.

Integrated Services Platform of International Scientific Cooperation

Innoscience Research (Malaysia), which is global market oriented, was founded in 2016.Innoscience Research focuses on services based on scientific research. By cooperating with universities and scientific institutes all over the world, it performs medical researches to benefit human beings and promotes the interdisciplinary and international exchanges among researchers.

Innoscience Research covers biology, chemistry, physics and many other disciplines. It mainly focuses on the improvement of human health. It aims to promote the cooperation, exploration and exchange among researchers from different countries. By establishing platforms, Innoscience integrates the demands from different fields to realize the combination of clinical research and basic research and to accelerate and deepen the international scientific cooperation.

Cooperation Mode



Clinical Workers



In-service Doctors





Foreign Researchers





Hospital



University



Scientific institutions

Our Journals



The *Journal of Architectural Research and Development* is an international peer-reviewed and open access journal which is devoted to establish a bridge between theory and practice in the fields of architectural and design research, urban planning and built environment research.

Topics covered but not limited to:

- Architectural design
- Architectural technology, including new technologies and energy saving technologies
- Architectural practice
- Urban planning
- Impacts of architecture on environment

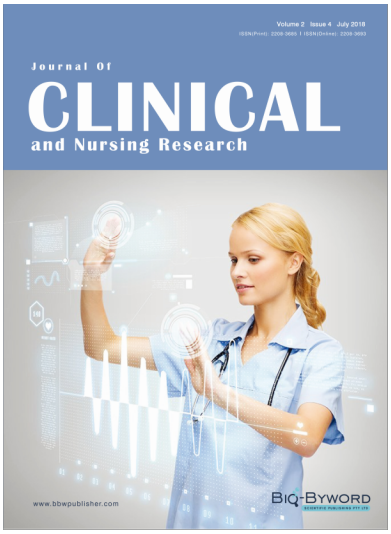

Journal of Clinical and Nursing Research (JCNR) is an international, peer reviewed and open access journal that seeks to promote the development and exchange of knowledge which is directly relevant to all clinical and nursing research and practice. Articles which explore the meaning, prevention, treatment, outcome and impact of a high standard clinical and nursing practice and discipline are encouraged to be submitted as original article, review, case report, short communication and letters.

Topics covered by not limited to:

- Development of clinical and nursing research, evaluation, evidence-based practice and scientific enquiry
- Patients and family experiences of health care
- Clinical and nursing research to enhance patient safety and reduce harm to patients
- Ethics
- Clinical and Nursing history
- Medicine



Journal of Electronic Research and Application is an international, peer-reviewed and open access journal which publishes original articles, reviews, short communications, case studies and letters in the field of electronic research and application.

Topics covered but not limited to:

- Automation
- Circuit Analysis and Application
- Electric and Electronic Measurement Systems
- Electrical Engineering
- Electronic Materials
- Electronics and Communications Engineering
- Power Systems and Power Electronics
- Signal Processing
- Telecommunications Engineering
- Wireless and Mobile Communication